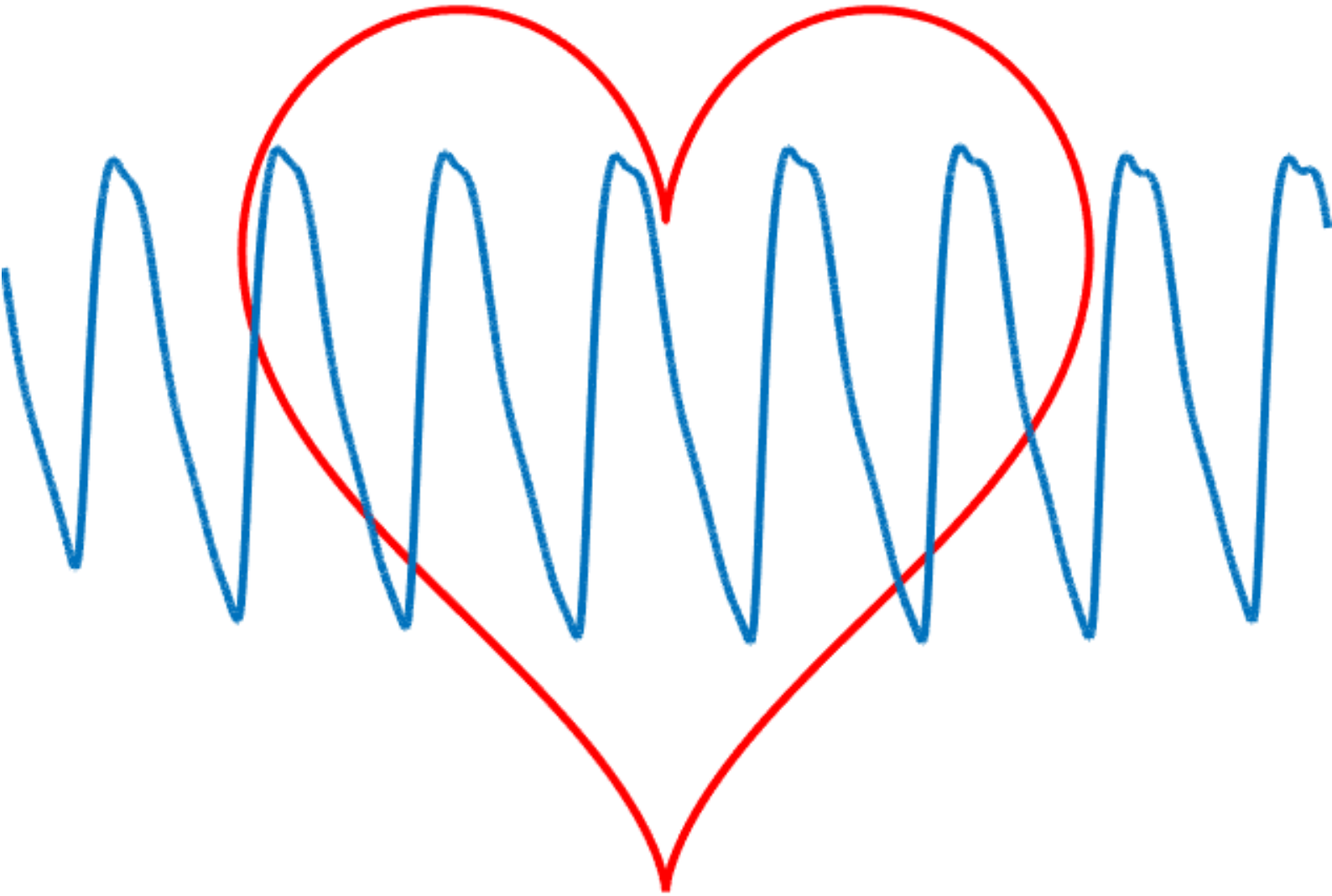

Nuno Henrique Pereira Martins Pinheiro

iLook over you

Thesis submitted to the University of Coimbra in compliance with the requirements for the degree of Master in Biomedical Engineering

January, 2017

· U C ·

UNIVERSIDADE DE COIMBRA

• U C •

FCTUC FACULDADE DE CIÊNCIAS
E TECNOLOGIA
UNIVERSIDADE DE COIMBRA

NUNO HENRIQUE PEREIRA MARTINS PINHEIRO

iLook over you

Dissertação apresentada à Universidade de Coimbra para cumprimento dos requisitos necessários à obtenção do grau de Mestre em Engenharia Biomédica

Thesis submitted to the University of Coimbra in compliance with the requirements for the degree of Master in Biomedical Engineering

Supervisors:

Paulo de Carvalho, PhD

Ricardo Couceiro, PhD

Coimbra, 2017

This work was developed in collaboration with:

Centre for Informatics and Systems of the University of Coimbra

This work is related with project LINK (H2020-692023)
and project HeartCycle (FP7-216695)

Abstract

Syncope refers to the temporary loss of consciousness caused by a reduction in the arterial systemic blood pressure (BP) that leads to the decrease of the global cerebral perfusion. BP, in turn, depends on the cardiac output and systemic vascular resistance, which are regulated by the autonomic nervous system. Due to these connections, any trigger that affects this equilibrium may originate syncope. When this is a neural trigger, the condition is called neurally mediated syncope (NMS).

Syncope is, in fact, a widespread and costly condition, implying a direct global annual cost of $1.7-$2 billion to health services. Therefore, it is essential to find ways of avoiding such large costs caused by syncope and related conditions – as cardiovascular diseases (CVD) and falls –, in favor of the investment in p-health and m-health preventive solutions.

Heart rate variability (HRV) is a promising marker of the autonomic regulation, which requires the acquisition of electrocardiograms (ECG) to reliably compute the heart rate (HR). However, such equipment is still not comfortably available in p-health applications. Due to the progress in single spot optical sensors (more convenient and less intrusive tools), the photoplethysmogram (PPG) is an interesting alternative for pulse rate (PR) measurements instead of HR, driving the interest in the assessment of HRV indexes from the PPG analysis (pulse rate variability – PRV).

In the first part of this thesis, the hypothesis of using PRV features as surrogates for HRV indexes is investigated in three different contexts: healthy subjects at rest, healthy subjects after physical exercise and subjects with CVD. Six different PPG characteristic points are also evaluated to find the most suited for PRV analysis in these contexts. The study is based on the assessment of the correlation, error and distribution of the signals.

The achieved results suggest that the PRV can be often used as an alternative for HRV analysis in healthy subjects, with correlations above 82%, for both time and frequency features. Contrarily, in post-exercise and CVD subjects, time and (most importantly) frequency domain features shall be used with caution (mean correlations ranging from 68% to 88%).

Several BP monitoring algorithms have been proposed to predict impending syncope in real time. However, they still present disadvantages regarding their usage in p-health contexts: while some use cuff-based BP, others use ECG-based approaches, with both implying the use of expensive and uncomfortable hardware. On the other hand, approaches more suitable for personal uses, such as algorithms built only with PPG are less reliable.

The aim of the second part of this work is to follow the group's effort on fulfilling this gap, providing a fully PPG-based algorithm to predict impending NMS, with increased reliability. A threshold-based classification model was used to predict impending syncope after applying the Minkowski distance metric (which was proved as the best metric in this context), with exponent $p=2^{-0.5}$. Numerous parameters were evaluated to feed the algorithm: PR, left ventricular ejection time (LVET), stiffness index (SI), reflection index (RI), as well as several indexes related with the PRV, the second derivative of the PPG, the systolic rise of the PPG pulse wave and the information dynamics of data.

From all the mentioned parameters, several features were computed, resulting in an evaluated set of 94 different features. The most appropriate to predict syncope were ranked using a score system and selected according to their scores. With these, different algorithm setups were assessed and the most relevant results were discussed. The highlighted setup, used in the third part of the thesis, was tested with an F-measure of 86%, 100% of sensibility, 85% of specificity, a false positive rate per hour of $1.9h^{-1}$, as well as 242.3±226.9 sec of prediction time, embedding features derived from SI, PR, LVET and RI.

The third and last step of the project concerns the development of a system to predict impending syncope in real time, using third-party hardware devices (biosignalsplux® with a PPG sensor and a Windows® PC). The back-end of the system consists of the algorithm setup presented above, written in MATLAB®. The front-end of the system was written in Java® and performs three tasks: it wraps the MATLAB® back-end, supports the real-time Bluetooth® communication between the terminals and interacts with the user through an interface. Since it depends on a PC, this is a limited p-health system, but it is already a satisfying proof of concept that provides, besides a valid research tool, a usable solution for hospital settings, the elderly, drivers and operators of heavy machinery.

Resumo

A síncope refere-se à perda temporária de consciência, causada por uma redução da pressão arterial (BP) sistémica, responsável pela queda da perfusão cerebral global. A BP, por sua vez, depende do débito cardíaco e da resistência vascular sistémica, que são regulados pelo sistema nervoso autónomo (ANS). Devido a estas conexões, qualquer fator externo que afete esse equilíbrio pode originar síncope. Quando esse fator é neuronal, o episódio é classificado como síncope neuromediada (NMS)

A síncope é, de facto, uma condição comum e dispendiosa, implicando um custo anual direto de $1.7 a $2 biliões para os serviços de saúde de todo o mundo. Assim sendo, é essencial encontrar formas de evitar custos tão elevados associados à síncope e a condições relacionadas – por exemplo, doenças cardiovasculares (CVD) e quedas –, a favor do investimento em soluções preventivas de *p-health* e *m-health*.

A variabilidade da frequência cardíaca (HRV) é um marcador promissor de regulação autónoma, mas que requer a aquisição de eletrocardiograma (ECG) para calcular a frequência cardíaca (HR) de forma confiável. Este equipamento, contudo, não é confortável para soluções de *p-health*. Devido ao progresso no desenvolvimento de sensores óticos (mais convenientes e menos intrusivos), o fotopletismograma (PPG) torna-se numa alternativa interessante para medições de pulso cardíaco (PR) em vez de HR, levando ao interesse na avaliação de índices de HRV baseados na análise de PPG (variabilidade do pulso cardíaco – PRV).

Na primeira parte desta tese, a hipótese de se utilizarem índices de PRV como substitutos para os índices de HRV é investigada em três contextos diferentes: sujeitos saudáveis em repouso, indivíduos saudáveis após exercício físico e sujeitos com CVD. Seis pontos característicos do PPG também foram avaliados, de forma a encontrar o mais adequado para análise de PRV nesses contextos. A análise é baseada na avaliação da correlação, erro e distribuição dos sinais.

Os resultados obtidos sugerem que a PRV pode ser utilizada como alternativa à análise de HRV em indivíduos saudáveis, tendo produzido correlações acima de 82%, tanto para tempo como para frequência. Contrariamente, nos sujeitos em pós-exercício e com CVD, as características do domínio do tempo e, mais importante, da frequência, devem ser usadas com precaução (correlações médias variando de 68% a 88%).

Vários algoritmos de monitorização da BP foram propostos para prever síncope iminente em tempo real. No entanto, ainda apresentam algumas desvantagens quanto ao seu uso em contextos de *p-health*: enquanto alguns usam BP adquirida com braçadeira, outros usam abordagens baseadas em ECG, sendo que ambos implicam o uso de hardware caro e desconfortável. Por outro lado, abordagens mais adequadas para usos pessoais, tais como algoritmos construídos unicamente com PPG, são menos confiáveis.

O objetivo da segunda parte deste trabalho é acompanhar os esforços do grupo para preencher essa lacuna, fornecendo um algoritmo totalmente baseado em PPG para prever síncope iminente, com maior confiabilidade. Utilizou-se a métrica da distância de Minkowski (que se provou ser a melhor métrica testada), com expoente $p=2^{-0.5}$. Diversos parâmetros foram avaliados para alimentar o algoritmo: PR, tempo de ejeção do ventrículo esquerdo (LVET), índice de rigidez (SI), índice de reflexão (RI), bem como vários índices relacionados com: o PRV, a segunda derivada do PPG, o crescimento sistólico da onda de pulso do PPG e a dinâmica de informação dos dados.

A partir dos parâmetros mencionados, foram calculados vários atributos, resultando num conjunto de 94 índices diferentes avaliados. Os mais apropriados para prever síncope foram classificados usando um sistema de pontuação e selecionados de acordo com as suas pontuações. Com estes, diferentes configurações do algoritmo foram avaliadas e os resultados mais relevantes foram discutidos. A configuração destacada, utilizada na terceira parte do trabalho, foi testada com *F-measure* de 86%, 100% de sensibilidade, 85% de especificidade, uma taxa de falsos positivos por hora de 1.9h-1, bem como 242.3±226.9 segundos de tempo de previsão, incorporando índices derivados de SI, PR, LVET e RI.

A terceira e última etapa do projeto diz respeito ao desenvolvimento de um sistema de previsão de síncope em tempo real, utilizando dispositivos comerciais (biosignalsplux® com um sensor PPG e um PC com Windows®). O *back-end* do sistema consiste na configuração do algoritmo apresentado acima, escrito em MATLAB®. O *front-end* do sistema é escrito em Java® e executa três tarefas: é *wrapper* do *back-end* MATLAB®, suporta a comunicação Bluetooth® em tempo real entre os terminais e interage com o utilizador através de uma interface. Uma vez que depende de um PC, trata-se de um sistema de *p-health* algo limitado, mas já é uma prova de conceito satisfatória que fornece, além de uma ferramenta de pesquisa válida, uma solução útil para meios hospitalares, idosos, motoristas e operadores de maquinaria pesada.

Agradecimentos

Na realização deste projeto, tive a enorme sorte de ser dirigido por uma equipa de orientadores extremamente acessível e competente, que sempre me propôs objetivos interessantes, reais e planeados, mantendo-se ativamente pronta para me ajudar a realizá-los. Assim, agradeço ao Doutor Ricardo Couceiro e ao Prof. Doutor Paulo de Carvalho por toda a ajuda, tempo despendido, comunicação e, acima de tudo, pelos ótimos conselhos e experiência de aprendizagem que me proporcionaram. Agradeço, ainda, à Philips Research pela base de dados que utilizei no Capítulo 5 desta tese e, em especial, ao Doutor Jens Muehlsteff, pelo apoio na realização do artigo científico associado ao Capítulo 4 deste trabalho. Quero, também, agradecer aos meus colegas de Laboratório pela sua boa-disposição e animação, bem como ao Prof. Doutor João Carvalho e Prof. Doutor Miguel Morgado, Coordenadores de Curso sempre presentes.

Muito obrigado aos meus amigos de “cá” e de “lá”, porque me fazem sentir em casa. Às vezes, bastam 10 minutos de conversa, basta um café e um sorriso, para todo o dia ser melhor, para “recarregar baterias” e, até, resolver uma tarefa “empancada”. As minhas terras, os meus sítios, não ficam onde estão; ficam onde estas pessoas vão e onde posso encontrá-las.

A ti, Catarina, porque um fardo é menor quando é dividido, e a felicidade é maior quando é partilhada. E dividir e partilhar contigo é algo de que não me poderei esquecer, porque me faz muito bem. Nestes anos, ninguém viveu as minhas coisas como tu viveste e como te esforçaste em fazê-lo. Por isso, estou imensuravelmente grato.

À minha família, pela presença, pelo carinho e pela preocupação. Porque me sinto abraçado com a sinceridade de quem se preocupa de verdade e de quem me quer o maior bem.

Mais do que tudo, aos meus pais e à minha irmã, porque não existe um momento em que não pensem em mim. Porque conto sempre com eles. Porque, para mim, estão sempre disponíveis, mesmo quando não estão, e durante o tempo que for preciso. A eles, tenho de agradecer todo o esforço, trabalho, dedicação e persistência. Tenho de agradecer o tanto que se mantêm na minha vida, o tanto que se interessam por mim, mesmo que eu viva longe e não os chame. Agradeço isto com todo o amor e, mesmo assim, não chega.

“Technology is a word that describes something that doesn’t work yet.”

Douglas Adams

Contents

Abbreviations

AC	Alternating current
AI	Aging index
ANS	Autonomic nervous system
API	Application programming interface
AR	Autoregressive
AUC	Area under the curve
AV	Atrioventricular
BMI	Body mass index
BP	Blood pressure
BV	Blood volume
BVP	Blood volume pulse
CNS	Central nervous system
CO	Cardiac output
CS	Cardiac syncope
CT	Crest time
CVD	Cardiovascular diseases
CVP	Central venous pressure
DBP	Diastolic blood pressure
DC	Direct current
ECG	Electrocardiogram
FFT	Fast Fourier transform
FPRh	False positive rate per hour
HF	High frequency
HR	Heart rate
HRV	Heart rate variability
HUTT	Head-up tilt table
ID	Information dynamics
KST	Kolmogorov-Smirnov test
LED	Light emitting diode
LF	Low frequency

LV	Left ventricular
LVET	Left ventricular ejection time
MAP	Mean arterial pressure
m-health	Mobile health
NMS	Neurally mediated syncope
NN	Normal-to-normal
NRMSE	Normalized root mean squared error
OH	Orthostatic hypotension
p-health	Personal health
PAT	Pulse arrival time
PC	Personal computer
PEP	Pre-ejection period
PNS	Parasympathetic nervous system
PP	Pulse pressure
PPG	Photoplethysmogram
PPW	Pulse pressure wave
PR	Pulse rate
PRV	Pulse rate variability
PSD	Power spectral density
PTime	Prediction time
PTT	Pulse transit time
PVC	Premature ventricular contraction
PVR	Peripheral vascular resistance
PWV	Pulse wave velocity
RI	Reflection index
ROC	Receiver operating characteristic
SA	Sinoatrial
SBP	Systolic blood pressure
SDK	Software development kit
SDPPG	Second derivative of the photoplethysmogram
SE	Sensibility
SI	Stiffness index
SNS	Sympathetic nervous system

SP	Specificity
SpO_2	Peripheral oxygen saturation
SRC	Spearman's rank correlation
STD	Standard deviation
STI	Systolic time interval
SV	Stroke volume
SVM	Support vector machines
SVR	Systemic vascular resistance
VLF	Very low frequency
VR	Velocity of rise
WRST	Wilcoxon's rank sum test

List of Figures

List of Tables

Chapter 1

Introduction

This chapter introduces the context of this thesis, justifying it with its global interest and motivation (section 1.1), as well as presenting its main goals (section 1.2). The performed tasks to achieve these goals are listed in section 1.3 and the organization of this document is briefed in section 1.4. Finally, the contributions and relevance of this thesis are addressed in section 1.5.

1.1. Contextualization and Motivation

Syncope refers to the temporary loss of consciousness caused by some trigger (*e.g.* orthostatic stress, emotions and physical exercise), producing a consequent decrease in the arterial systemic blood pressure (BP) and global cerebral perfusion/blood flow, which will instigate the syncope [1, 2, 3].

Syncope is responsible for 0.9 to 1.2% of the emergency department visits per year in Europe [4] and for about 1-3% in the USA (where it accounts for 1-6% of all the hospital admissions per year [5], with an associated global annual cost of $1.7-$2 billion – $5000-$14000/inpatient [6, 7]). Despite the presented cost being similar to that of HIV, asthma and chronic obstructive pulmonary disease [7], up to 80% of the acknowledged causes of a syncope event determined during a full hospital admission are identified in the emergency department, and most of them are benign and self-limited [5], with an overall mortality rate of only 0.28% (0.36-1.26% in the elderly). Furthermore, this cost is reported to increase with age [6]. The high costs may be justified with the high rates of hospital admissions seen in more than 60% of the cases, which, in most of the times, do not result in a conclusive diagnosis [7].

Since the incidence of this condition is mainly related to individuals over 45 years old [5] and given that the populations in Europe and in the USA are growing older, it is expected that the presented costs will tend to increase [7], in the absence of countermeasures.

Given the revealed discrepancy (with possibilities of increasing) between the large costs of syncope for health systems and its diagnostic and mortality rates, the need to find ways to avoid unnecessary hospitalizations is clear, in order to reduce the presented phenomenon and let the health institutions take care of exclusively unavoidable acute cases, improving their efficiency and quality of service.

Most of the times, the occurrence of a syncope event makes the subject fall uncontrolledly, causing potentially dangerous side effects, such as fractures and bruises. In fact, falls account for 3% of the total expenditure of the National Health Service from the UK, with the fall of elder people accounting for 8% of all the emergency ambulance responses in London and for 7.5% in the urban areas of the USA [8]. More specifically, 39% of all the accident and emergency department attendances in patients over 50 years old are due to falls or syncope. The UK government spent nearly £1 billion per year because of unintentional falls, only in patients older than 60 years (50% in hospitalizations and 41% in institutionalizations) [9].

As already mentioned, a marked decrease in systemic BP (equal or lower than 60mmHg [10]) is associated with syncope. Systemic BP depends on the cardiac output (CO) and total peripheral vascular resistance (PVR) – representing the systemic vascular resistance (SVR) –, which are influenced by the autonomic nervous system (ANS) [2]. This suggests that the prediction of syncope events may be enabled by an early detection of changes in indicators such as BP, CO and others. These may include the heart rate (HR) – evaluating cardiovascular chronotropic changes –, the left ventricular ejection time (LVET) – assessing inotropic changes –, the stiffness index (SI) and the reflection index (RI), surrogating the vascular tone and BP itself [11]. Heart rate variability (HRV) parameters quantify the change of time periods between consecutive cardiac cycles, and they have been proven to be valuable tools to characterize and understand the regulation of the cardiovascular system by the ANS [12]. Functions related to information dynamics (ID) have also been used in physiological time series to characterize short-term complexities of/between systems of the body. This includes beat-to-beat evaluations on the cardiovascular system, variability signals and the influence of the neural system on the cardiac function [13].

A major strategy to diminish the presented costs on syncope, CVD and falls' handling is to avoid the happening of such events, by preventing its occurrence. This implies the permanently monitoring of the potential patients, in a concept commonly

named as personal health (p-health), which promotes a fundamental transformation on healthcare systems, from conventional hospital-centered to individual-centered schemes [14]. The monitoring may be made using telemedicine and mobile health (m-health) [15], benefiting from technologies such as smartphones and smartwatches.

The listed parameters are potential evaluators for syncope management in m-health settings. However, the hardware of support must be carefully chosen, because, in addition to be reliable and accurate, it must be inexpensive, non-invasive, easy-to-use, comfortable and a well-known diagnostic device [16].

The photoplethysmogram (PPG), for allowing the calculation of the referred indicators and complying with the stated operational characteristics, is a tempting technique to use in such personal scenarios. It is acquired with standard peripheral oxygen saturation (SpO_2) sensors [11], using low-cost hardware: a light emitting diode (LED) placed at peripheral sites (*e.g.* the fingertip, earlobe or wrist) to measure, with a photodiode, transmitted or reflected light [14]. The major drawback in the use of PPG (especially, in fingertip PPG) is the easy introduction of motion artifacts during acquisitions [17], which decreases its reliability and accuracy.

1.2. Objectives

The aim of this thesis is to extend the work presented in [11, 18, 19, 20, 21], proposing a PPG-based algorithm to predict syncope episodes in an accurate, consistent, reliable and valuable manner, in a real-time setting, standing on BP surrogating features. This main goal is divided in three large steps, as follows:

1. Comparison between HRV parameters derived from electrocardiogram (ECG) and from PPG, evaluating the usefulness of the PPG-related ones, in different life scenarios;
2. Construction of a robust and low complexity algorithm to predict impending neurally mediated syncope (NMS) in real time, solely based on cardiovascular features derived from PPG, in compliance with m-health conditions;
3. Development of a concept demo application to show the usefulness of such algorithm, demonstrating its function on PPG signals acquired in real time with a third-party wearable hardware.

1.3. Planning

This section outlines the schedule of the performed work and the respective milestones. It must be noticed that, despite the official starting date of this thesis (February 2016), the work was started voluntarily in October 2015, in order to elaborate a more through thesis. The referred schedule is detailed in Table 1.

Table 1 – Fulfilled schedule of the defined milestones.

Task Description	2015			2016												2017
	Oct	Nov	Dec	Jan	Feb	Mar	Apr	May	Jun	Jul	Aug	Sep	Oct	Nov	Dec	Jan
Planning of milestones																
Analysis of PPG systems to use in m-health contexts																
Familiarization with cardiovascular evaluation through PPG																
Comparative study between PPG and ECG in HRV analysis																
Writing of the first scientific paper																
Familiarization with previous works on syncope prediction																
Investigation of new features to embed in a syncope prediction algorithm																
Study of algorithm variations to predict impending syncope																
Comparison of the achieved results with previous ones																
Writing of the second scientific paper																
Evaluation of technologies to construct a PPG p-health system																
Familiarization with the chosen technologies																
Planning of a p-health PPG-based software to predict impending syncope																
Development of the PPG-based software to predict syncope																
Testing of the developed system																
Writing of the final report																

1.4. Structure of the Dissertation

The document is structured as follows: Chapter 2 dissects the theoretical physiological concepts that are of interest to the goal of the thesis. Chapter 3 approaches the utility of the PPG to assess BP regulation indexes, pointing down its advantages and drawbacks, outlining its use to calculate features and listing the state-of-the-art p-health algorithms and m-health applications of the technology. Chapter 4 matches the first step of the main goal of the thesis, evaluating the computation of HRV features using PPG, in comparison with the ECG as gold standard. Chapter 5 details on the actual construction of the impending syncope prediction algorithm, showing the produced advances and achieved results (corresponding to the second step of the main objective). Chapter 6 reports the development of the concept demo application (last step of the project), outlining its requirement analysis, design, implementation and test. Finally, Chapter 7 presents the global conclusions resulting from the project and launches new ideas and suggestions for future work.

1.5. Contributions

Besides this report and related with this thesis, two scientific papers were produced.

The first, in Appendix A, summarizes the work presented in Chapter 4, corresponding to the evaluation of the PPG signal as source for HRV indexes, traditionally derived from ECG. It was orally presented in the 2016 38th Annual International Conference of the Engineering in Medicine and Biology Society (EMBC'16) of the Institute for Electrical and Electronics Engineers (IEEE), in Orlando, Florida, the USA, on August 16-20, 2016 [22].

The second, in Appendix B, presents the work outlined in Chapter 5, reporting the development of the PPG-based algorithm to predict syncope in real time. It was submitted for presentation in the 2017 joint event of the European Medical and Biological Engineering Conference (EMBEC'17) and the Nordic-Baltic Conference on Biomedical Engineering and Medical Physics (NBC'17), in Tampere, Finland, on June 11-15, 2017.

The work in Chapter 5 was also assigned for presentation in the IEEE 5th Portuguese Meeting on Bioengineering (5 ENBENG), organized by the Portuguese Chapter of IEEE Engineering in Medicine & Biology Society (EMBS), in Coimbra, on February 16-18, 2017.

Chapter 2

Underlying Physiology

In this chapter, the fundamental aspects concerning the physiological background of the thesis are presented. It starts with the description of the anatomy and physiology of the cardiovascular and autonomic systems. Their interactions and consequent regulation of BP are addressed. Finally, the particular case of syncope is outlined, based on the previously considered sections.

2.1. Cardiovascular System

2.1.1. Overview and Blood Circulation

The cardiovascular system is composed by three components: the heart, blood vessels and the lymphatic system (which does not contain blood, but serves as an exchange system, together with blood vessels) [23]. In optimal conditions, the heart and blood vessels form a system that allows a fast and effective transportation of oxygen, nutrients and waste products around the tissues of the body – in this case, the human body. The cardiovascular system also takes part in the distribution and secretion of hormones and in the regulation of the body temperature (delivering heat on the organs) [24].

The heart has two intermittent adjacent pumps that correspond to its right and left sides, which are constituted, each one, by an atrium and a ventricle. The atria function as reservoirs of blood that fill the underneath ventricles, which performs the actual action of pumping [23, 24].

As illustrated in Figure 1, the right ventricle injects deoxygenated blood – filled with carbon dioxide – to the lungs, allowing the exchange of gas and the return of oxygenated blood – filled with oxygen – to the heart, through the left atrium, in a process that defines the pulmonary circulation. Simultaneously, the left ventricle pumps oxygenated blood to the aorta, which distributes it through all the body tissues, via the

arterial system. In the different tissues, oxygen is diffused from the blood to cells, and carbon dioxide is diffused in reverse, deoxygenating the blood. The newly deoxygenated blood is returned to the right atrium through the superior/anterior and inferior/posterior venae cavae, completing the systemic circulation. Then, the blood flows to the right ventricle [23, 24].

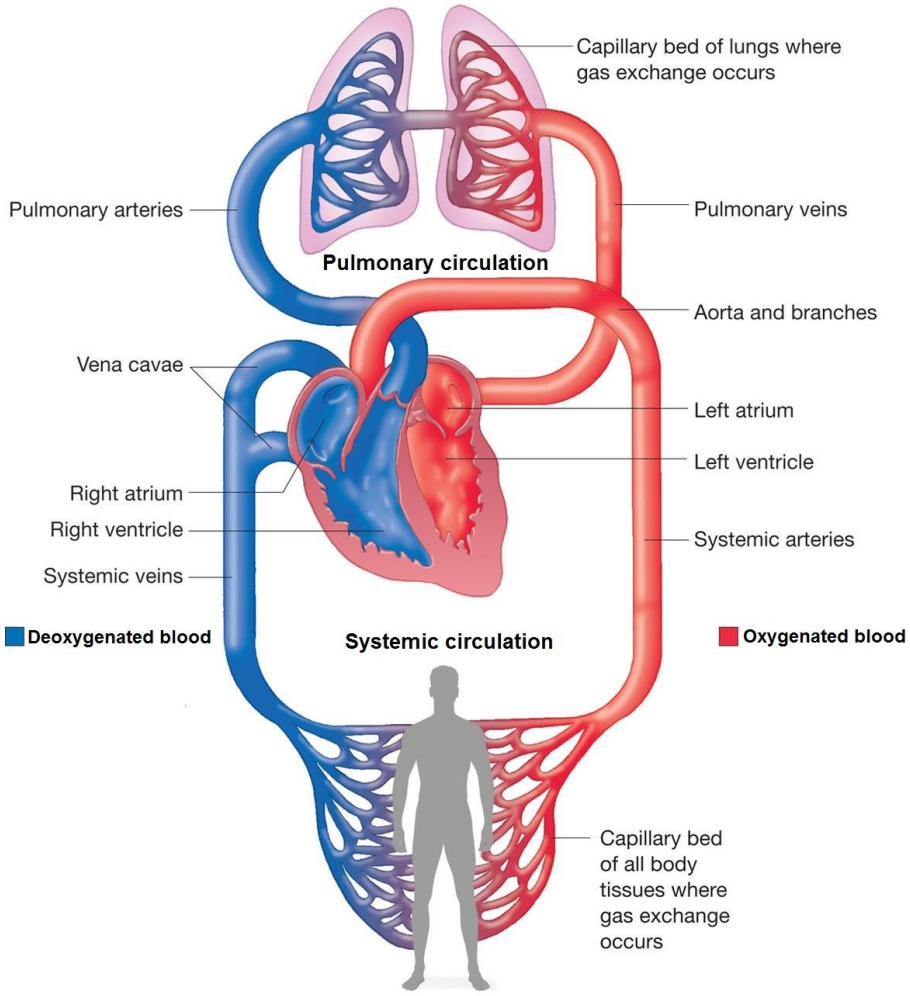

Figure 1 – Schematic representation of the cardiovascular system and blood circulation. Adapted from [25].

It is noticed that the arrangement of the vascular network allows the travelling of blood from the heart to tissues through arteries, and the returning through veins, no matter the circulation type. Larger arteries divide into smaller ones, highly innervated with ANS-related nerves (autonomic nerves) – influencing their constriction or dilation. These smaller arteries (arterioles), with variable resistance in their walls, are responsible for the regulation of BP. The arterioles give rise to narrower capillaries, which delay the flow speed and ease the exchanges between the blood and the surrounding cellular environment. Afterwards, this capillaries' network converges in progressively wider

venules and, then, veins, which concentrate most of the blood flow, being the vessels with larger capacitance [18].

2.1.2. The Heart

The heart consists of the four already mentioned muscular chambers: right atrium, right ventricle, left atrium and left ventricle, as stated in Figure 2. The right atrium connects with the right ventricle through the tricuspid/pulmonary valve, whereas the left atrium communicates with the left ventricle through the bicuspid/mitral valve. These two valves are known as the atrioventricular (AV) valves and control the one-way blood flow from the atria to the ventricles. The blood flow from the heart to the body is allowed by the semilunar valves, which are located in the exit of each ventricle. The pulmonary valve controls the flow from the right ventricle to the pulmonary circulation; the aortic valve rules the exit of blood to the systemic circulation. It is the synchronized action of these valves, responding to pressure changes inside and outside the ventricles that prevents the regurgitation of blood to its previous location [23, 24].

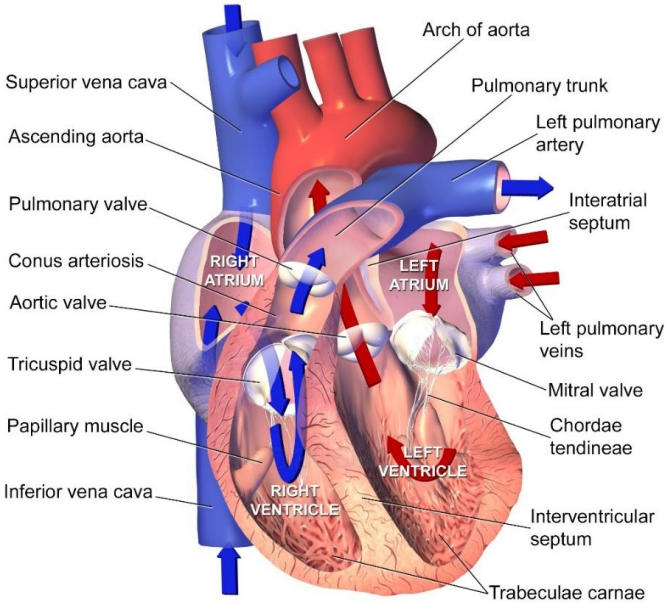

Figure 2 – The internal anatomic structure of the heart [26].

The perceptible periodicity of the blood pumping by the heart is maintained by an important system of electrical conducting fibers that generate and propagate electrical impulses through the heart [18], and that can be influenced by the ANS [23] (see next sections). This system includes the sinoatrial (SA) and the AV nodes, as well as the system of His-Purkinje [18] – Figure 3.

In fact, the mammalian heartbeat is initiated by specialized pacemaker fibers in the SA node with membranes that have an unstable resting potential. As a result, these cells generate an action potential almost every second, provoking a wave of depolarization that spreads across the two atria, initiating the atrial systole – see section 2.1.3. Then, the electrical impulse reaches the AV node, suffering a delay of about 0.1 sec (in healthy subjects at rest). This grants sufficient time for the atria to contract before the ventricles are activated (to pump the blood out of the heart). After this delay, the impulse is relayed to the AV bundle (bundle of His) – fast-conducting muscle fibers –, running down the septum through the bundle branches and achieving an extensive network of wide cells – the Purkinje fibers – that distributes the impulse, making the both ventricles contract as near simultaneously as possible [18, 24].

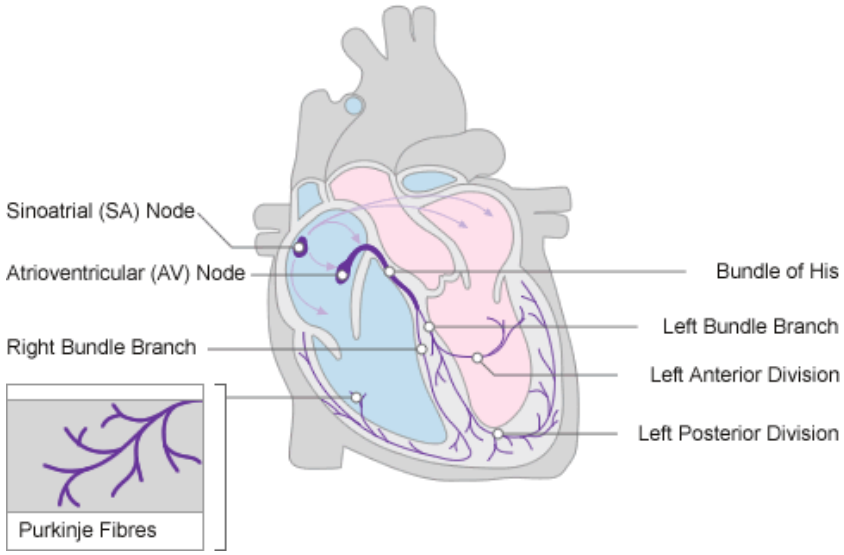

Figure 3 – The cardiac conduction system [27].

2.1.3. Cardiac Cycle

The sequential contraction of the atria and ventricles results in a repeated cycle (the cardiac cycle) of characteristic pressure and volume changes, whose comprehension enables the detection of diseases, namely valvular defects. The cardiac cycle consists of two main stages: systole defines the ventricular contraction and consequent blood ejection, as well as the associated events; diastole is longer (approximately 2/3 of the cycle time, in healthy subjects at rest) and refers to the rest of the cycle (with ventricular relaxation and filling). Beyond these two main stages, and based on the shape of the ECG (whose signal illustrates the electrical activity of the heart), seven different phases are distinguished in the cardiac cycle (Figure 4) [23, 24]:

1) Atrial systole: The P wave of the ECG arises, representing the depolarization of the atria, which leads to their contraction (increasing atrial pressures) and consequent blood flow to the ventricles (the AV valves are opened and the semilunar valves are closed);
2) Isovolumetric contraction: This represents the beginning of systole, with the depolarization of the ventricles (marked with the QRS complex of the ECG). As all valves are closed at this point, the intraventricular pressure increases rapidly and the ventricular shapes change, but their volume remains constant;
3) Rapid ejection: Due to the increased intraventricular pressures, the semilunar valves open, leading to the ejection of blood into the aorta (systemic circulation) and pulmonary arteries (pulmonary circulation), provoking the decrease of the ventricular volumes. The atria are already being filled with blood and their volumes increase;
4) Reduced ejection: The occurrence of the T wave in the ECG indicates the repolarization of the ventricles, whose pressures and ejection rates fall. This is the last phase of systole;
5) Isovolumetric relaxation: The ventricular relaxation continues and their inner pressures remain decreasing, leading to the closure of the semilunar valves, marking the beginning of diastole. This closure is associated with the occurrence of a notch in the aortic and pulmonary arterial pressure signals. As in phase 2, this is an isovolumetric process;
6) Rapid filling: The low intraventricular pressures induce the opening of the AV valves. This, together with the maximal atrial volumes that are felt, causes a rapid passive filling of the ventricles with blood;
7) Reduced filling: This phase is not clearly demarked from the last. However, this refers to the period during diastole when passive filling is nearing completion, which implies increased intraventricular pressures and the reduction in the velocity of the blood flow. After this, the process returns cyclically to phase 1.

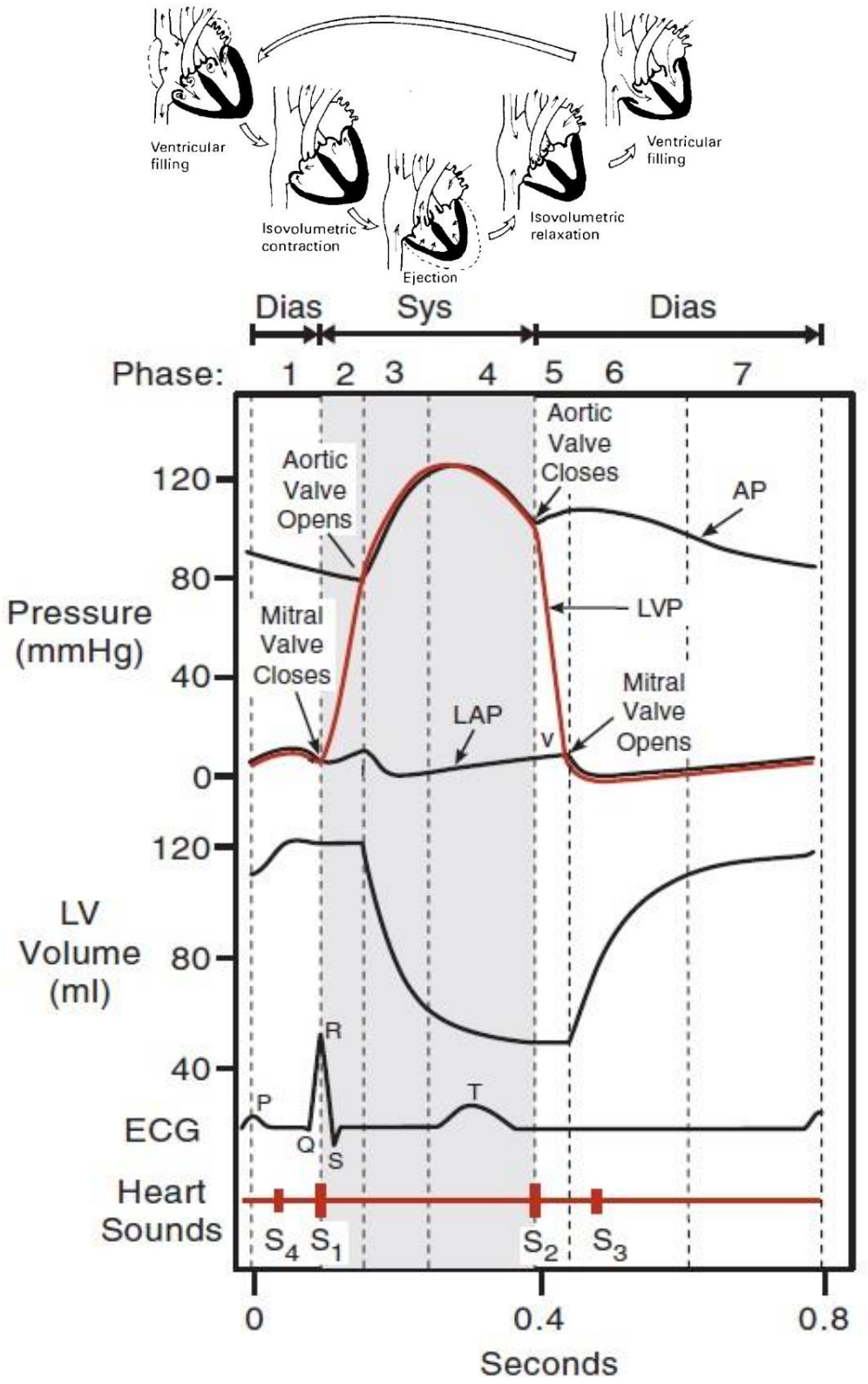

Figure 4 – The seven cardiac cycle phases and the variation of pressures and volumes in the heart, correlated in time with an ECG signal and the correspondent heart sounds. These are aquired with a phonocardiogram and help in the mapping of the cardiac cycle. As seen, the sound S_1 is associated with the isovolumetric contraction of the ventricles, whereas the S_2 is associated with the isovolumetric relaxation. Adapted from [23, 24].

Legend: *AP: aortic pressure; LVP: lenft ventricular pressure; LAP: left atrial pressure; LV: left ventricle.*

2.2. Autonomic Nervous System

2.2.1. Overview

The ANS defines a part of the nervous system that innervates several tissues/organs of the body and acts automatically, without voluntary control (the reason for being called “autonomic”) [28]. The supplied tissues/organs include the cardiovascular system (especially heart, muscular arteries and arterioles), the gastrointestinal tract (stomach and intestine), the urinary tract (kidneys, ureter, bladder and urethra), the genital tract, part of the airway (trachea and bronchi), the eyes (pupils) and sweat, salivary, and digestive glands [28, 29]. Thus, the ANS influences processes, such as: BP, HR, body temperature, digestion, the breathing rate, metabolism, defecation, urination, the balance of water and electrolytes, the sexual response and the production of body fluids [29].

The ANS consists, anatomically, of a central and a peripheral part. The central part is made of large aggregates of neurons in the hypothalamus and columns of neurons in the brainstem and spinal cord – organs belonging to the central nervous system (CNS). The peripheral part consists of nerves that emerge from the brainstem and the spinal cord and reach autonomic ganglia throughout the body, from which other nerves connect with the previously named target organs [28].

ANS receives internal (from the body) and external (from the environment) stimuli, reacting to the information by triggering body processes in the target tissues. This implies the existence of two different pathways:

- Afferent (or sensory) neurons provide the sensory side of the system and support both sensation and reflexes, providing the CNS with inputs from peripheral and brain sensors;
- Efferent (or motor) neurons are projected into the target organs, manipulating their activity based on responses from the CNS [23, 28].

The produced reactions can be of stimulation or inhibition of processes, triggered by one of two divisions of the ANS (Figure 5): the sympathetic nervous system (SNS), usually for stimulation; or the parasympathetic (vagal) nervous system (PNS), typically for inhibition [28, 29].

Generally, the sympathetic division prepares the body to face stressful situations, secreting norepinephrine through adrenergic nerve fibers, as neurotransmitter. This division increases HR, BP, the force of heart contractions and muscular strength. It also dilates the airways to ease the breathing, leads the body to release stored energy and slows body processes that are less important in emergencies, such as digestion and urination. It causes palms to sweat, pupils to dilate and hair to stand on end.

The parasympathetic division actuates during ordinary situations, using acetylcholine secreted by cholinergic fibers. It slows HR, decreases BP and stimulates the digestive tract to process food and eliminate wastes. Energy from the processed food is used to restore and build body tissues [29].

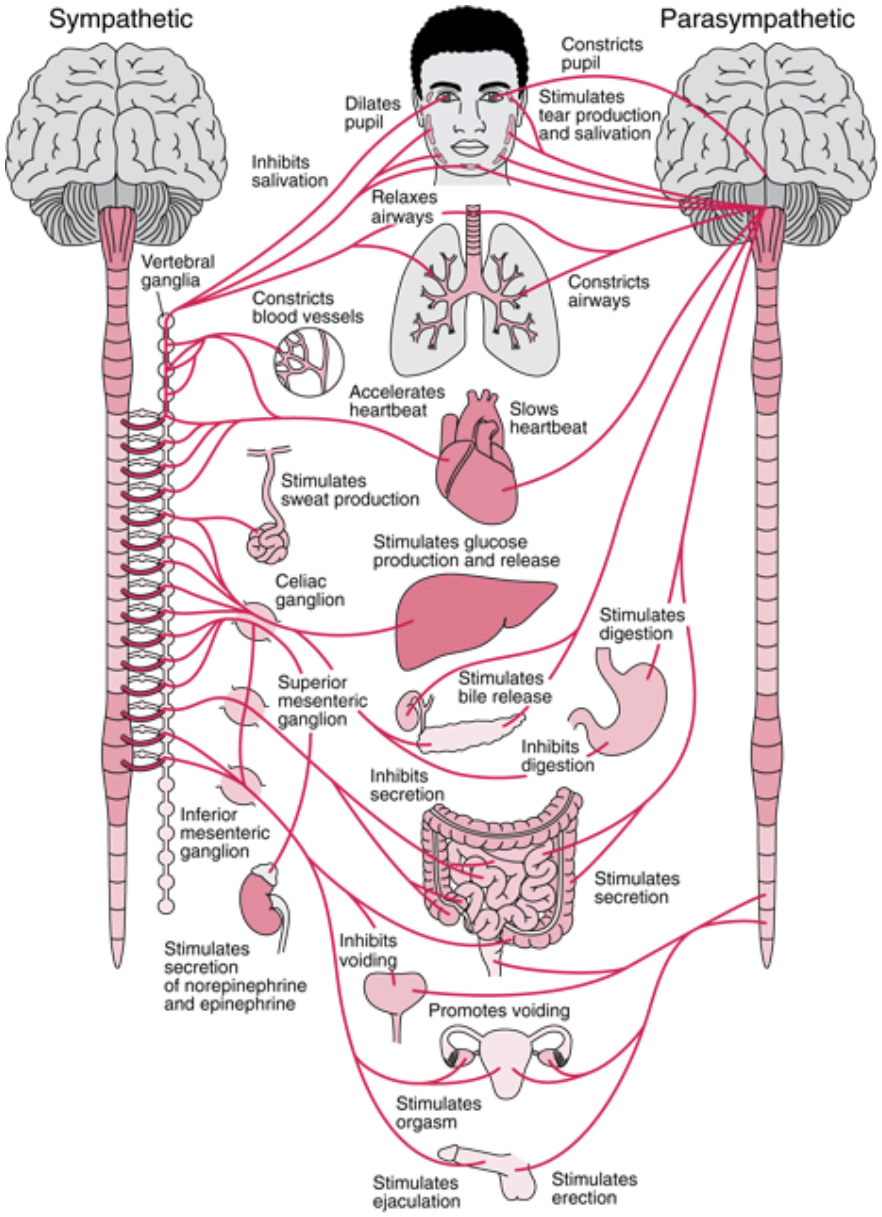

Figure 5 – SNS and PNS of the ANS, in its central and peripheral parts, emphasizing the origin of the nerve fibers in the CNS [29].

2.2.2. Autonomic Cardiovascular Innervation

As aforementioned, the ANS plays an important role regulating the cardiac function.

The SA node, AV node and atrial muscle are innervated by vagal efferent nerves (parasympathetic innervation through the vagus nerve), whereas the vagal innervation of the ventricular myocardium is sporadic. Concerning the sympathetic efferent nerves, they are presented in the SA node and throughout the atria and ventricles (Figure 6).

The effects of the efferent pathways in the heart are clear. Parasympathetic activation leads to the decrease of HR (negative chronotropy), heart contractility (negative inotropy) and conduction velocity of blood within the heart (negative dromotropy). Sympathetic activation causes opposite effects, since it increases HR, contractility and conduction velocity [23].

All these changes have chain effects in the cardiovascular system. In fact, the HR has a strong outcome in the myocardial force, which increases/decreases with HR, since the evolution in HR within a few beats is able to improve/diminish the isometric contractile force plateau of the heart. As for the stroke volume (SV) – the amount of blood ejected per beat by the left ventricle into the aorta [30] –, it varies in the same way of the inotropy, based on the Frank-Starling law. Preload – initial stretching of the cardiac myocytes prior to contraction [31] – and afterload – pressure that the heart must eject blood against [32] – fluctuate in accordance [33].

The heart also contains vagal and sympathetic afferent nerve fibers that relay information from stretch and pain receptors. The stretch receptors (baroreceptors) are involved in the feedback regulation of blood volume (BV) and arterial BP. The pain receptors produce chest pain when activated during myocardial ischemia [23] – despite being autonomous, the ANS induces pain when issued, allowing the perception of one's self [28, 34].

Regarding the autonomic action over blood vessels, these are more constricted or dilated depending on its activation, which is prominent in arterioles (much innervated by ANS nerves) [18].

As depicted from previous considerations, the sympathetic activation leads to the rise of the vessels' constriction. Nonetheless, the parasympathetic system has little

(almost inexistent) direct results on blood vessels, provoking inhibitory effects (vasodilatation) indirectly, through their influence on sympathetic nerves [23].

The already mentioned baroreceptors (stretch receptors) are mostly located at the carotid sinus and the aortic arch [34], being tension-sensitive afferent nerve fiber endings that act as monitoring sensors of BP, transmitting the information to the CNS (Figure 6). This information corresponds, precisely, to changes in BP, which motivate a change in the frequency of the afferent nerve activity.

The arterial baroreflex (baroreceptor reflex) is the negative feedback mechanism that starts with the sensing of the baroreceptors. It is a critical physiological process of the greatest importance, since it regulates the short-term arterial BP, eliciting reciprocal responses of the ANS. When afferent baroreflex nerve traffic intensifies (because of BP increments), the efferent sympathetic traffic decreases, and the efferent parasympathetic traffic increases, inducing the aforementioned cardiovascular changes that lead to a new drop in BP. When BP lowers, an inverse response occurs. This allows, in healthy subjects, a beat-to-beat regulation of the BP, with a fast reaction to environment deviations [34, 35, 36].

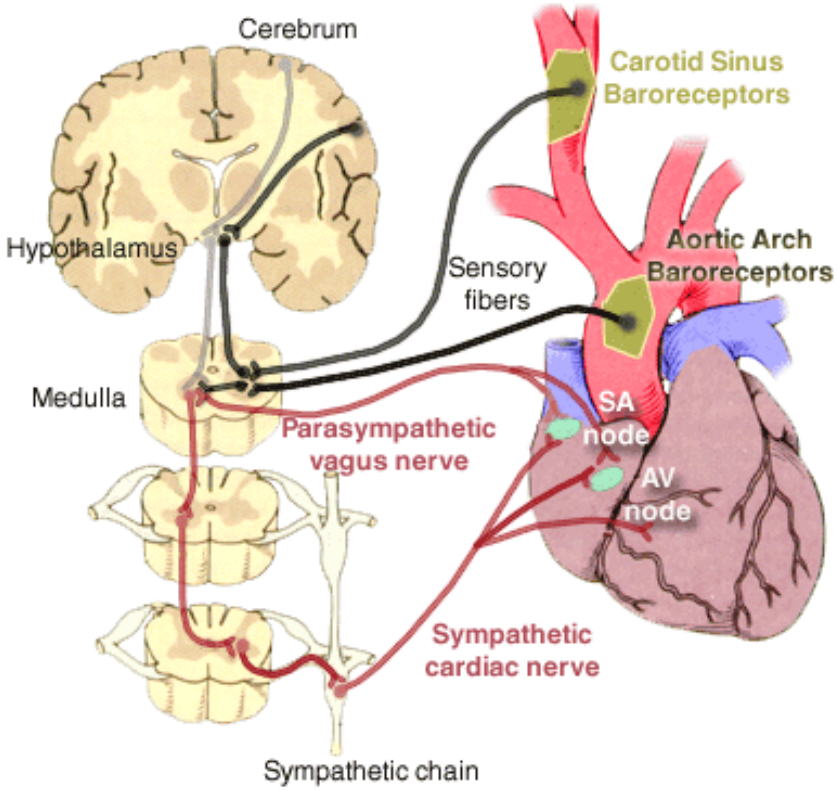

Figure 6 – Illustration of the different ANS pathways (afferent/efferent and sympathetic/parasympathetic) concerning the cardiovascular system.

2.3. Arterial Blood Pressure

The ejection of blood into the aorta by the left ventricle produces a pulse pressure wave (PPW) that has a characteristic shape, depending on the site that is monitored (Figure 7). This illustrates the variation of the pressure that blood exerts against the walls of the arterial system, as the blood travels through the network of arteries, and defines the arterial BP (in the literature, when BP is mentioned, it implies arterial BP) [23, 24, 37].

The exerted tension creates a gradient of pressure along the vessels that drives the blood, in a pulsatile (not steady) variation, since the heart ejects blood intermittently. Between successive ejection phases, in healthy adults, the systemic arterial BP (BP in the systemic circulation) decays from, approximately, 120 mmHg to 80 mmHg, while pulmonary BP (BP in the pulmonary system) decays from 25 mmHg to l0 mmHg. The conventional way of writing this is 120/80 mmHg and 25/10 mmHg [24], defining the systolic blood pressure (SBP) and diastolic blood pressure (DBP) in both circulations, which are traditionally measured with an arm BP cuff (sphygmomanometer). SBP describes the highest BP against the aorta – immediately after the left ventricular (LV) ejection – and DBP refers to the lowest aortic pressure – immediately before the ventricular ejection. The aortic pulse pressure (PP) is the difference between SBP and DBP [23, 24].

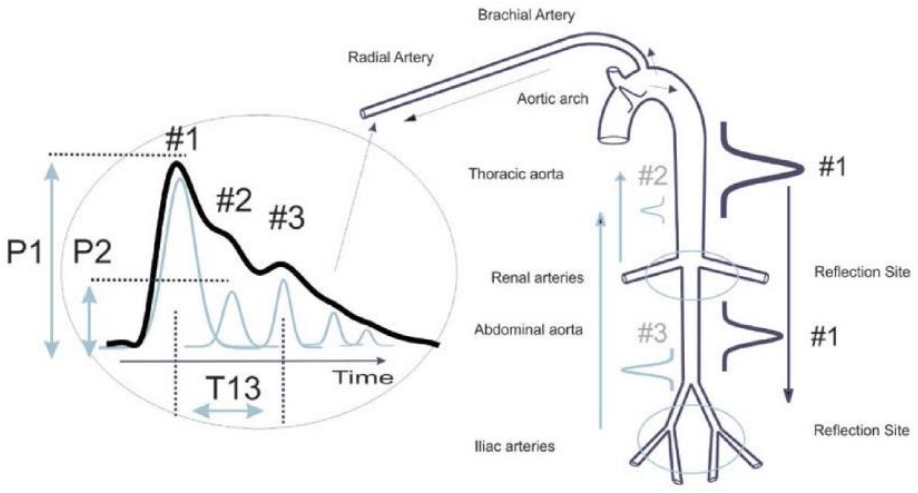

Figure 7 – Morphology of the PPW at the radial artery, with the anatomical schemed location [37]. It sums the main wave #1 from the aortic arch with the reflection waves #2 and #3. #2 is called the second/late systolic wave, as the peak in #1 of the PPW refers to the SBP. The onset of the PPW defines the DBP.

As blood flows down the aortic arch, the change in the velocity, morphology and amplitude of the PPW is related with several factors that include decreased compliance

(distensibility [24]) of distal arteries and the existence of reflective waves, especially from arterial branching points to peripheral sites that act as reflection sites. These reflective waves counter-propagate to the direction of the single arterial pressure wave, which is seen in the shape of PPW, since it sums all the pressure waves (Figure 7) [18, 23, 37].

The mean arterial pressure (MAP) decreases as the PPW travels down distributing arteries, but with a small reduction, due to the low resistance of the arteries. MAP depends on the CO, SVR and central venous pressure (CVP), with the equation:

$$MAP = CO.SVR + CVP \quad (1)$$

SVR defines the resistance that the systemic vasculature applies against the blood flow. CO refers to the volume of blood leaving the heart per minute, based on the HR and SV:

$$CO = HR.SV \quad (2)$$

MAP can also be defined in terms of SBP and DBP:

$$MAP = DBP + {}^{(SBP - DBP)}/_{3} \quad (3)$$

However, this relation is only valid for healthy resting HR, since when it fastens, diastole shortens more than systole, leading the PPW to change its shape and the MAP to approximate to the arithmetic average of SBP and DBP [18, 23].

CO, SVR and CVP change because of diverse triggers on the basis of their calculation. Nevertheless, they are dependent between each other. For example, the increase of the SVR also increases the heart's afterload, decreasing CO and changing CVP. Moreover, control mechanisms operated by the ANS affect these dynamics. The respiratory system is also an influencer, since the breathing cycle induces variations in the intra-thoracic pressure, which have impact on the deoxygenated blood flow, venous return and CVP. In fact, all the interdependencies are created in order to stabilize the BP in healthy levels that are required to preserve an equilibrium in the blood flow throughout the body, allowing the demanded nutrient and gas exchanges [18, 23, 24]. Issues arise when this balance is not maintained, and it is in such scenarios that syncope events occur.

Figure 8 presents a scheme from [18] that characterizes the physiological interactions regarding BP that have been approached throughout this document.

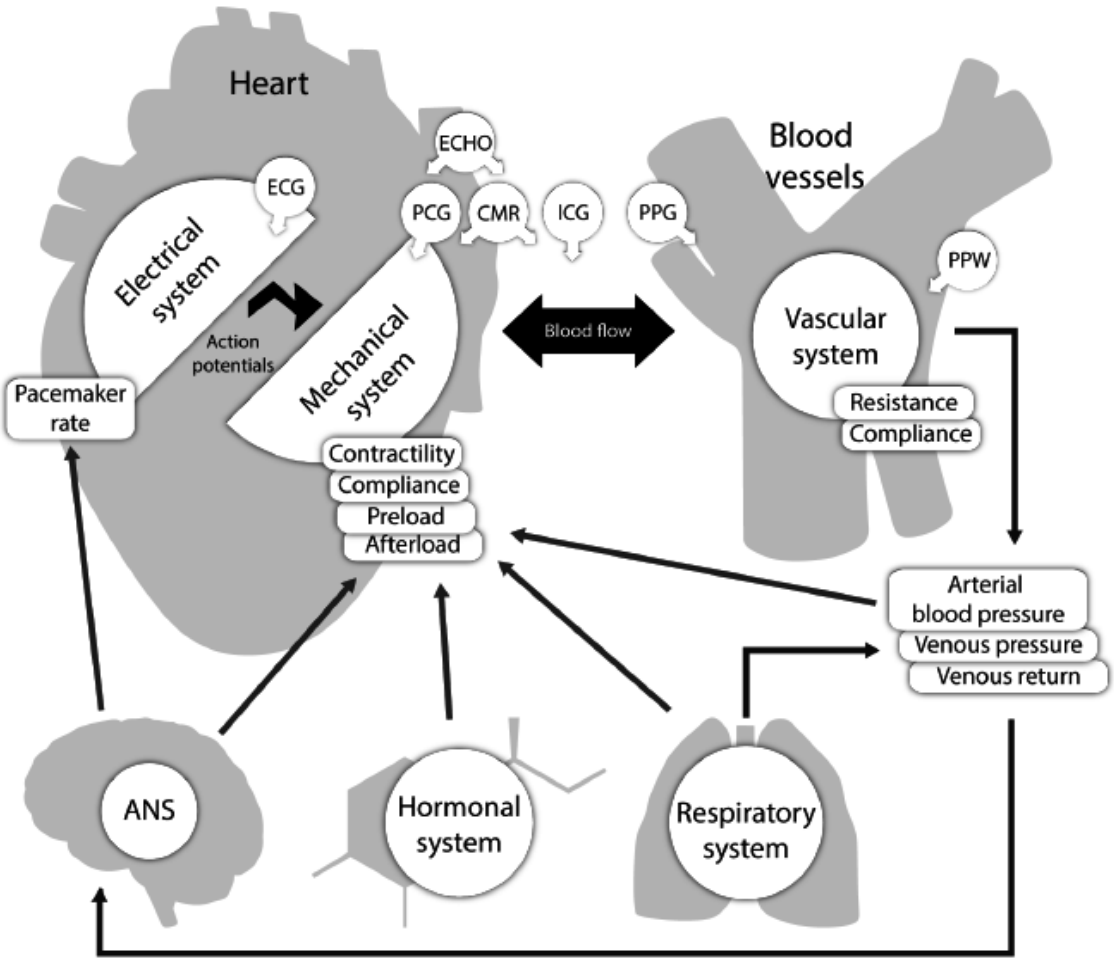

Figure 8 – Interactions involving the cardiovascular dynamics and techniques to assess them [18].
Techniques: *ECG: electrocardiography; ECHO: echocardiography; PCG: phonocardiography; CMR: cardiac magnetic resonance; ICG: impedance cardiography; PPG: photoplethysmography; PPW: pulse pressure wave.*

2.4. Syncope

As suggested in the former Chapter 1, syncope (or, more commonly named, fainting) is a complex symptom that defines a sudden and transient loss of consciousness associated with an inability to maintain postural tone, with a rapid onset, short duration and spontaneous complete recovery. It is due to the occurrence of a temporary global cerebral hypoperfusion event, caused by unexpected cardiovascular reflexes in response to some kind of stimulus. These reflexes instigate a decrease in systemic BP (to equal or lower than 60 mmHg [10]) and consequent diminishing of the cerebral blood flow, which occurring during more than 6 sec may induce the syncope episode [2, 5, 7]. During the episode, the subject may exhibit erratic movements of the

arms and legs [3]. Furthermore, the occurrence of syncope is a uniquely human characteristic, since no other species is shown to experience it [1].

A syncope event is self-limited, meaning that the loss of consciousness does not require resuscitation – it recovers spontaneously and independently, with the reestablishment of baseline neurologic status and sense of orientation [2, 7]. However, some post-recovery fatigue may happen [2], as well as retrograde amnesia, especially in older subjects [38].

It is the cause of the unconsciousness (the transient global cerebral perfusion) that defines syncope (Figure 9). Without it, syncope may be confused with other disorders associated with temporary loss of consciousness, such as seizures, vertigo, dizziness, drop attacks, coma, shock, strokes or head injuries [2, 5, 7].

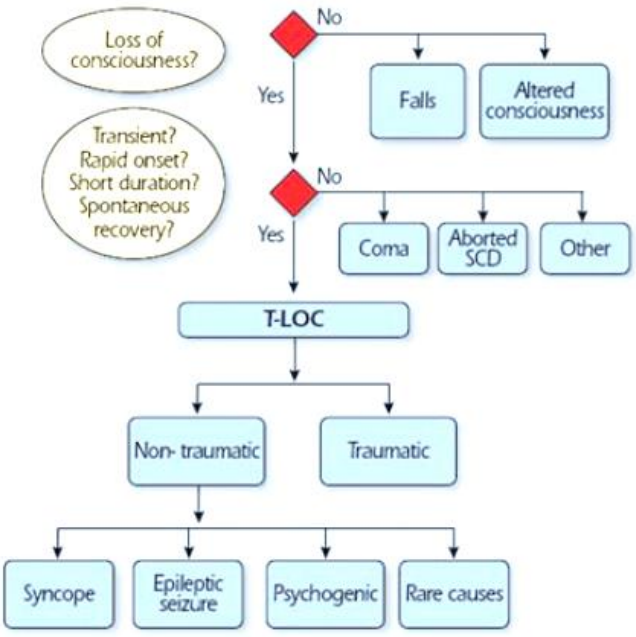

Figure 9 – Decision tree specifying the diagnosis of syncope, in the context of the transient loss of consciousness [2]. SCD: sudden cardiac death; T-LOC: transient loss of consciousness.

A syncope event may be preceded of some prodromal symptoms, such as nausea, vomiting, weakness, sweating, lightheadedness, visual disturbance, etc. [2, 5, 7]. However, it often happens without any previous distinguishable warning, hampering its anticipation. The duration of the episodes is regularly inaccurately estimated [2], too, which is a major difficulty in the management of an occurred episode by others.

As previously depicted, the fall in systemic BP that induces syncope may happen due to the combination in the decrease in the CO and/or in the total SVR. Inappropriate reflex activity, through vasodepressor (vasodilatation), cardioinhibitory (bradycardia) or

mixed reflexes may lead to low SVR. Impairments in the ANS by drugs, primary and secondary autonomic nervous failure (ANF) – when, in upright position, sympathetic vasomotor pathways are unable to increase SVR – can also cause inadequate SVR.

Three general causes are known to drive a fall on CO:

- cardioinhibitory effects (as for SVR);
- cardiovascular causes, due to arrhythmia and structural diseases (*e.g.*, pulmonary embolism, hypertension,...);
- inadequate venous return, due to volume depletion or venous pooling.

The third is also influenced by ANF, when the gravitational stress, in combination with vasomotor failure, results in venous pooling of blood below the diaphragm and a decrease in venous return.

Table 2 – Classification of syncope, based on its influencing mechanisms. Adapted from [2].

<table>
<tr><th>Syncope Type</th><th>Cause</th><th>Physiological background</th><th>Main consequence</th><th>Last consequence</th></tr>
<tr><td rowspan="3">NMS</td><td>Cardioinhibitory</td><td rowspan="3">Unsuited reflex</td><td rowspan="2">Low CO</td><td rowspan="7">Low BP
+
Cerebral hypoperfusion</td></tr>
<tr><td>Mixed</td></tr>
<tr><td>Vasodepressor</td><td rowspan="3">Low PVR</td></tr>
<tr><td rowspan="4">OH syncope</td><td>Drug-induced ANF</td><td>Normal ANS</td></tr>
<tr><td>Primary ANF</td><td rowspan="2">Structural damage ANS</td></tr>
<tr><td>Secondary ANF</td></tr>
<tr><td>Volume depletion</td><td rowspan="2">Unsuited venous return</td><td rowspan="3">Low CO</td></tr>
<tr><td>Venous pooling</td></tr>
<tr><td rowspan="3">CS</td><td>Arrhythmia</td><td rowspan="3">Cardiac or pulmonary issue</td></tr>
<tr><td>Structural cardiac issue</td></tr>
<tr><td>Others</td></tr>
</table>

The mentioned mechanisms underlying syncope define its 3 pathophysiological types (Table 2): NMS, syncope due to orthostatic hypotension (OH) and cardiac syncope (CS) [2, 3].

Brignole *et al.* [39] quantified the prevalence of each type of syncope in two groups of Emergency Department patients that were diagnosed with different guidelines, during one month: usual-care group, with 929 subjects (62±21 years old) from 28 hospitals (Nov.-Dec. 2001); standard-care group, with 745 patients (66±21 years old) from 19 hospitals (Oct.-Nov. 2004). The results in Table 3 prove that NMS is the predominant type of syncope, which is fully confirmed in other recent studies [40, 41, 42, 43, 44],

producing 30-40% of the emergency department visits per year in Europe [4]. The choice of the showed results was based on the balance between the representativeness and topicality of the studies.

Table 3 – Distribution of syncope cases in [39].

Diagnostic	Standard-care	Usual-care
NMS	46%	65%
OH syncope	6%	10%
CS	13%	13%
Unexplained syncope	20%	5%
Not a syncope	15%	6%

2.4.1. Neurally mediated syncope

NMS or reflex syncope defines a syncope event that occurs when cardiovascular reflexes suffer intermittent abnormalities, responding to a trigger. These reflexes lead to vasodilatation (vasodepressor effects) – through the sympathetic efferent pathway – and/or bradycardia (cardioinhibitory effects) – parasympathetic pathway –, which will origin the decrease in BP and cerebral perfusion (Table 2). These efferent processes are used to classify the type of NMS: vasodepressor, if the main cause of NMS is the loss of upright vasoconstrictor tone leading to hypotension; cardioinhibitory, if bradycardia or asystole largely predominate; mixed, when both mechanisms contributed to the episode.

The efferent and afferent mechanisms are not linearly correlated, since there are innumerous possible triggers. Because of this, the most involved afferent pathway is also used for classification, as listed below:

- Vasovagal syncope: it is usually preceded by ANS-related prodromal symptoms (nausea, vomiting, sweating, pallor,…) and is mediated by emotional distress (phobias, fear, pain,…) or orthostatic stress, but it is not indicative of neurologic diseases;
- Situational syncope: it is due to some specific circumstances, such as cough/sneeze, gastrointestinal stimulation (swallow, defection,…), micturition, post-prandial, post-exercise, etc.;
- Carotid sinus syncope: it happens after a mechanical stimulation of the carotid sinuses;
- Atypical forms: this is to describe uncertain situations [2, 3].

At the onset of a NMS event, there is a preceding sympathoexcitation that happens in response to the trigger. The NMS event can, then, be divided in three stages (Figure 10) [34]:

1) Oscillation phase: The exaggerated sympathetic response may provoke hyperactivity of the LV wall, activating the baroreceptors in it. The CNS will promote vagal-mediated bradycardia, vasodilation and hypotension (Bezold-Jarisch reflex [45]) to suppress the sympathetic activity and protect the myocardium. The double feedback mechanism between sympathetic and parasympathetic activations oscillates to maintain BP, enhancing the low frequency (LF) component of HRV;
2) Imbalance phase: Venous return reduces because the enhanced venous pooling is not recouped, and the falling BP due to decreased SV is compensated not only with peripheral vasoconstriction, but also with much increased HR. The double feedback mechanism fails, as the high frequency (HF) component of the BP wave and HRV enhances. It is estimated that the sympathetic activity is overwhelmed by the parasympathetic activation;
3) Catastrophe phase: HR drops abruptly due to the cessation of sympathetic activity, leading to an immediate and characteristic fall of BP. A sympathetic activation is generated, triggering a sudden tachycardia and the onset of the NMS.

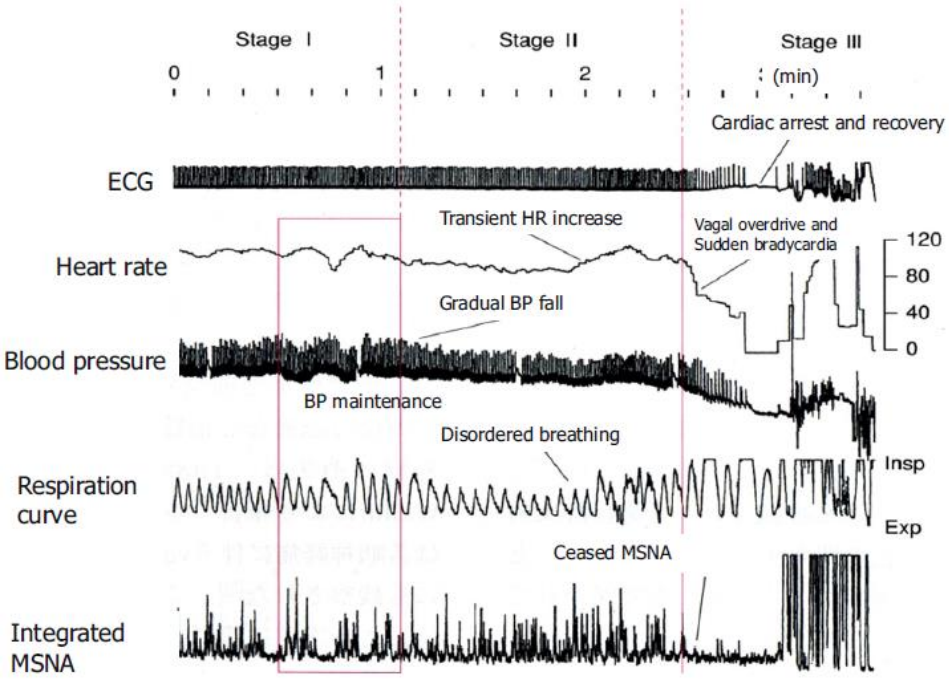

Figure 10 – Stages of NMS, with typically related biosignals [34]. ***Legend:*** *MSNA: mean sympathetic nerve activity.*

2.5. Concluding Remarks

This chapter allows the comprehension of the physiological processes that are of interest to the focus of this thesis.

An anatomic approach is firstly made, in order to present the cardiac and vascular structures that are analyzed. Then, the mechanical processes of the cardiovascular system are inspected, showing the importance of the heart and vessels to distribute blood inside the body, allowing the effective oxygenation and exchange of molecules with the tissues.

This is followed by a description of the ANS, considering its importance and action mechanisms to regulate the cardiovascular function, influencing BP depending on the needs of each situation.

BP itself is then approached, integrating the previous concepts and understanding how it is influenced by the several parameters, while considering its great importance to maintain the blood flow.

Finally, syncope is presented as a result of a combined failure of the previous physiological concepts, which instigate the decrease in BP and in the global cerebral perfusion that induce the transient loss of consciousness.

Chapter 3

Assessing Blood Pressure Regulation with the Photoplethysmogram

In this chapter, the photoplethysmography (and corresponding PPG signal) is approached as the technology that mostly matters to the scope of this work and its importance to m-health is outlined. Next, several features that can be derived from the PPG to evaluate the cardiovascular function are explored, explaining their connection with physiological aspects.

As one of the key goals of the project is to investigate a real-time PPG-based m-health algorithm to predict impending syncope, a state-of-the-art on this subject is presented. This concerns the most recent works on related algorithms, as well as m-health systems capable of assessing BP using PPG.

3.1. Photoplethysmogram and its Value

3.1.1. The Photoplethysmography

The plethysmograph is an instrument mainly used to monitor variations in blood volume (BV) that occur in a part of the body, within each heartbeat. It can be of different types, depending on the transducer that is used to catch and convert the signal: water (*e.g.* water-filled cuffs or chambers), air (air-filled cuffs), strain gauge (rubber tubes with mercury), impedance (electrodes) and photoelectric (photo detectors) [16].

The photoelectric plethysmography, or photoplethysmography, is, as suggested, a noninvasive optical technique that uses a light source (typically, a LED) – to illuminate the tissue – and a photodetector (typically, a single phototransistor) – to assess the light intensity –, in order to measure the propagated PPW in the microvascular bed of tissues of some body part, through time [16, 18, 46, 47].

These components can be arranged in two different operational configurations: transmission mode, where the tissue sample is placed between the two components; reflectance mode, where the LED and detector are placed side-by-side. Although the transmission mode imposes more restrictions than the reflection one on the usable body locations, it is the most commonly used approach [46, 47].

The enlarged flowing of the blood inside a body structure increases its optical density and absorbance of light (the number of erythrocytes carrying light-absorbing hemoglobin arises). In the transmission mode, this decreases the light intensity measured by the photodetector, and the resulting signal is inverted to correlate positively with the BV variation. As for the reflectance mode, the same effect leads to the increase of the light caption (enhanced by the nonhemolyzed erythrocytes that are reflective) [47].

The probe of the photoplethysmography can, in theory, be applied in any body site, depending mostly on the shape of the equipment. However, the relation between the captured light and the actual BV is complicated, being susceptible to phenomena of scattering, reflection and refraction. In this way, the monitoring of a more uniform and diffuse vascular bed, as in the fingertips or earlobes [48], is more adequate [47]. In fact, these are, together with the toes, the most used body sites to attach probes of photoplethysmography [46, 49, 50]. Other locations are reported in the literature, such as inside the auditory canal, focusing on a more comfortable use and on the reduction of motion artifacts (described below) [51].

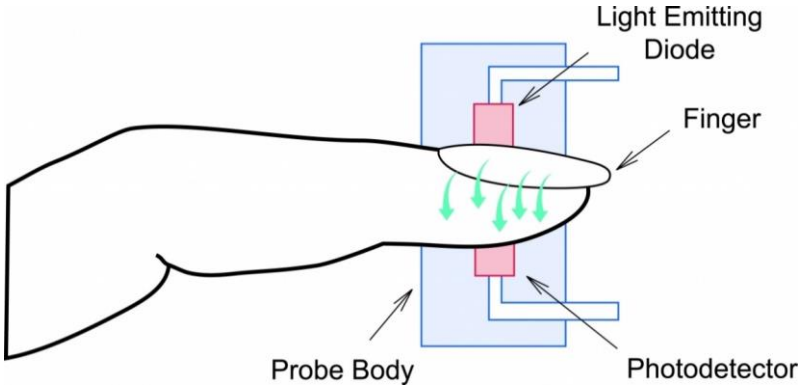

Figure 11 – Functionality scheme of a fingertip photoplethysmography probe with transmission mode [52].

In medical settings, the light source of the probe typically emits at a wavelength of around 900 nm (infrared) [16, 48]. Nevertheless, with the advent of the wearable systems, providing a long battery life is a need [14]. So, nowadays, despite wavelengths of less than 630 nm (yellow, blue, green,…) having their penetration blocked by the

hemoglobin in the blood [53], there are instruments applying such short wavelengths. It must be noticed that the range from 650 to 1350 nm is reported to be where light has its maximum depth of penetration in tissues [54], since water (the main constituent of tissues) strongly absorbs light in the ultraviolet and longer infrared wavelengths. The shorter wavelengths of light are also strongly absorbed by melanin [46].

In clinical contexts, the photoplethysmography is commonly used as pulse oximeter, which is accepted by the International Standards Organization (ISO) and the European Committee for Standardization as the standard non-invasive measure of oxygen saturation level (since 1987) [48, 55]. This technology is, then, frequently used in anesthesia, critical care and emergency medicine settings, allowing the real-time monitoring the arterial SpO_2 [18, 46, 47].

Figure 12 - Example of a pulse oximeter using PPG [56].

3.1.2. The Photoplethysmogram

PPG is the signal that is returned by the photoplethysmography. It is, then, a cyclic signal that correlates with the pulsatile volume of circulating blood, in each cardiac cycle, showing the total sum of volume changes in the vascular system of the analyzed body site, including all vessels. However, the arterial pulsations are the most significant [47], being directly driven by LV contractions [48].

The PPG signal can be decomposed into two components (Figure 13): the direct current (DC) and alternating current (AC) components.

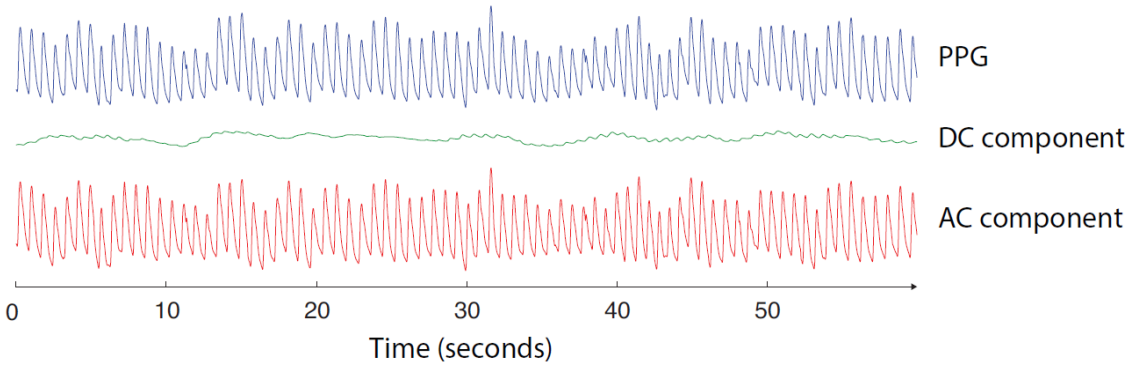

Figure 13 – The PPG signal with its AC and DC components [18].

The DC component refers to the baseline of the PPG, which displays slow oscillations of LF, due to changes in capillary density (derived from episodic sympathetic outflow or local autoregulation, for example) and fluctuations in venous volume (due to respiration-induced fluctuations in CVP). As seen, the baseline is not steady and is dependent on external factors, which makes it very prone to distortions and of no use for health contexts (in p-health or hospital settings), as it changes the amplitude of the AC (Figure 14) pulsatile waveform [46, 47]. Its removal is, in fact, a common signal processing step [16], and it is performed in most of the commercial pulse oximeters [47].

The AC component is superimposed on the DC one, and it defines the characteristic pulsatile waveform of the PPG, being the component that is affected by the cardiac cycle and, consequently, by the HR. This is, then, the component that has medical interest in terms of diagnostic [46, 47].

As the AC component illustrates the changes in peripheral BV due to the activity of the heart, it is natural that it presents a morphology that is similar to the arterial BP waveform. However, this implies a volume-pressure relation that is not linear, since the arterial volume is determined by the balance of internal BP and external pressure, not by only by BP alone. This also matters because of the dynamic compliance and stress-relaxation of arteries and veins, which define that vessels are stiffer when their pressure changes quickly and more compliant when their pressure changes slowly. Therefore, there is a lack of HF-related features of on the PPG signal, comparing to the arterial BP waveform, and this is dependent on each subject's physiologic state and vessels' mechanical properties [47].

Furthermore, as already suggested, the PPG is mostly a qualitative measurement where reductions in light intensity indicate relative increases in BV, whereas the

quantitative relation is more complicated to achieve, because of the aforementioned irregular network of vessels that exists in each body site [47].

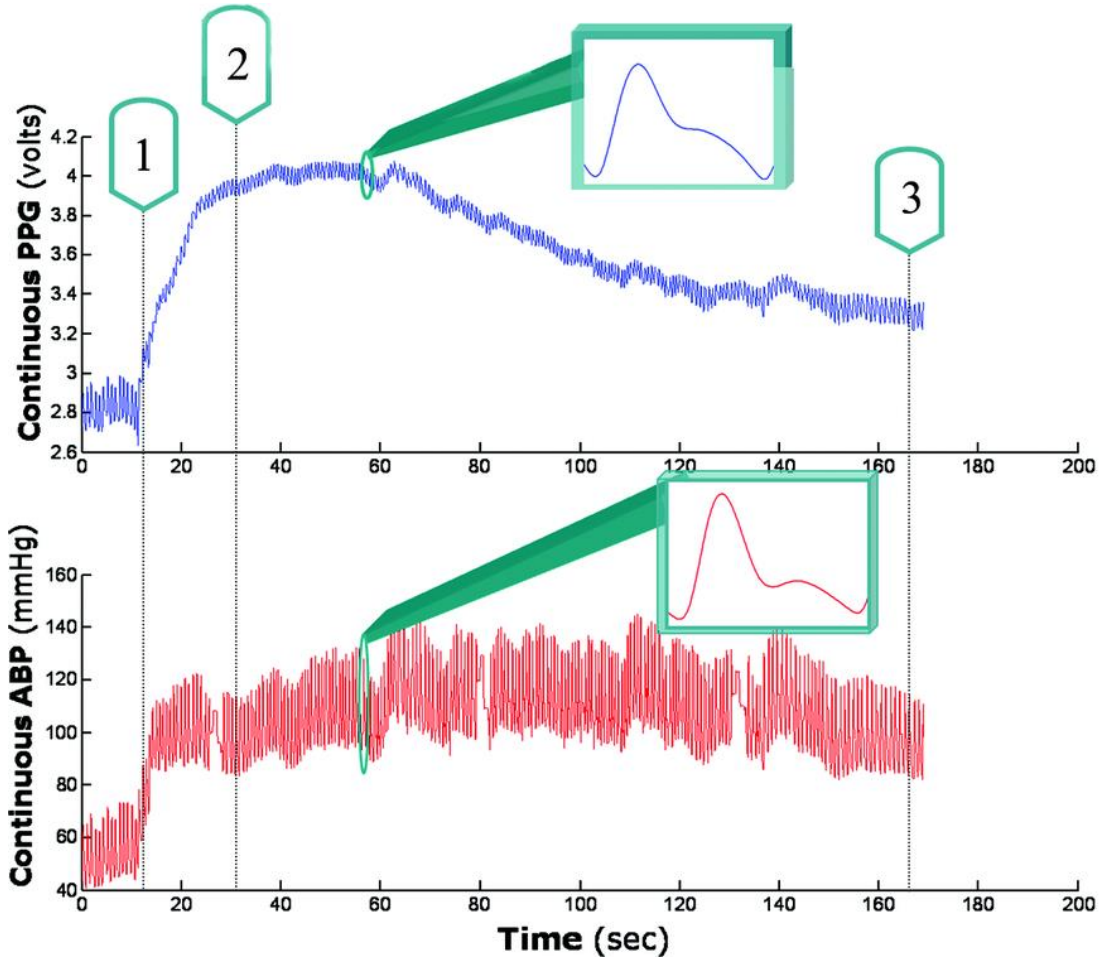

Figure 14 – Relationship between the PPG and arterial BP (ABP), collected in an ipsilateral hand [47]. In 1, the subject lowers the hand, increasing the BV and BP. In 2, the PPG's baseline tends to decrease after a peak, despite the ABP's remaining constant, because of the reduction in vessels' compliance. In 3, the subject puts the hand back to its position, but, due to autoregulation, ABP's amplitude remains increased.

A PPG pulse is perceptibly divided in two different phases [16], as in Figure 15:

- Anacrotic phase: It refers to the rising edge of the pulse, being mostly concerned with systole (it includes the systolic peak);
- Catacrotic phase: It defines the falling edge of the pulse, being related with diastole (including the systolic peak) and wave reflections from the peripheral vasculature.

Moreover, a dicrotic notch is usually noticeable in the catacrotic phase of healthy subjects with compliant arteries [16]. However, the perception of this also depends on the used PPG probe, especially on the light source. In fact, shorter wavelengths have less ability to penetrate tissue than longer ones, which may smoothen the signal, since only more superficial tissues are being examined. On the other hand, this may reduce

motion artifacts in movement settings (for example, in an acquisition while walking), because of acquiring less non-pulsatile sources (essentially coming from veins) [57, 58].

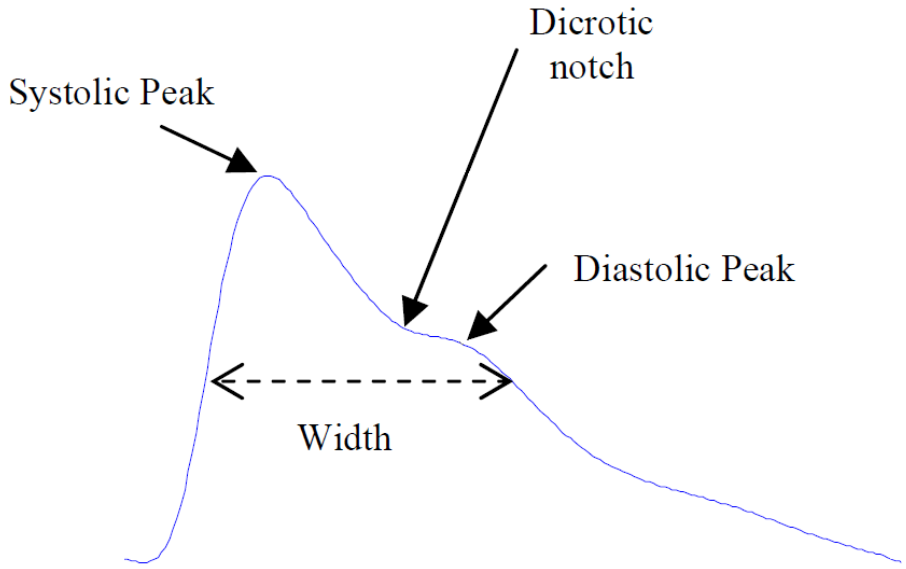

Figure 15 – PPG pulse with a typical waveform in healthy subjects, with the identification of reference characteristics [16].

3.1.3. Advantages

PPG is, then, presented as an apparently simple signal, but that contains a lot of information about the cardiovascular system and the systems that interact with it, with its morphology still not being fully understood and, therefore, its complete range of applications [16, 46, 47].

Beyond these facts, photoplethysmography is, for its operation and instrumentation, a very interesting and competitive technique. With the recent advances in the hardware and software technologies, better tools (more efficient and fast) are available for lower prices, both for signal acquisition and processing. This means that the PPG technique, besides the pulse oximetry, achieved a broader spectrum of potential applications, such as: continuous clinical physiological monitoring, vascular assessment and autonomic function evaluation [17, 55, 59].

Being constituted of, basically, a LED and a photodetector, the modern PPG sensors use low-cost semiconductor equipment that allows accurate acquisitions. Furthermore, LEDs are mechanically robust and compact, have a very long operating life ($>10^5$ h) and operate over a wide range of temperatures with small shifts in the peak-emitted

wavelength, being very reliable. As for photodetectors, they are sensitive and operate with fast responses, and they are also compact and cheap [46].

In contrast with other plethysmographs, PPG sensors do not require direct contact with the skin surface [16]. In addition, the simplicity of their operability does not require trained personnel to handle them (contrarily, for example, to the electrocardiography or other plethysmographs). It is a non-invasive, convenient, unobtrusive and portable technology [55], and it does not consume much energy.

The social-economic difficulties imposed to the health systems around the globe (see Chapter 1), together with all these advantages, make the plethysmography a very enthusiastic technology to work on and, even, to invest. Leading the health paradigm to the perspective of p-health and m-health, this makes even more sense [14].

3.1.4. Challenges

The challenges/drawbacks that the photoplethysmography presents focus mainly in the quality of the PPG. As already seen, this signal depends on many variables through complex ways that relate nonlinearly with the recorded optical phenomena. These variables include subject's movement, skin structure, skin temperatures, blood oxygen saturation, blood flow rate and the measuring environment [16, 46, 47]. All these factors provide information to the PPG, necessarily bringing artifacts to the signal.

Four issues are identified as the main challenges of photoplethysmography [16]:

- Powerline interference: It introduces a sinusoidal component of characteristic frequency in the signal, which can be due to power sources interferences, to the electronic amplifiers of the system or because of any other electromagnetic signal (*e.g.* surrounding light or an external magnetic field);
- Motion artifact: This is, perhaps, the main issue on bringing PPG to m-health settings, being related with voluntary or involuntary vibrations or movements of the analyzed body site (very clear to observe in fingertip PPG), variations in temperature, poor interaction between the probe and the skin. The unpredictable behavior of this kind of artifacts is the major problem in the analysis, mostly in applications that do not use other sensors beyond the PPG to help on the detection of movement (as accelerometers);

- Low amplitude signal: Despite the fact that this can be due to decreased BP or more constriction in the arterial vasculature, the gain controller of the PPG probe may induce some automatic unexpected changes in the signal, leading the wave to saturate in some limit or to rest in some random fixed value;
- Premature Ventricular Contraction (PVC): PVCs are extra, abnormal heartbeats that begin in one of the ventricles [60], causing a brief arrhythmia. If not happening repeatedly, this can be harmless, but it affects the accuracy in the detection of events and features (*e.g.* the calculation of the HR itself).

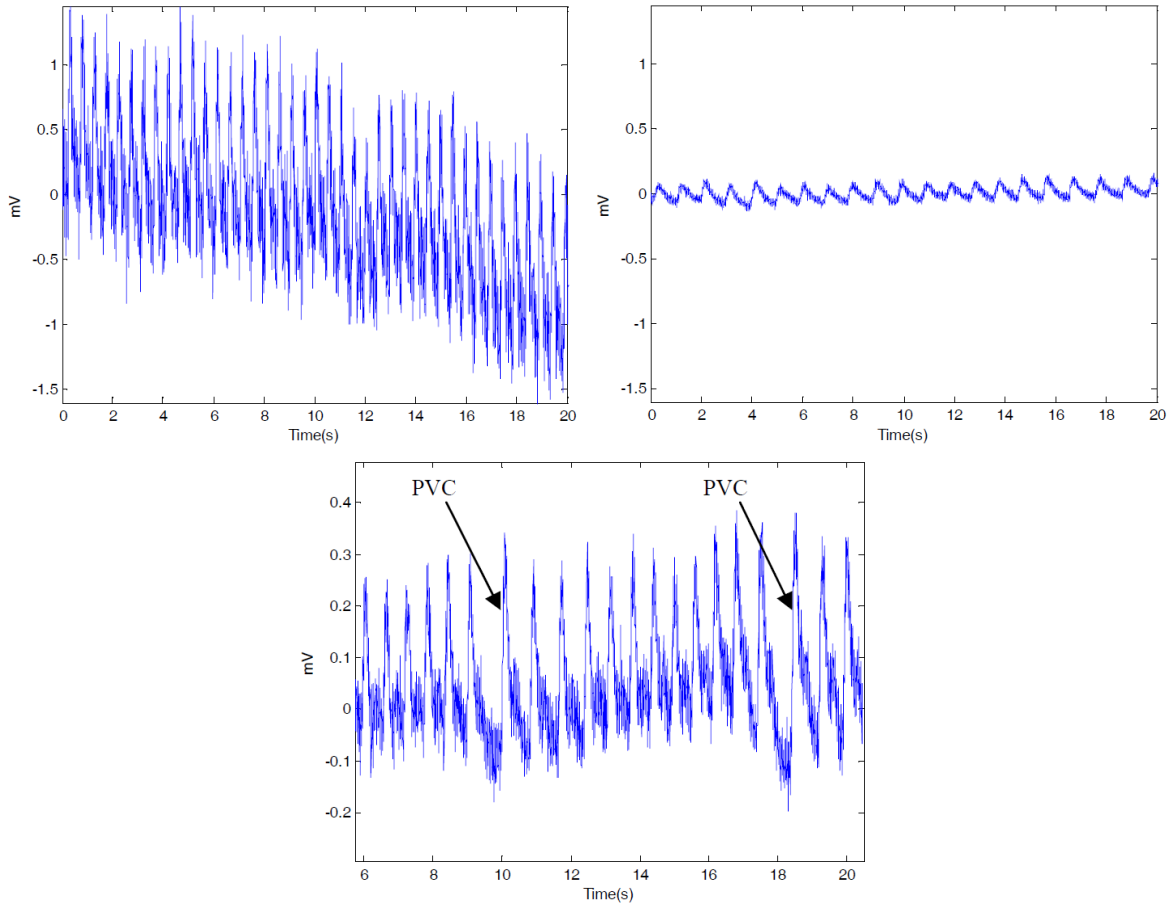

Figure 16 – Artifacts of PPG [16]. ***Top-left:*** *Powerline and motion artifacts.* ***Top-right:*** *Signal with low amplitude.* ***Bottom:*** *Ocurrences of PVC damaging the PPG.*

3.2. Evaluating the Cardiovascular Function

As previously observed, although PPG does not provide a direct reading on BP and despite its apparent simplicity, it carries complex information not only about peripheral

vasculature (and the site where the measure is taken), but also about the proper dynamics on the heart and vessels, characterizing the movements of systole and diastole throughout its pulses. Consequently, PPG allows the computation of many different features (that can be related between each other), illustrating cardiovascular phenomena around the body and, specifically, the symptoms associated with syncope.

3.2.1. Chronotropy, Inotropy, Vascular tone and Blood pressure

Chronotropy and Heart/Pulse Rate

The chronotropic changes refer to the time interval variations that happen in the heart movement/cycle, influencing the heartbeat. In this way, the chronotropy is specifically evaluated using the HR. The HR refers to the number of beats per unit of time that the heart produces. Each beat corresponds to one complete cardiac cycle. This is, then, the feature that illustrates the beating frequency of the heart [11, 16, 19], being essential to match body's metabolic demands with the subject's CO [61].

The gold standard to calculate HR accurately is the use of the R-peaks of the ECG, because of their distinct profile that is easily demarked. In this approach, two consecutive R-peaks are detected, and the time interval between them indicates the duration of one single heartbeat (Figure 17) [16, 17].

Nevertheless, in principle, any signal capable of showing accurate inter-beat intervals provides enough information to calculate HR. When working with PPG, since pulse signals are used, the terminology is pulse rate (PR), instead of HR [17]. Any point of the PPG pulse (or other signal) can be used to count the heartbeat (Figure 17), provided that the measurement is always made accurately in that point, over the pulses – otherwise, the produced data will be corrupted.

HR (or PR) reflects the balance between the sympathetic and parasympathetic systems, being related with the action of the SA node [62]. Increased resting HR has been associated with cardiovascular death, ischemic heart disease and sudden cardiac death, both in subjects with CVD and, even, in asymptomatic ones [61, 63, 64].

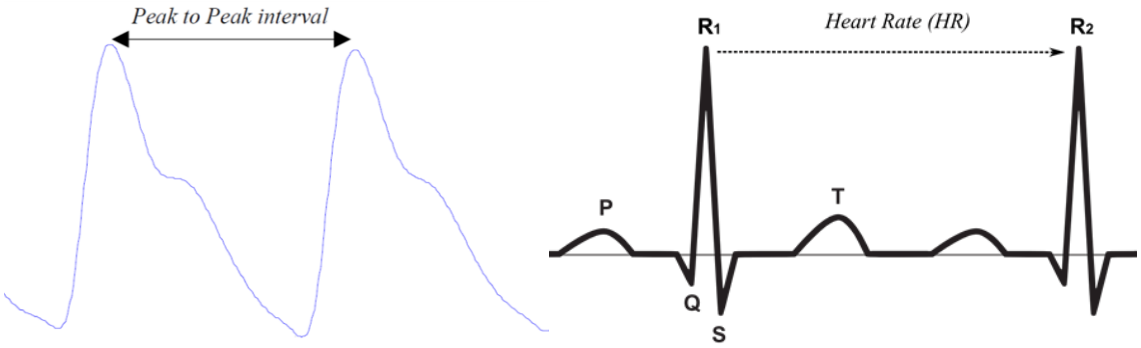

Figure 17 – Common determination of the PR and HR.
Left: *Interval between systolic peaks of the PPG that can be used to define PR [16].*
Right: *Common definition of the HR as the RR intervals of the ECG [65].*

Inotropy and Left Ventricular Ejection Time

LVET is one of the two systolic time intervals (STIs) that are commonly defined in the literature – the other is the pre-ejection period (PEP). PEP defines the time interval between the beginning of the ventricular electrical depolarization (represented by the Q-wave of the ECG) and the opening of the aortic valve. LVET refers to the next step of systole, defined as the time interval between the opening and the closure of the aortic valve (period of ejection of blood from the left ventricle) [18].

Whereas the calculation of PEP requires the ECG, accurate LVET values can be computed only with PPG [66]. The gold standard technique for the non-invasive evaluation of STIs is the echocardiography, which uses Doppler and M-mode analyses. However, in p-health and m-health contexts, this is not a viable technique [18]. To face this issue, some approaches on the computation of LVET only with PPG have been proposed [66, 67].

A healthy LV function is characterized by short PEP and long LVET levels [68], which can be quantified with the ratio of PEP/LVET [69]. LVET is an indicator of inotropic changes in the heart (changes in the contractility of the heart), being associated with SV and a prognostic parameter related to hypovolemia [70]. Moreover, changes in LVET were connected with poor prognosis in hospitalized patients with heart failure and precapillary pulmonary hypertension [71].

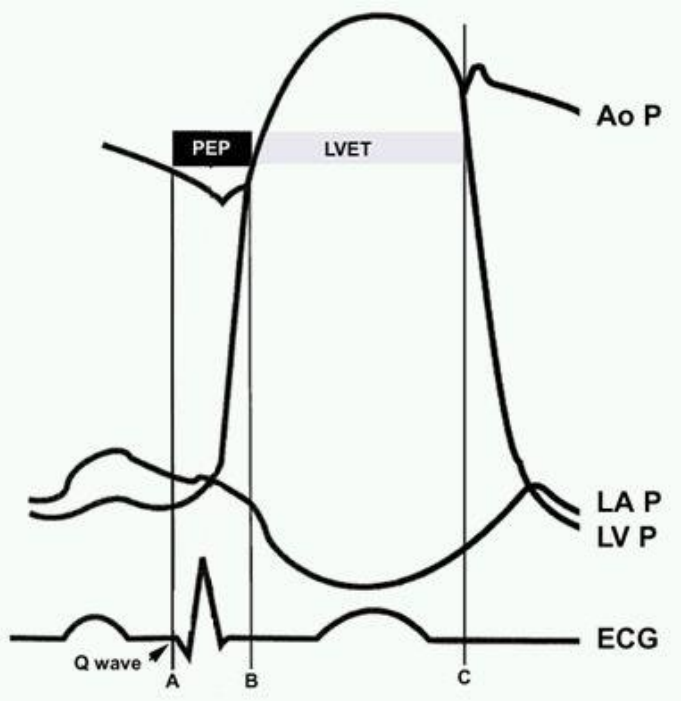

Figure 18 – LVET and PEP indication, with an ECG as reference. Adapted from [72].
***Legend:** Ao P: aortic pressure; LA P: left atrial pressure; LV P: left ventricular pressure.*

Volume Tone, Blood Pressure, Stiffness Index and Reflection Index

To investigate effects on the cardiovascular volume tone and BP, the study of the morphology of the PPG pulse may be of much interest. In fact, Figure 7 highlights the evolution of the PPW in the vascular system, shown in a PPG pulse. SI and RI are features calculated, precisely, through the identification of the several waves in one single PPG pulse, as in Figure 19.

SI refers to the time interval that initiates with the main wave that propagates from the aortic arch and finishes with the reflected waves (time interval between the peak of the systolic wave and the peak of the diastolic wave). As for RI, it defines the ratio between the amplitude of the diastolic wave and the amplitude of the systolic wave [66].

Based on Figure 19, these features are extracted, in each PPG pulse, as follows [66]:

$$SI = B_d - B_s \tag{4}$$

$$RI = A_d - A_s \tag{5}$$

SI was significantly correlated with PP by Baruch *et al.*, during lower body negative pressure sessions [37]. Furthermore, SI relates with large artery stiffness (and age-related issues) [73], as well as with the velocity of the PPW – named as pulse wave velocity (PWV) – [74], especially in large arteries, too.

Contrarily to the relation between SI and large arteries, RI is associated with the stiffness of small arteries [74]. It has also been related with variations of the volume tone [75, 76].

Couceiro *et al.* found a solid relationship between the two features and both BP and total PVR [66], two important physiological direct predictors of impending syncope.

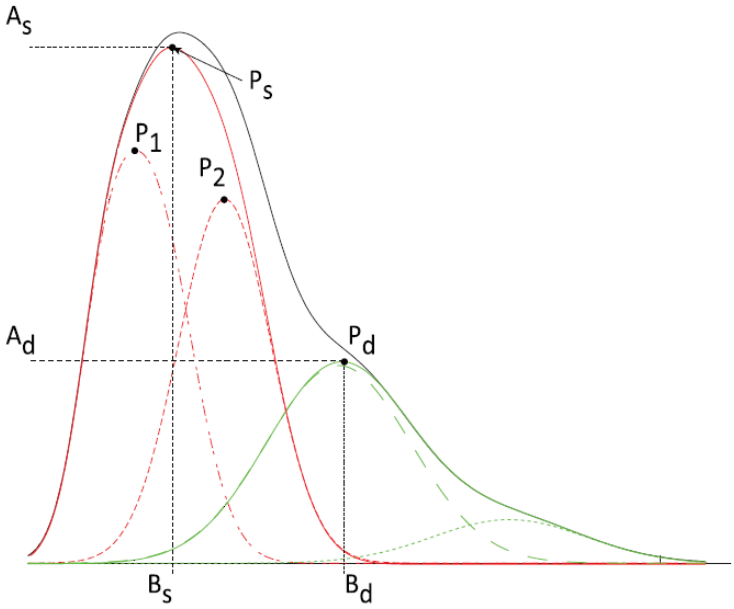

Figure 19 – PPG pulse and characteristic points used to extract SI and RI [66].

3.2.2. Heart and pulse rate variability

HRV refers to the variations that happen in HR through time, quantifying the change of time periods between consecutive cardiac cycles [12]. Since this is based on the discrete observation of HR values through time, the gold standard technique for its measurement is the quantification of RR intervals from the ECG (Figure 20) [77]. However, following the same logic of HR and PR, when characteristic points from PPG signals are used to get HRV information throughout several pulses, the used terminology for the concept is pulse rate variability (PRV) [17].

HRV (or PRV) may vary due to age, cardiac disease, respiration and cardiac load, being clinically linked to arrhythmias, hypertension, coronary artery disease, congestive heart failure, organ transplant, tachycardia, neuropathy and diabetes [78].

Since the ANS influences the cardiac cycle, HRV is a valuable framework to investigate the sympathetic and parasympathetic function and balance. In fact, the most

important application of HRV analysis is the surveillance of post-infarction and diabetic patients, in whom it helps to evaluate the risk for sudden cardiac death [12].

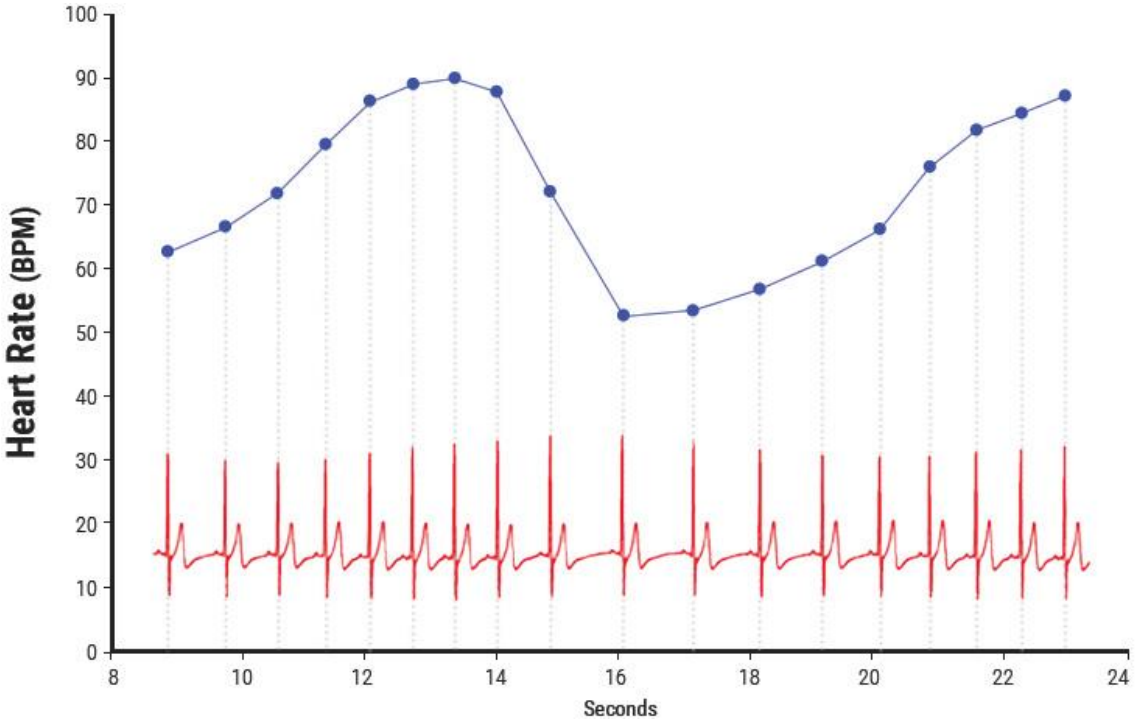

Figure 20 – Example of a HRV record (top, blue), based on the RR intervals of an ECG (bottom, red) [79].

Based on the registry of the successive HR values directly measured, several HRV-related features can be extracted. These features belong to one of two domains: the time domain (Table 4) or the frequency domain (Table 5).

Frequency domain variables are nowadays possible to extract and embed in p-health and m-health applications because of the advances in technologies such as low-cost microprocessors, which enable the relatively rapid computation of the power spectral density (PSD) of the HR registry through methods like the Fast Fourier transform (FFT) or autoregressive (AR) models [77].

HRV framework allowed the association between HR, diastolic BP, systolic BP, mid-frequency band power of HR and plasma adrenaline concentrations, which showed significant increases in subjects that changed from supine to sitting to standing posture [80]. Moreover, it has been suggested that aerobic athletes present an increased power in all frequency bands of the HRV [81].

The rhythmic contributions of the sympathetic and parasympathetic systems to the heart modulate the heartbeat at distinct frequencies. Sympathetic activity is associated with the LF range (0.04–0.15 Hz), while parasympathetic activity is associated with the

HF range (0.15–0.4 Hz) of modulation frequencies of the HR. This difference enables the distinction between sympathetic and parasympathetic contributions in the cardiovascular system [12, 78]. In this way, the ratio between the power of low and high frequencies is commonly defined as a marker of sympatho-vagal balance [78].

As a consequence, the influence of the ANS on the cardiovascular system provides deeper information through HRV tools, as the neurologic status of patients [82] and its evolution (following the evolution of HRV parameters). In fact, since possible imbalances in the sympatho-vagal equilibrium are shown through these indexes, it is possible to compute the relative cholinergic and adrenergic modulation of HRV [12].

Table 4 – Typical time domain HRV indexes [12, 77, 78].

Parameter	Description
Mean	Mean of the registered time intervals
SDNN	Standard deviation (STD) of normal-to-normal (NN) intervals
SDNN index	Mean between several SDNN, in a different time window
SDANN	STD of the averages of several intervals, in a different time window
SDSD	STD of successive differences between adjacent NN intervals
RMSSD	Square root of the mean squared differences between adjacent NN intervals
NN50	Number of interval differences of successive NN intervals greater than 50ms
pNN50	Ratio between NN50 and the total number of NN intervals
MAX-MIN	Difference between the shortest and the longest RR intervals
HRV index	Total number of all counted intervals, divided by the amplitude of each interval

Table 5 – Typical frequency domain HRV indexes [12, 77, 78].

Parameter	Description	Frequency
Total Power	Variance of all RR intervals	Approximately <= 0.4 Hz
ULF	Power in ultra-low frequency range	<= 0.003 Hz
aVL	Power in very low frequency (VLF) range	0.003 Hz – 0.04 Hz
aLF	Power in LF range	0.04 Hz – 0.15 Hz
aHF	Power in HF range	0.15 Hz – 0.4 Hz
aLF Norm	Normalized LF power	LF / (Total power – VLF) x 100
aHF Norm	Normalized HF power	HF / (Total power – VLF) x 100
RaLH	Ratio of low and high frequencies	LF/HF

3.2.3. Second derivative of the photoplethysmogram

The second derivative of the PPG (SDPPG) is a commonly used signal, much more than the first derivative. It is also referred to as the acceleration PPG since it is an indicator of the acceleration of the blood flow in the measurement site [16] (and, extrapolating, in the whole body).

The SDPPG waveform is mainly composed by four systolic waves and one diastolic wave (Figure 21): *a*-wave (early systolic wave, positive to the reference), *b*-wave (early systolic wave, negative to the reference), *c*-wave (late systolic increasing wave), *d*-wave (late systolic decreasing wave) and *e*-wave (early diastolic positive wave) [16, 83].

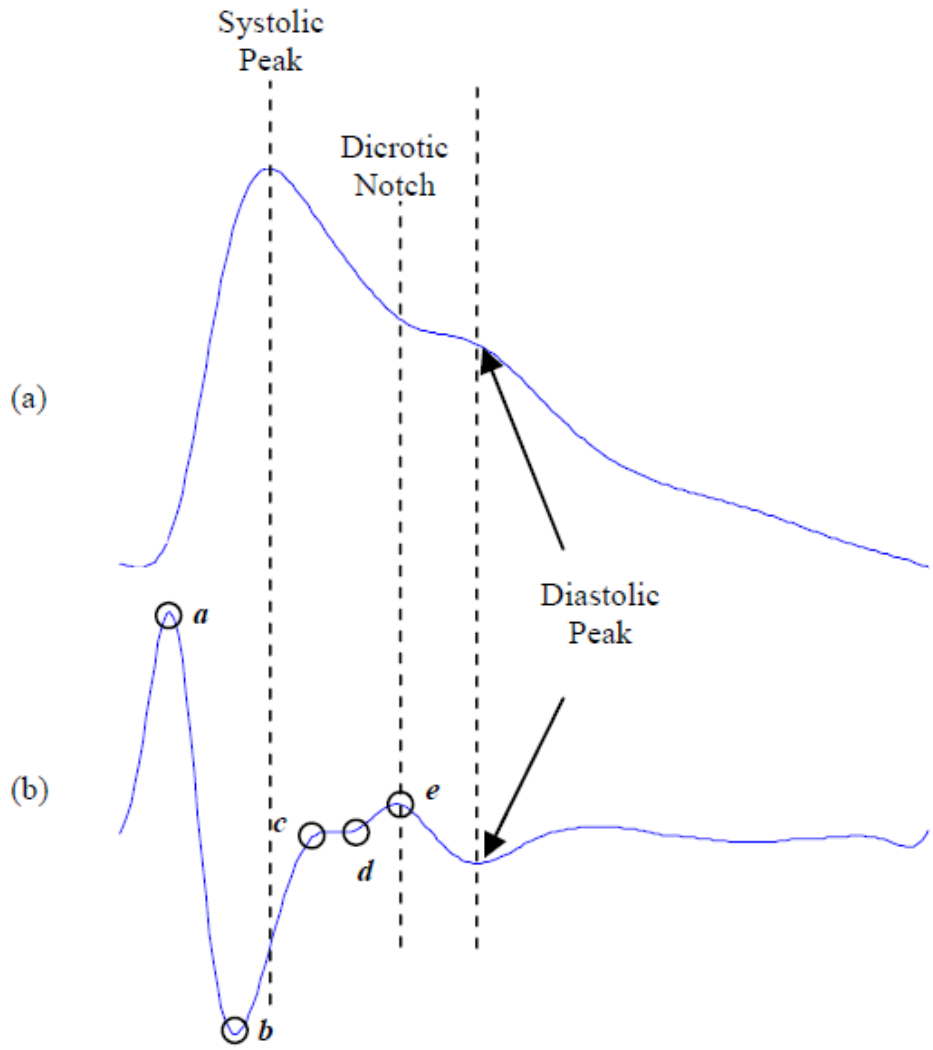

Figure 21 – Representation of a PPG pulse (a) and its respective SDPPG (b), with the location of the waves a, b, c, d and e [16].

The relative heights/amplitudes of each wave to the *a*-wave (*b/a*, *c/a*, *d/a* and *e/a*) are frequently used ratios that relate with the dynamics of the vascular system in aspects such as: atherosclerosis, age, drugs, arterial BP and arterial stiffness. In fact, an *aging index* (SDPPG-AI) was defined: *(b-c-d-e)/a* [16, 83, 84].

The ratio *b/a* has been related to increased arterial stiffness and decreased compliance, especially in the peripheral circulation (which is normal, since the PPG directly analyzes this circulation). As the arterial stiffness increases and compliance diminishes with age and arteriosclerosis, *b/a* is indicated as a non-invasive index of these conditions [85, 86, 87]. Furthermore, it was shown to be a useful evaluator of the risk of heart disease [88] and of the existence of hypertension [89].

The ratios *c/a*, *d/a* and *e/a* were shown to increase with decreased arterial stiffness [85], which means that they tend to decrease with age [16, 86].

The *c/a* ratio was also used to distinguish subjects with hypertension [89], whereas -*d/a* was used as an index of LV afterload and for the assessment of vasoactive agents [85]. *d/a* was associated with the risk of developing metabolic components [90]. As the *e*-wave represents the dicrotic notch of the PPG pulse and, consequently, the closure of the aortic valve in the cardiac cycle (signaling the subsequent decreasing blood flow), it can be used to monitor the cardiac function [91, 92].

Concerning the index SDPPG-AI, it was shown to grow with the advance of age, being useful to evaluate arteriosclerosis and assess the subject's vascular age [85, 93].

3.2.4. Systolic rise of the photoplethysmogram pulse wave

As already discussed, the first peak of a PPG pulse refers to the anacrotic phase of the pulse, which relates with systole and the flowing of blood through the aortic valve to the aorta, being associated with the rise of BP towards the SBP [16, 23, 24].

This implies that the systolic amplitude (the height of the systolic peak that relates with the SBP) of the PPG is an indicator of the pulsatile changes in blood volume, assessing the arterial blood flow on the measurement body site [94, 95]. It is, therefore, an evaluator of the stroke volume [96], being indicated as a potentially better surrogate for BP than the pulse arrival time (PAT) [97]. It was also demonstrated as a directly proportional feature of the local vascular compliance on the measurement site, over a wide range of CO values [98].

PAT refers to the time interval that, in a cardiac cycle, corresponds to the sum of PEP with pulse transit time (PTT). PTT refers to the time taken by the PPW to travel between two distinct arterial sites, being, for that, inverse to the PWV [18].

The time that spans between the onset of the PPG pulse and the systolic peak, named crest time, is also a parameter worth of evaluation, since it also allows the assessment of CVDs. Since it relates with the PWV, it provides an interesting insight on the risk of a subject to suffer from CVD [99].

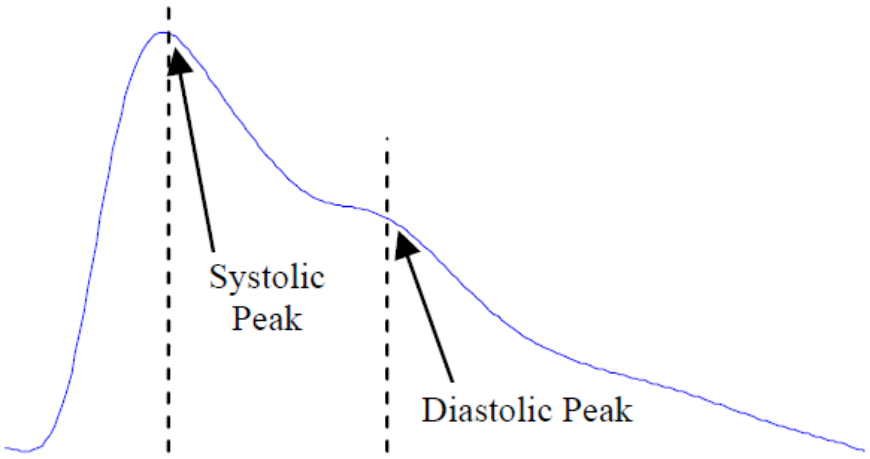

Figure 22 – Indication of the systolic and diastolic peaks in a PPG pulse. Adapted from [16].

3.2.5. Information dynamics

The communication and mutual influence that the ANS and cardiovascular system present between each other is just one of the many examples of multisystem interactions existing in the body. In fact, an organism is seen as an integrated and organized network of organs that influence each other, in order to find the best state of equilibrium [100]. When these interactions are not well-known, data-driven approaches are used to explore the system and, in these terms, the information-theoretic framework allows the study of the system dynamics from a nonlinear and model-free perspective [13].

This framework is based on the quantification of the entropy of a studied process, which refers to the amount of information carried by itself, in terms of the average uncertainty also about itself. Considering a process Y, this is translated to:

$$H(Y) = -\sum p(y) \log p(y) \tag{6}$$

where $p(y)$ defines the probability of Y to take the value y. Considering a coupled process X, the conditional entropy quantifies the average uncertainty that remains about Y when X is known, as below:

$$H(Y|X) = -\sum p(x,y) \log p(y|x) \tag{7}$$

where $p(y|x)$ is the conditional probability of observing y given that x was observed. The amount of shared information between the two processes is quantified with the calculation of the mutual information, defined as:

$$I(X;Y) = \sum p(x,y) \log \frac{p(y|x)}{p(y)} \quad (8)$$

where $p(x,y)$ is the joint probability of observing the values y and x simultaneously [13].

Faes *et al.* developed an ID toolbox based on the estimation of conditional entropies that is suitable for the analysis of physiological systems, which typically present a problem of dimensionality – they are high-dimensional state spaces that provide limited length time series [13].

They have been using this to study several short-term physiological complexities, such as: the effects of postural and mental stress on HR and BP [101]; the effect of orthostatic stress alone on HR and BP [102]; the underlying mechanisms of cardiovascular and cerebrovascular regulation in orthostatic syncope [103] and; the dynamics within the brain and between the brain and the heart during sleep [104].

3.3. Prediction of Syncope in Real Time

The prediction and diagnosis of syncope has been made through the application of the head-up tilt table (HUTT) test to previously identified subjects [3, 18]. This test is made in clinical facilities and consists of the patient lying on a bed and being tilted at different angles (from 30º to 60º), while the BP, electrical impulses of the heart and oxygen level are monitored. During the test, the individual may feel the sensation of passing out, or effectively pass out [105]. Several algorithms to predict impending syncope in real time are trained with data recorded during HUTT tests, and that is the case for the studies presented here.

The investigation of real-time predicting algorithms of impending syncope is driven by the need of finding ways to avoid unnecessary hospitalizations, in order to reduce health expenses and let the hospitals take care of exclusively indispensable cases (which improves the quality of the healthcare services and frees the population from more frequent medical appointments). This translates to the attempt of permanently monitor the patient's health, recording important data, retrieving alarms and giving suggestions to avoid some kind of crisis, in a p-health/m-health context [14]. This approach increases the useful diagnostic data about the patient and empowers him to take

countermaneuvers to prevent the syncope event, such as bending at the waist, toe-raising, leg-crossing, thigh contraction or handgrip [106]. In this way, such algorithms are supposed to be used at home, in ambulatory scenarios and in wearable systems (implying the use of inexpensive and convenient technologies).

Virag *et al.* [107], in a study with 1255 patients, used BP and ECG to predict vasovagal syncope in real time. The algorithm consists of a cumulative risk function that is compared with a threshold, analyzing the normalized HR (the RR intervals of the ECG), the normalized SBP and the LF powers of both parameters. The system was optimized in a set of 100 subjects and validated on the remaining 1155, achieving 95% of sensibility (SE), 93% of specificity (SP) and 128±216 sec of prediction time (PTime).

Mereu *et al.* [108] also used cuff-based BP and ECG as sources to predict NMS. The following features were extracted: RR intervals, SBP, DBP, mean (mBP) and pulse (pBP) BP, the ratio RR/SBP, the first derivative of the ratio RR/SBP, the first derivative of the ratio RR/DBP, the first derivative of the ratio RR/mBP, and the first derivative of the ratio RR/pBP. The study was specifically designed to be applied inside clinical facilities and counted with 145 volunteers. The validation of the algorithm presented 86.2% SE, 89.1% SP and 44.1±6.6 sec PTime.

Piccirillo *et al.* [109] used ECG and BP in 106 subjects. They applied the following HRV and BP variability normalized indexes to their algorithm: total power, HF power, LF power and very-LF power of both RR intervals and SBP. They achieved a validation result of 76% SE and 99% SP.

In p-health and m-health settings, the use of a cuff-based tool to assess BP is not suitable, comfortable nor practical. Given this, there has been a greater interest in the development of cuffless BP estimation techniques.

Eickolt *et al.* [110] and Muehlsteff *et al.* [111] used ECG and PPG as sources, in studies with 44 and 43 patients, respectively. The first one's validation results were 81% SE, 85% SP and 203±227 sec PTime. The second one's were 90.48% SE, 83.33% SP and 77.71±71.78 sec PTime. In [111], a threshold approach was applied to classify syncope events, being based on the HR (corresponding to RR intervals) and on several PAT values. These different PAT measures were defined, in each cardiac cycle, as the time intervals between the R-peak of the ECG and one of five characteristic points of

the PPG: the onset of the pulse, the systolic peak or 20%, 50% or 80% of the total amplitude of the systolic peak.

Couceiro *et al.* [19], also with an ECG and PPG-based system (applied in the same dataset used in [111] and in this work), achieved cross-validation results of 95.2% SE, 95.4% SP, 116.4±155.5 sec PTime and a false positive rate per hour (FPRh) of 0.14 h^{-1}. This algorithm applies the Minkowski distance and a threshold-based classifier in consecutive windows of 10 sec. The following parameters are extracted: HR (ECG-derived), PAT (defined as the time interval between the ECG R-peak and 80% of the PPG systolic amplitude), LVET, SI and RI (computed from the PPG, as in [66]). These parameters produce features that correspond to their normalization and to their normalized variation in 1.5 min windows, and these features feed the classification model.

The system of [19] overcame the performance of another algorithm proposed by Couceiro *et al.*, which applied Support Vector Machines (SVM) instead of the Minkowski distance [21]. In spite of the improved PTime (341.75±286.33 sec), this model had worst results of SP (84.6%) and FPRh (0.29 h^{-1}).

In [20], Couceiro *et al.* proposed the integration of HRV indexes into the algorithm of [19]. To choose the most suitable features for the system, a score metric based on the area under the curve (AUC) of the receiver operating characteristic (ROC) curve was applied, showing that the parameters SDNN, aHF and aLF (refer to Table 4 and Table 5) could improve the algorithm. In fact, the performance was better, with a cross-validation scheme producing 93.3% SE, 100% SP, 56.1±36.8 sec PTime and 0.00 h^{-1} of FPRh.

Despite BP and ECG being clinically recommended for syncope diagnosis [2, 7], in a p-health perspective, PPG, for its cheapness and easiness-to-use, is, as previously seen, more interesting.

In [11], Couceiro *et al.* compared the algorithm from [19] with a version of it based only on PPG. As a result, all the PAT features were not possible to compute (as PAT depends directly on the ECG), and the ECG-derived HR was substituted by the PR (corresponding to the time intervals between 80% of the systolic peak's amplitudes of consecutive PPG pulses). This version performed expectedly worse, since the best scored parameter of the original approach was, precisely, the normalized PAT. In a

cross-validation scheme, this PPG-based algorithm achieved 65.3% SE, 94% SP, 0.14 h^{-1} FPRh and 82.6±44.9 sec PTime.

3.4. Wearables to assess Blood Pressure

3.4.1. Context

Nowadays, there are several wearable hardware solutions that allow, through the use of specialized software, the estimation of cardiovascular features that can act as BP surrogates. Moreover, most of these tools provide their own application programming interface (API) that eases the interaction through programming with the system, allowing the development of related software by third-party developers.

As depicted in section 1.2, the third step of this work involves the use of such a solution to acquire PPG signals in real time, feeding a concept demo application that shows the usefulness of the syncope prediction algorithm developed in the second step. In this case, the key point in the interaction with the system is to ensure the access to the raw data of the PPG sensor (the actual PPG signal), as this is needed to compute several features studied in this work (as presented above, in sections 3.2 and 3.3).

As the investigation in this section based the choice on which hardware to link to the concept demo application, the collection of the presented information was mainly performed on October-November, 2015, to give time to, eventually, buy equipment. This is important to point out, since the market of wearable devices change rapidly, with new improvements in the technology every year.

3.4.2. Wearable devices: State-of-the-art

There are five commercial categories of wearable devices:

- Fitness: Solutions usually sold by sports brands and addressed to clients that play sports frequently. They show information about the physiological performance of the user, when exercising;

- Lifestyle: Its main objective is to give users the tools to maintain a healthy lifestyle (the information produced by these devices is very similar to those of fitness);
- Medical: Solutions designed to be used in clinical settings. Therefore, they must be medically validated in order to ensure that the results of their measurements are accurate and reliable;
- Stress: Devices with the purpose of estimating the client's stress level;
- Research: Since many of the tools belonging to the previous categories only provide the processed results of their sensors, these devices provide their data without any – or almost any – processing (raw data), so that any researcher can apply own algorithms [112].

Table 6 – Wearable devices that use plethysmography to extract HR information [112, 113, 114, 115].

Category	Device	Body site	HR sensor	Movement sensor	Compatibility	Connectivity
Fitness	*Polar Loop*	Wrist	Chest band	Accelerometer 3D	*iOS*; *OSX*; *Windows*	*USB*; *Bluetooth* (*Offline*)
	Motorola MotoActv	Wrist	Chest band	Accelerometer 3D	*Android*	*USB*; *ANT+*; *WiFi*; *Bluetooth* (*Online*)
	Adidas MiCoach Smart Run	Wrist	Optical	Accelerometer 3D; GPS	*Android*; *iOS*; *Windows Mobile*; *OSX*; *Windows*	*WiFi*; *Bluetooth* (*Online*)
	Garmin Vivofit	Wrist	Chest band	Accelerometer 3D	*Android*; *iOS*; *Windows*	*ANT+*; *USB*; *Bluetooth* (*Offline*)
	Basis B1	Wrist	Optical	Accelerometer 3D	*Android*; *iOS*; *OSX*; *Windows*	*USB*; *Bluetooth* (*Offline*)
	Microsoft Band	Wrist	Optical	Accelerometer 3D; Gyroscope; GPS	*Android*; *iOS*; *Windows Phone*; *OSX*; *Windows*	*USB*; *Bluetooth* (*Online*)
Lifestyle	*Samsung Gear*	Wrist	Optical	Accelerometer 3D; Gyroscope	*Android* (partially)	*Bluetooth* (*Online*)
	Saphire Wellness Watch	Wrist	Optical	Accelerometer 3D; gyroscope; magnetometer	*Android*; *iOS*; *Windows Phone*	*Bluetooth* (*Online*)
	Amiigo	Wrist	Optical	Accelerometer 3D	*Android*; *iOS*	*Bluetooth* (*Online*)
	LG Lifeband Touch	Wrist	*Earphone*	Accelerometer 3D; Altimeter	*Android*; *iOS*	*Bluetooth* (*Online*)
	Epson Pulsense Watch	Wrist	Optical	Accelerometer 3D	*Android*; *iOS*; *OSX*; *Windows*	*Bluetooth* (*Online*)
	Apple Watch	Wrist	Optical	Accelerometer 3D	*iOS*	*BLE* (*Online*)
Medical	*Gobe (Healbe)*	Wrist	Pressure	Accelerometer 3D	*Android*; *iOS*	*Bluetooth* (*Offline*)
	Withings Pulse	Wrist; neck; hip	Optical	Accelerometer 3D	*Android*; *iOS*	*Bluetooth* (*Offline*)
Research	*biosignalsplux*	Fingertip (coupled hub)	Optical	Accelerometer 3D (optional)	*Android*; *Windows*	*Bluetooth* (*Online*)
	E4 wristband	Wrist	Optical	Accelerometer 3D	*Android*; *iOS*	*BLE* (*Online*)

For this thesis, a research solution that provides a PPG sensor was already available to work – biosignalsplux® (extended below) [113].

Table 6 presents a list of wearable devices that use PPG technology to calculate HR and that allow the interaction of the user through programming. It is noticed that most of the devices are wrist-worn smartwatches or smart bands and, most of the times, acquire the PPG from the wrist (none of this is the case for biosignalsplux®). However, as it will be analyzed below, the majority of these gadgets do not allow the access to the raw PPG signal (contrarily to biosignalsplux®), which is a basis requirement for the project.

Given the information provided so far, it was possible to select the devices that, according to their functionalities, may be suitable for the project: Apple Watch®, Samsung Gear S® – for their dissemination in the market –, Microsoft Band®, E4 wristband® – for their compatibility – and biosignalsplux®. The characteristics of interest of each equipment are highlighted below.

Apple Watch®

Apple Watch® is an iOS®-compatible smartwatch produced by Apple®.

Its photoplethysmograph is consisted of two LED lights and two photodiodes. LEDs emit green light (495-570 nm) [116] for most of the time, hundreds of times per second. The sensor can also emit and capture infrared light at intervals of 10 minutes [117].

In addition to the PPG sensor, it has a 3-dimensional accelerometer, which functions as a motion/activity sensor.

Samsung Gear S®

Samsung Gear S®, on the other hand, is a smartwatch that works with Android Wear®, being compatible with Android®.

It also monitors HR using PPG with green LED lights to acquire the PPG signal [118].

It has a 3-dimensional accelerometer and a gyroscope to supervise user's activity.

At the time of writing, Samsung® is optimizing a research wrist-worn wearable (with a design similar to Gear S®), called Simband®. This device turns out to be a smart band fully dedicated to the field of healthcare, allowing the collection of HR, BV and

BP, skin temperature, oxygen levels and carbon dioxide, as well as raw ECG and PPG with several wavelengths [119, 120].

Microsoft Band®

Microsoft Band® is compatible with both Android® and iOS®, through its own software development kit (SDK) [121] and the Microsoft Health® platform, which allows an easy consultation of all the physiological data collected for the user [122].

In addition to the photoplethysmograph, Microsoft Band® has the following motion sensors: 3D accelerometer, gyroscope and GPS.

The photoplethysmograph captures the reflection of the green light emitted from a LED. This process can be done in different time intervals, depending on the active mode: in exercise modes, the heart rate is stored every second; in sleep tracking, the recording is done during periods of 2 minutes, interspersed with pauses of 8 minutes; in manual mode, the user can consult his heart rate at any time, by activating the respective command; in all other ways, the process is done in successions of periods of 1 minute of recording and intervals with 9 minutes of pause [123].

Despite the qualities, this device is not available for sale in Portugal, which excludes the possibility of its purchase to this project.

E4 Wristband®

This is a wrist-worn research solution that is compatible with Android® and iOS® through its own APIs, connecting through BLE – Bluetooth Low Energy® [124]. Besides the PPG sensor, it includes, among others, a 3-axis accelerometer [115].

The PPG sensor uses red and green LEDs, which is used to cancel some motion artifacts (except for this processing, the device provides raw signals). Furthermore, the company delivers much information and help regarding the equipment and related algorithms and theoretical foundations [125, 126].

In spite of all the positive insight, the cost of the purchase is very expensive [127].

Biosignalsplux®

This is a research solution provided by the Portuguese company PLUX, Wireless Biosignals®. The biosignalsplux® consists of a wireless tool package, which includes different integrable biometric sensors (available separately, according to the customer

needs) in a central hub. It serves as the basis for the development of many applications for academic purposes [113], providing the possibility of access to the raw data of the sensors.

There are many solutions for biometric data acquisition offered by this company, with a variety of 18 available sensors [128].

The fingertip PPG sensor, presented as blood volume pulse (BVP) sensor, has the following characteristics:

- Type: transmittance;
- Gain: 34;
- Wavelength: 670 nm;
- Bandwidth: 0.02-2.1 Hz [129].

The company also provides several binding APIs for different platforms: Android®, C++®, Java®, Python® and C#® [130].

Figure 23 – PPG sensor of biosignalsplux® [129].

3.4.3. Software to develop m-Health applications

Apart from all the diversity of fitness wearables, smartwatches (which fall into the category of lifestyle wearables) are more promising devices, with a bigger market. In this segment, there are three main platforms: Pebble®, Android Wear® and Apple Watch®.

These three systems present a series of functionalities quite dependent on their synchronization with a smartphone and the use of the greater computing capacity of this tool. Thus, using a smartwatch alone will typically reduce its potential and, therefore, the communication channels between these two types of devices are very well

developed, in order to use both in association. Given the dissemination, market potential and operational features of the smartwatches (linked with smartphones), they are seen as major drivers on p-health and m-health contexts [131].

However, the use of such technologies is dependent on the operations that the software provided by the three mentioned platforms allows. This subject is addressed below.

Pebble®

Pebble® is considered as the company that started the phenomenon of the smartwatch market in 2013 [132]. Pebble® watches synchronize with iOS® and Android®, since the company provides communication frameworks between the parties. In addition, Pebble® also provides its own SDK for free.

Despite the advantages in compatibility, this company had not included any PPG sensor in its products, by October, 2015. Nowadays, it is already available, but it only provides the HR data, with the PPG signal being inaccessible [133, 134]. Thus, Peeble® becomes an invalid option for this project.

Apple Watch®

Apple Watch® was launched only on April 24, 2015, and, in 2015, it was not sold in Portugal yet.

Despite the most restrictive compatibility issues associated with Apple® products, the company launched the HealthKit® and ResearchKit®: the first framework enables the integration and sharing of all information about the health status of a particular customer, while the second enables the development of third-party health applications [135, 136].

The possibility of accessing raw PPG signals remains unclear in the commonly available sources, so, we contacted Apple® to verify this condition. In fact, without a third-party software (as in the case of the E4 wristband®), the provided software kits by Apple® do not allow the access to the signal, only to the values of HR. Because of this, Apple Watch® also becomes an invalid option for the project.

Android Wear®

Unlike Pebble® and Apple®, since March 18, 2014, Google® only provides operating systems for smartwatches (Android Wear®) [137], and has created a number of partnerships with brands that develop the associated hardware (Samsung®, Sony®, Motorola®, LG®, HTC® and Asus®, for example) [138]. This hardware is then connected to an Android® smartphone via Bluetooth®.

Through the Wear API®, any developer can create applications for Android Wear® (or rely on signals generated by the device). This software does not support the access to raw PPG signals, either, only to already computed HR. The access to raw signals becomes dependent on external software provided by other manufacturers, as in the cases of the E4 wristband® and the biosignalsplux® [139].

3.5. Concluding Remarks

This chapter provides a technological insight regarding the photoplethysmography and the PPG signal. The available knowledge about the underlying physiological phenomena of a PPG pulse is approached, outlining the chronotropic and inotropic effects that influence the morphology of the signal. There is, though, a warning on the still limited clear information that is available on the subject, since the optical PPG sensors tend to capture many complexities occurring in deeper vessels – always depending on the functional characteristics of the sensors, more specifically, on the wavelength of the emitted light. Other disadvantages – most of all, motion artifacts – and advantages regarding the usefulness of PPG sensors on p-health and m-health systems are referred.

Several features extractable from the PPG are stated as interesting surrogates for the variation of BP, PVR and CO, as well as for the influence of the ANS on the cardiovascular system. The utility of each one of them is explored, since they will be used in the next two chapters.

Furthermore, some of these features has already been used to predict impending syncope, which is also discussed. In fact, despite the existence of some interesting predictive algorithms, none of them is actually prepared for the application in a fully m-

health accurate system comfortable to the user. This fact drives the interest on iterating over PPG-based models, since there is still room for improvements.

In the end, from a more commercial/operational point of view, the state-of-the-art technologies applied on m-health contexts are discussed, regarding both wearable hardware and development software.

Chapter 4

Evaluating Heart Rate Variability with the Photoplethysmogram

This chapter approaches the evaluation of the PPG signal as a source for the analysis of HRV, producing PRV features. In this way, a statistical analysis is made, concerning the comparison between PRV features and HRV ones, considered as gold standards.

This analysis is made on healthy subjects at rest and after a light physical exercise, and on subjects with CVDs, providing different conclusions depending on the analyzed context. Furthermore, the most suitable characteristic points on the PPG to derive PR intervals is also assessed, from a total set of six different characteristic points: the onset, the peak of the first derivative and the systolic peak of the PPG pulse, as well as the points corresponding to 20%, 50% and 80% of the total height of the systolic peak.

The work on this chapter resulted in a conference paper [22], orally presented in the EMBC'16 conference of the IEEE, in Orlando, Florida, the USA, on August 16-20, 2016.

4.1. Introduction

As already referred, HRV defines the change of time periods between consecutive cardiac cycles, during a larger time interval. It has been proved to be a good analytical tool to understand the neural regulation of the cardiovascular system, which is performed by the ANS (comprising the SNS and the PNS) [12].

The gold standard technique to study this is the analysis of series of RR intervals from signals of ECG. Nevertheless, in principle, any signal providing accurate inter-beat heartbeat intervals can be used instead. A similar analysis of series of pulse cycle intervals from PPW – such as PPG signals – can provide analogous results, under

specific conditions. Since pulse signals are used, it shall be called PRV instead of HRV [17].

The use of PPG signals is a tempting technique, because of the previously discussed advantages of the underlying technology, such as being inexpensive, non-invasive, convenient and a well-known diagnostic device that can potentially be used in ambulatory and wearable systems [16, 17, 59, 140]. It is, then, of great interest to evaluate the frequency and time domain features produced by both analysis, assessing the similarities between each other. Due to its technological and practical advantages, PPG is becoming increasingly popular in wrist-worn devices for PR detection [17, 59], driving the interest for PRV analysis (rather than HRV) in different physiological, demographic and biometric circumstances. In fact, the PRV may even achieve better estimates than HRV under some circumstances, such as when the ECG is subject to ECG-specific electrical artifacts, e.g., during clinical interventions [59].

Recent studies showed a sufficient accuracy of PRV compared to HRV in healthy mostly young subjects at rest [17], with high correlations (r) of both time and frequency domain parameters ($r > 0.94$, p-value < 0.0001) [49], and suitable limits of agreement: from [-0.1, 0.1] min^{-1} (in HR) to [-7.0; 19.8] % (in pNN50) and from [-1.38; 0.9] n.u. (in LF/HF ratio) to [-202; 343] ms^2 (in LF) [50]. In non-stationary conditions evaluated through HUTT tests, similar results were found in [141].

It has also been shown that PRV-derived parameters tend to overestimate HRV values representing physiological processes related with short-term variability [17], but without impairing the evaluation of ANS in individuals at rest: absolute differences from 0.0 ± 0.7 min^{-1} (in HR) to 6.4 ± 0.8% (in pNN50), and from 0.31 ± 0.21 n.u. (in LF/HF) to 54 ± 44 ms^2 (in HF) [50]. The overestimation of the HRV values comes from the main difference between the HRV and PRV, which is the time delay caused by the PTT, commonly measured as the difference between the appearance of the R-peak on the ECG and the corresponding peak value in BP. However, this value is susceptible to change between heartbeats [142].

A major challenge on using PPG in HRV analysis is its sensitivity to motion artifacts, as mentioned in the previous Chapter 3 [17, 49]. Suppression of these artifacts by improved algorithms is a popular research topic [55, 143]. The strategy to suppress motion artifacts may also be complemented with the acquisition of the PPG from other body sites rather than the most common fingertips, like the earlobe [49, 50] or inside the

auditory canal [51]. Often, an acceleration signal is synchronously acquired as well [49, 143], enhancing the deletion of motion artifacts using sensor fusion approaches.

Rauh *et al.* [50] achieved appropriate limits of agreement between the ECG-derived HR and the PPG-derived PR in healthy subjects for paced breathing. However, worse ranges were observed for some parameters. In the time domain, from [-0.4, 0.5] min^{-1} (HR) to [-10.2; 21.3] % (pNN50). In the frequency domain, from [-4.56; 3.31] n.u. (LF/HF) to [-715; 1260] ms^2 (LF). This was interpreted as a higher influence of breathing effects on the PPG compared to the ECG. Similar results were reported during obstructive sleep apnea events [144].

Furthermore, Han *et al.* [145] found that different breathing patterns lead to unequally altered characteristics of HRV and PRV. Breathing frequency had a higher impact than breathing volume.

It was also demonstrated that the agreement between HRV and PRV-derived frequency features diminishes (e.g., a decrease of 28% in HF) during mental stress like the Stroop Color-Word Test, when compared to resting conditions [146].

Since moderate physical or mental stress has been associated with a compromised agreement between PRV and HRV [17], the aim of this study is to extend these observations and to compare the HRV and PRV parameters, extracted using a time-variant analysis, in three experimental settings (healthy subjects at rest, healthy subjects after physical exercise and subjects with CVD) and using six different characteristic intervals to compute PRV indexes (detailed below).

4.2. Collected Data

Three datasets were collected at the “Centro Hospitalar de Coimbra” covering different populations and circumstances:

- Case 1: Healthy subjects at rest in supine position;
- Case 2: Healthy subjects (same subjects as in case 1) after brief and moderate physical exercise on a treadmill;
- Case 3: Subjects with CVD (such as hypertension, acute infarction, heart failure and coronary artery disease) at rest in supine position.

Our datasets comprise ECG and PPG signals collected from all enrolled individuals using a HP-CMS monitor extended with a data logger functionality. The PPG signal (@125Hz) was recorded from the tip of the index finger using an infrared transmission finger probe, while the ECG waveform (MLII lead) was digitized at 500Hz.

The first and second sets consisted of 33 subjects, while the last one was composed by 35 individuals (both men and women).

The biometric characteristics of the enrolled subjects (51 males and 17 females) are presented in Table 7.

Table 7 – Biometric characteristics of the study populations (average ± STD).

Dataset	Age (years)	BMI (kg/m^2)
Cases 1 and 2	29.72±8.54	24.48±2.41
Case 3	58.97±17.22	25.38±3.10

Our data analysis is based on a sliding window of 180 sec. with increments of 5 secs. Because of this, the minimum length of the analyzed signals must be at least 185 secs. to retrieve two data points. This requirement could not be achieved for some subjects, which had to be excluded from the analysis:

- Case 1: Patient 19;
- Case 2: Patients 3, 4 and 5;
- Case 3: Patients 4 and 34.

4.3. Methods

4.3.1. HR *vs.* PR from different PPG characteristic points

To perform a HRV and PRV analysis, it is essential to first extract the HR and the PR. HR was calculated from detected consecutive R-peaks in the ECG signal, while PR was inferred as the time span between the chosen characteristic points of two consecutive PPG pulses.

The consecutive characteristic points used to compute PR were defined as the time intervals corresponding to:

1. the onset of the PPG pulse – PPG_{onset};

2. 20% of the PPG pulse's total amplitude, at the systolic rise – $PPG_{20\%}$;
3. the local maxima of the PPG pulse's first derivative – PPG_{der};
4. 50% of the PPG pulse's total amplitude, at the systolic rise – $PPG_{50\%}$;
5. 80% of the PPG pulse's total amplitude, at the systolic rise – $PPG_{80\%}$;
6. the peak of the PPG pulse – PPG_{peak}.

Each one of these characteristic points produced a set of PRV features (described below) that were statistically compared between each other, in the three datasets described above.

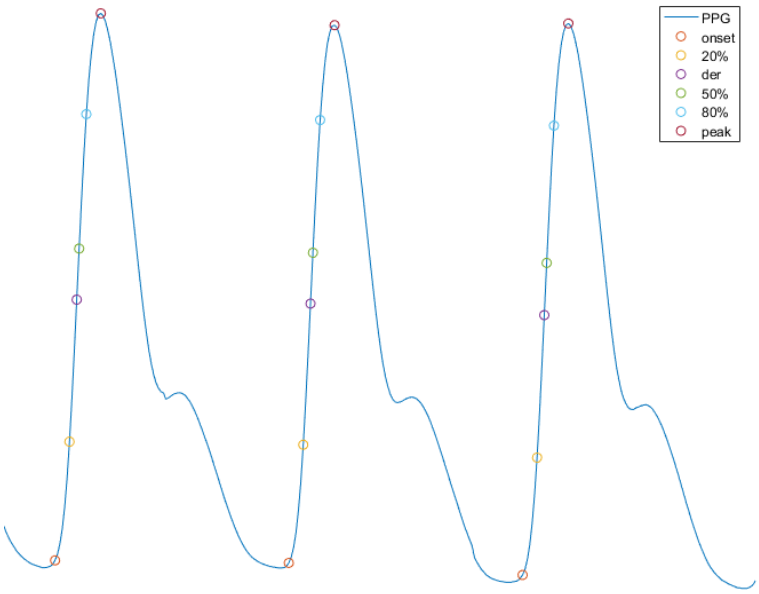

Figure 24 – Three PPG pulses (two PR intervals) showing the relative location of the six different characteristic points analyzed.

4.3.2. HRV and PRV analysis

Using a 180 sec. sliding window shifted by 5 sec. increments, time and frequency domain HRV and PRV features were extracted following the same procedure. Noisy segments and signal artifacts in the ECG and PPG signals were carefully removed from the analysis, as a starting point. Before the extraction of features, both signals, for each patient, were processed with a low-pass finite impulse response digital filter [147], using a Hamming window [148] and with a cutoff frequency of 0.5 Hz.

Recalling the indexes approached in section 3.2.2, the following six time domain features (besides the proper HR or PR) were extracted and analyzed:

- *Mean* – mean of the time intervals within the sliding window;

- SDNN – STD of NN intervals;
- SDSD – STD of successive differences between adjacent NN intervals;
- RMSSD – square root of the mean squared differences between adjacent NN intervals;
- NN50 – number of interval differences of successive NN intervals greater than 50ms;
- pNN50 – ratio between NN50 and the total number of NN intervals [16].

Additionally, using a Blackman window [149] followed by the Burg's method [150] to estimate the autoregressive power spectral density, four frequency domain parameters were extracted:

- aVL – normalized area of the spectrum of VLF band (0.003-0.04 Hz);
- aLF – normalized area of the spectrum of (LF) band (0.04-0.15 Hz);
- aHF – normalized area of the spectrum of (HF) band (0.15-0.4 Hz);
- RaLH – ratio between aLF and aHF [17].

As already discussed, on one hand, the HF component is widely accepted as a marker of parasympathetic activity (and influenced by the respiratory activity). On the other hand, the LF component is thought to result from both sympathetic and parasympathetic activities [12, 144], being controversially identified as a primary indicator of SNS modulation [12, 78]. RaLH is commonly defined as a marker of the balance between the sympathetic and vagal influence [144].

4.3.3. Statistical evaluation methods

This study comprises a statistical evaluation of the accuracy of the extracted PRV features (in the time and frequency domains, extracted from different characteristic intervals) by comparing them to the corresponding HRV features, extracted from the analysis of the ECG signal (considered as ground truth). The data were synchronized in time, ensuring the correct correspondence between the analyzed features.

This comparison was performed using the Spearman's rank correlation (SRC), the normalized root mean squared error (NRMSE) and the Wilcoxon's rank sum test (WRST). MATLAB R2014b® was used for signal processing and subsequent data analysis.

First, a one-sample unequal-tailed Kolmogorov-Smirnov test (KST) was performed in each set of parameters' values to test if each vector of data belonged to a standard normal distribution, or not (at the 5% significance level) [151]. The results showed that almost none of the data fulfilled this criterion (including the parameters of HR and PR themselves). Exceptions were observed in:

- Case 1: Patient 20 – feature pNN50 (p-value = 0);
- Case 2: Patients 1, 2, 17 and 30 – feature pNN50 (p-value = 0) –, and patient 2 – feature RaLH (p-value ∈ [0.0482, 0.1565]).

From these exceptions, only patient 30 in case 2 provided more than three analyzed windows of signal (19 values were registered for each feature). Patient 17 in case 2 produced three windows, while patients 1, 2 (case 2) and 20 (case 1) provided only two values of data per feature.

Therefore, non-parametric methods were applied to assess the agreement between the extracted features and to test the hypothesis that those features came from the same distribution [152].

To assess the agreement between the HRV and PRV features, *i.e.* the existence of a monotonic relationship between each pair of features, a two-tailed SRC was used [152, 153]. The normalized error between each PRV feature and its homologous HRV feature was assessed using the NRMSE, defined as:

$$NRMSE = \frac{\sqrt{\frac{1}{N}\sum_{m=1}^{N}(PRV_{feat_i}^{j}[m] - HRV_{feat_i}[m])^2}}{\overline{HRV_{feat_i}}} \quad (9)$$

where HRV_{feat_i} is the i^{th} extracted feature (*e.g.*: aVL, …, pNN50) from the ECG analysis, $PRV_{feat_i}^{j}$ is the i^{th} extracted feature from the analysis of the j^{th} PPG interval (e.g.: PPG_{onset}, …, PPG_{peak}) and $\overline{HRV_{feat_i}}$ is the mean of the values of the i^{th} HRV-derived feature. N is the total number of samples that compose each feature and m corresponds to each one of the samples.

A two-sided WRST was performed in order to test whether the HRV and PRV features could be considered as samples coming from continuous distributions with equal medians, *i.e.* if they belonged to the same population, with p-value < 0.05. This

test has a similar use of the Student's t-test, but does not require the data to be normally distributed [152, 154].

4.4. Results and Discussion

The achieved results are summarized in Figure 25 (Table 8) and Figure 26 (Table 9), which present the averages of the mean results of SRC and NRMSE (detailed in Table 22 and Table 23 of the Appendix C). These results are organized by feature domain (time and frequency domains) and according to the different PPG characteristic points and to the different analyzed datasets.

Table 8 – Average and STD of the means of SRC (%) between ECG-derived and each PPG interval-derived features, in time and frequency (freq.) domains. The best result in each domain is highlighted.

Feature Domain	**Intervals between PPG characteristic points**					
	PPG$_{onset}$	***PPG$_{20\%}$***	***PPG$_{der}$***	***PPG$_{50\%}$***	***PPG$_{80\%}$***	***PPG$_{peak}$***
Dataset: Case 1						
Time	86.5±12.3	85.1±15	**87.2±11.9**	85.4±12.7	84.8±15.7	82.4±17.1
Freq.	89±7.4	89.8±6.5	90.4±5	**90.6±6.2**	89.6±7	88±7.1
Dataset: Case 2						
Time	75.9±20	79±17.8	77.9±18.1	79±16.8	**80.6±16.2**	78.7±18
Freq.	83.2±11	**88±8.4**	83±11.1	84.3±12.3	84.8±10.1	81.9±13.4
Dataset: Case 3						
Time	73.3±20.4	72.4±21.7	**74.1±17.6**	71.7±20.3	72.3±19	68.5±22.5
Freq.	**76.4±7.1**	71±9.9	72.6±8.8	68±9.7	70.5±10.7	69.8±10.3

Table 9 – Average and STD of the means of NRMSE (%) between ECG-derived and each PPG interval-derived features, in time and frequency (freq.) domains. The best result in each domain is highlighted.

Feature Domain	**Intervals between PPG characteristic points**					
	PPG$_{onset}$	***PPG$_{20\%}$***	***PPG$_{der}$***	***PPG$_{50\%}$***	***PPG$_{80\%}$***	***PPG$_{peak}$***
Dataset: Case 1						
Time	6±4.7	5.7±4.2	5.5±4.2	**5.3±3.9**	5.5±3.9	5.4±4
Freq.	17.4±6.4	15.7±5.4	16.5±6.4	14.8±4.8	**14.7±5.3**	14.9±2.6
Dataset: Case 2						
Time	15.6±18.3	14.6±16.4	14.4±15.2	**13.7±14.6**	13.9±14.5	14.2±14.9
Freq.	30.5±19.9	28.6±17.6	32.9±16	30.3±15	29.6±15.7	**26.9±11**
Dataset: Case 3						
Time	9.8±7.3	9.6±6.9	10±7.3	**9±5.9**	9.5±6.3	9.8±6.3
Freq.	38.9±11.7	45.2±13.6	47.1±13.2	42±9.6	**38.9±8.5**	42.5±8.6

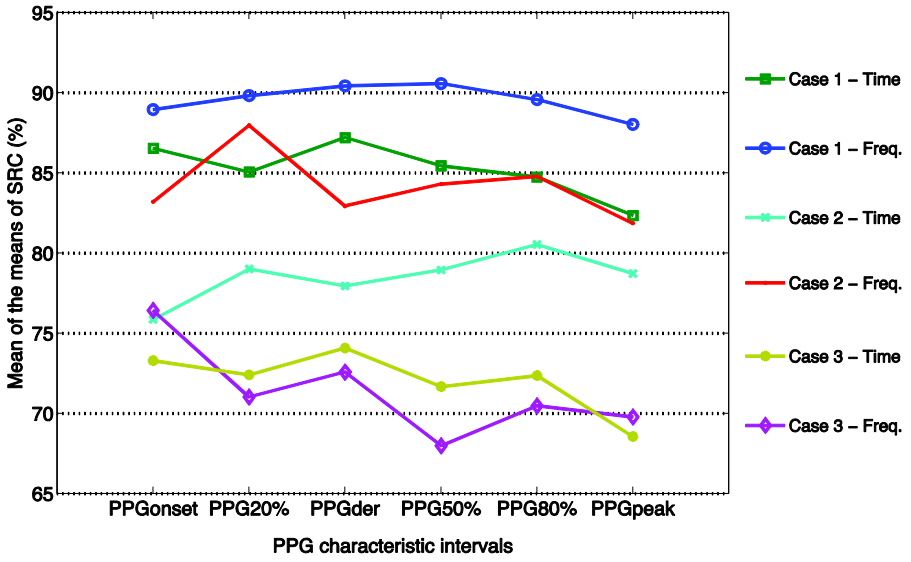

Figure 25 – Average of the means of SRC (%) between ECG-derived and each PPG interval-derived features, in time and frequency (freq.) domains. More details in Table 8.

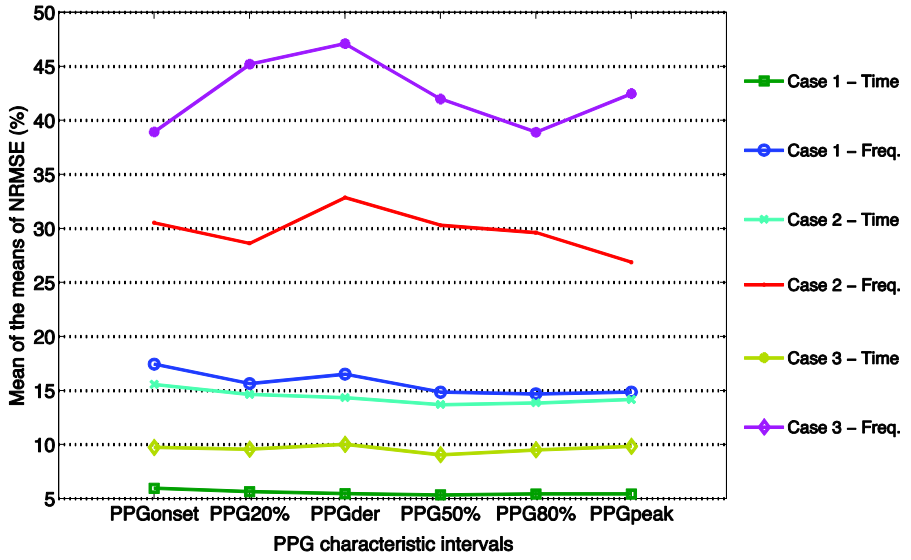

Figure 26 – Average of the means of NRMSE (%) between ECG-derived and each PPG interval-derived features, in time and frequency (freq.) domains. More details in Table 9.

Almost all the correlation values were statistically significant (p-value < 0.05), except for those found to belong to a standard normal distribution through the KST discussed previously, which was expected.

From Figure 25, it is possible to observe that under ideal conditions, *i.e.* healthy patients at rest (case 1), the agreement between the features extracted from HRV and PRV analysis is high (SRC ∈ [82.4±17.1; 90.6±6.2] %) in most of the analyzed parameters. As seen in Table 22, the exceptions were found for NN50 and pNN50 (SRC ∈ [56.1±37.5; 69.1±30.6] %).

Contrarily, in cases 2 and 3, the agreement between the analyzed features decreases drastically (SRC ∈ [68±9.7; 80.6±16.2] %). An exception was found for the frequency domain features in case 2, which range from 81.9±13.4 % to 88±8.4 %. It is also shown that the agreement between PRV and HRV features tend to decrease from case 1 to case 3, and that the achieved correlations within frequency domain features present higher values when compared to the time domain features (except for case 3).

Regarding the estimation error of the PRV features, it is possible to observe from Figure 26 that the time domain features extracted from PRV analysis achieved the lowest estimation errors (comparing to frequency features), in all the three cases (NRMSE ∈ [5.3±3.9; 15.6±18.3] %), being the case 2 where the worst estimates were achieved (NRMSE ∈ [13.7±14.6; 15.6±18.3]). As for the frequency features, it is shown that there is a drastic increase in the estimation error from case 1 (NRMSE ∈ [14.7±5.3; 17.4±6.4] %) to case 3 (NRMSE ∈ [38.9±8.5; 47.1±13.2] %).

From the analysis of each specific feature in the time domain, it is observed in Table 22 and Table 23 that the direct comparison between HR and PR signals (specified as HRV-PRV) returns excellent estimation errors (NRMSE ∈ [1.3±0.6; 2.8±2.6] %), followed by high correlations (SRC ∈ [88.6±16; 98.3±2.1] %) in the three cases under study. This observation shows a close agreement and high similarity between the estimated PR and HR signals under different physiological conditions. It is also noticed that the features presenting better accuracy (*i.e.* lowest NRMSE) are the *mean* (NRMSE ∈ [0.1±0.1; 0.4±0.6] %) and SDNN (NRMSE ∈ [2.6±2; 8.7±8.2] %), which may be related with the fact that these indexes are direct descriptors of the distributions of HR and PR values (that have, themselves, a close agreement and high similarity).

It shall be noticed that the features NN50 and pNN50 present a very low agreement in all the three cases, ranging from 36.2±46.2% to 69.1±30.6% (see Table 22), representing one of the main contributions to the decrease in the global correlation of the time domain features depicted in Figure 25. Nevertheless, these two features presented a good estimation error (NRMSE ∈ [5.7±3.6; 10.6±7.7] %). The reason for such observations was investigated through the construction of a histogram of the errors between each pair of values of each compared feature (for each PRV characteristic interval and including all the patients). The error was computed according to:

$$Error_{feat_i}^{j} = HRV_{feat_i} - PRV_{feat_i}^{j} \quad (10)$$

where HRV_{feat_i} is the i^{th} extracted feature (*e.g.*: aVL, …, pNN50) from the ECG analysis, $PRV^{j}_{feat_i}$ is the i^{th} extracted feature from the analysis of the j^{th} PPG interval (e.g.: PPG_{onset}, …, PPG_{peak}) and $Error^{j}_{feat_i}$ defines a vector of errors that correspond to the differences between each pair of values of HRV_{feat_i} and $PRV^{j}_{feat_i}$.

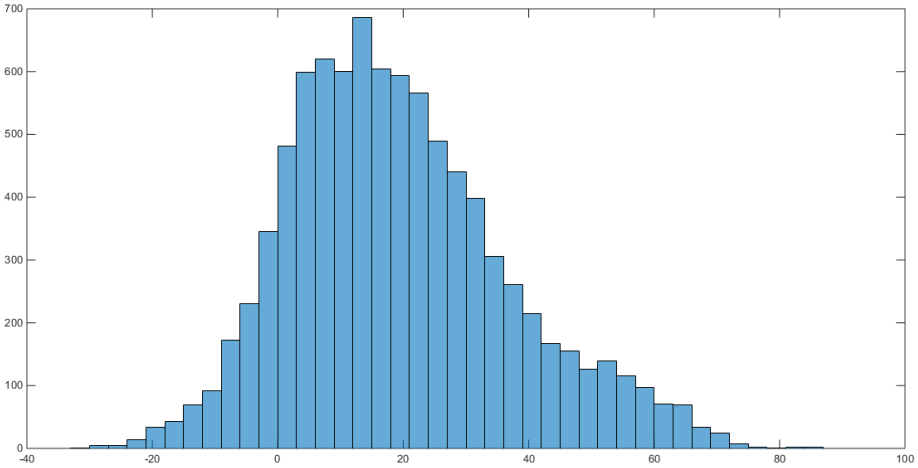

Figure 27 – Histogram of the error between the ECG and the PPG_{peak}-derived NN50.

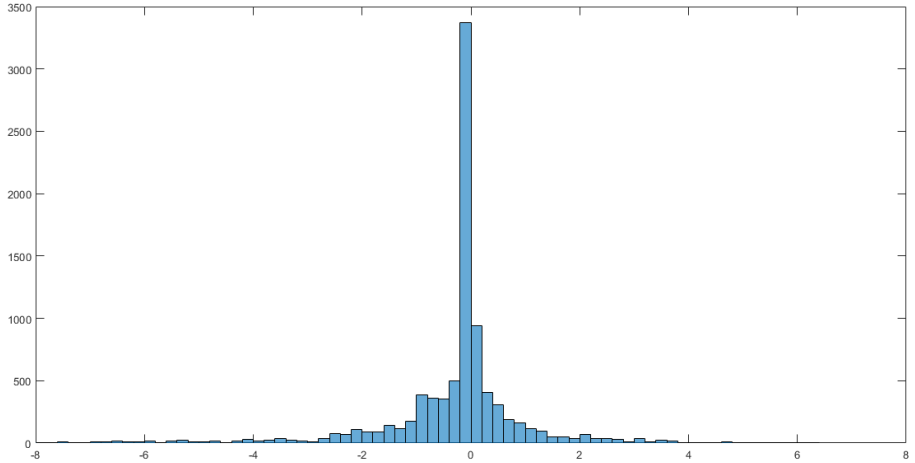

Figure 28 – Histogram of the error between the ECG and the PPG_{peak}-derived Mean.

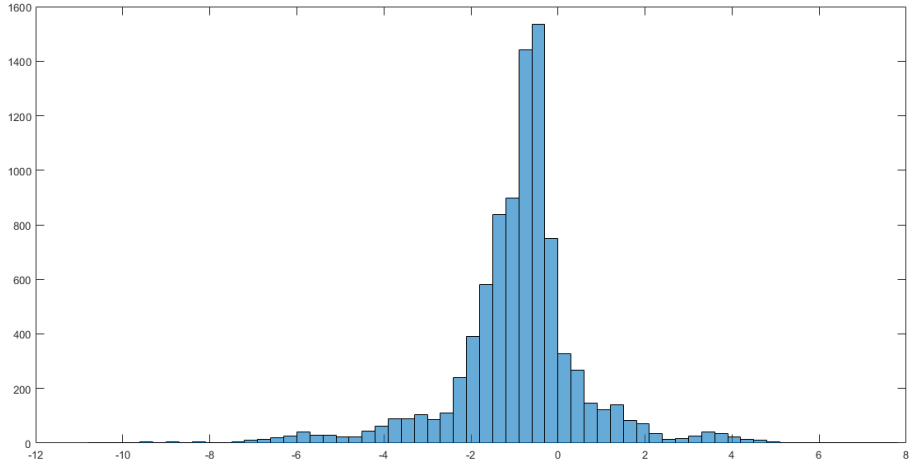

Figure 29 – Histogram of the error between the ECG and the PPG_{peak}-derived SDNN.

The analysis of the histograms showed that almost all the PRV features overestimated the HRV ones, as mentioned in the literature [17, 50] (as in Figure 28 and Figure 29), with the only exceptions being NN50 (as in Figure 27) and pNN50. Moreover, the tails of the histograms of NN50 and pNN50 are larger, with more widespread values of error.

Figure 27, featuring NN50 derived from PPG_{peak}, is used as an example to validate that the produced error values are, in fact, mostly positives (HRV NN50 is larger than PRV NN50) and with a wider distribution. The other PPG characteristic points, as well as the feature pNN50, lead to similar results.

Figure 28 and Figure 29 show the errors of PPG_{peak}-derived *Mean* and SDNN, as opposite examples to Figure 27. In these examples, the errors are concentrated in values closer to zero (as these are two of the most accurate PRV features), and their distribution tends to negative values, displaying that the PRV features are larger than HRV ones (corresponding to the referred overestimation). This is verified for the other features and PPG characteristic intervals.

One possible reason for the low correlation within NN50 and pNN50 relies on the fact that they are based on the counting of interval differences among a very short amount of time (50 ms), which is approximately 5% of the RR interval (considering a HR of 60 min^{-1}). Therefore, it is expected that even the smallest estimation error produces a highly negative impact on the agreement of these features with their reference.

It is worth mentioning that the analogous results of SRC (Table 22) and NRMSE (Table 23) concerning NN50 and pNN50 are explained by the linear relationship that is established by the two features. This is also noticed for SDSD and RMSSD.

Regarding the frequency domain features, the RaLH presented a complex behavior, since the accuracy in the estimation of this feature is highly dependent on the estimation errors of both aLF and aHF. This implies that the uncertainty in the estimation of one (or both) of these two features propagates as a dramatic increase of the estimation error of RaLH.

Table 22 shows that the agreement between the PRV frequency features and their HRV references tends to decrease from VLF (aVL) to HF (aHF). This trend is also clear

when inspecting the estimation error, with a special emphasis on aHF, where the NRMSE is clearly higher in all the three cases.

Issues for HF-related features have already been previously reported [17, 59, 146]. In fact, the HF component is influenced by many typical PPG artifacts (*e.g.* motion artifacts), as well as by stronger breathing patterns induced by exercise or mental stress [50, 144, 145] (such as in case 2), which lead to higher uncertainty in the estimation of aHF.

Similarly, in case 3 subjects (older subjects and with CVD), abnormal patterns in breathing and in the Frank-Starling mechanism (which cause stronger fluctuations in HR/PR) [17, 50], as well as the existence of a poorer blood perfusion and a lower compliance (stiffer arteries), can represent an obstacle to the correct detection of the PPG characteristic points. Moreover, the elderly are known to have distinct skin characteristics that prevent the reflectance/transmittance of light to the photodetector of PPG sensors (mimicking a low-pass filtering behavior), which can also prevent the correct identification of the PPG pulse characteristic points. These aspects increase the uncertainty in the calculation of the heartbeat intervals and consequently have a negative impact on the agreement between aHF estimated from PRV and the reference HRV.

Analyzing the characteristic points that achieved the best results, it is possible to observe, from Figure 25 and Figure 26, a small variation in the correlation and NRMSE values for most of the PPG characteristic points of case 1 (approximately less than 3%). The only exception was observed in the correlation of time domain features for PPG_{peak}.

As for cases 2 and 3, although the NRMSE within time domain features increases when compared to case 1, it is shown in Figure 26 that it remains with a low range of values ([9±5.9; 15.6±18.3] %). A worse agreement within the time domain features of cases 2 and 3 was also observed (Figure 25), being the best values achieved for $PPG_{80\%}$ (in after-exercise individuals) and for PPG_{der} (in subjects with CVD). In these cases, a higher range of correlation values was also seen for the frequency domain features (SRC $\in$ [68±9.7; 88±8.4] %), suggesting that the selection of a suitable PPG characteristic interval is much more important in these sets, than in healthy individuals.

The characteristic points exhibiting the best estimation error (NRMSE) were, in general (taking time and frequency categories into account), the $PPG_{50\%}$, $PPG_{80\%}$ and

PPG_{peak}, while the agreement between features did not follow a consistent pattern, depending on the context and analyzed feature domain. However, there is more accordance between the intervals with best correlation and with best NRMSE in case 1 subjects, rather than in the remaining cases.

PPG_{peak} underperformed in almost all cases. One plausible reason for this is the change in the characteristics of the PPG pulse depending on the situation, leading to the existence of a very broad maximum of the PPG pulse, which prevents the correct estimation of PR intervals and, consequently, the derived PRV features. Effects such as breathing are reported to have a strong influence on PR detection accuracy [50, 145].

The WRST was used to test the hypothesis in which HRV and PRV features are samples obtained from continuous distributions with equal medians, at the 5% significance level.

Table 24 in Appendix C describes the average, among all patients, of p-values achieved with the WRST, for each feature, characteristic point and dataset case. The analysis of this table reveals that most of the features in case 1 failed to reject the null hypothesis, not achieving the condition of p-value<0.05. The only exceptions whose mean p-values fulfilled this condition were: SDSD and RMSSD ($PPG_{80\%}$), NN50 and pNN50 ($PPG_{20\%}$, PPG_{der} and PPG_{peak}).

For case 2, similar conclusions were found, since the same referred features were the only ones rejecting the null hypothesis in some characteristic points. However, despite some increased values (relatively to case 1) in parameters such as HRV-PRV and *Mean*, there is a reduction in most of the averaged probabilities. In case 3, the unique features that actually rejected the null hypothesis through the mean results in Table 24 were NN50 and pNN50, but a generally marked decrease in the p-values of all the features is noticed.

The features with higher WRST averaged p-values are, as expected, the ones already presented as being more correlated and accurate among HRV and PRV: *Mean*, SDNN, aVL and the proper HRV-PRV. Moreover, HRV-PRV was predictably distinguished as the feature with much higher p-values, which follows the observation of being the most correlated and accurate one.

The spread among the least and the most accurate values between the three datasets suggest that the choice of the best PPG characteristic point is dependent on the

physiological condition of the subject and on the analysis' context, which highlights the need for an automatic decision-making algorithm to select the most suitable PPG intervals. To our knowledge, in such a system, the SRC may provide better guidelines, since the trend between HRV and PRV features can be corrected through algebraic means.

4.5. Concluding remarks

This study focuses on the evaluation of commonly used HRV features calculated from PR signals, both in frequency and time domains. The evaluation was made through the statistical comparison of HRV and PRV-derived parameters (including HR and PR) using the Spearman's rank correlation (SRC), the normalized root mean squared error (NRMSE) and the Wilcoxon's rank sum test (WRST).

Our results confirm that the majority of PRV indexes may be used as surrogates for ECG-based HRV in healthy subjects at rest, as reported in the literature [17, 49, 50, 141]. Accurate results can be observed in subjects after exercise, especially for aVL, aLF, HRV-PRV, *Mean* and SDNN. However, in CVD patients, we found a lower performance in the estimation of PRV features, with the exception of the abovementioned features, where some acceptable results were achieved. Low agreement and/or high estimation errors within aHF, NN50 and pNN50 were identified and justified.

In general, time domain features present a mean NRMSE below 15% in the three case studies, whereas frequency domain features show such a result only in healthy subjects at rest. As for the achieved correlation values, the features extracted from CVD patients are the only ones with average results below 75%. Therefore, time domain features may be used for PRV analysis covering the three presented protocols, whereas frequency domain features require more caution.

Our general averaged results (considering both time and frequency domains) show that, for healthy subjects at rest, the most suitable PPG characteristic point (with highest agreement with the reference) is PPG_{der}, while for healthy subjects after exercise the best characteristic point is $PPG_{20\%}$. As for the subjects with CVD, the characteristic point achieving the highest agreement was the PPG_{onset}.

To conclude, this study provides a ranking of PRV parameters that is useful for practical applications and that may be used depending on the obtained PPG characteristic interval and analyzed context.

One of the applications of this study is the adoption of its findings on the subject of Chapter 5, which comprises the development of a PPG-based prediction system for impending syncope. In fact, to our knowledge, the study of a PPG-based algorithm to predict syncope embedding several PRV indexes was not available in the literature until the writing of this thesis.

However, this Chapter 4 is not fully directed to such a use. It provides insight on the potential usefulness of different HRV features derived from PPG, in general different physiological and operational contexts. Since this comparison of PRV features is based on statistical techniques and not on models with established targets, the subject of this chapter provides a broad vision on the usage of PRV features in various contexts (hospital/clinical settings, p-health, m-health or other) for any practical application, considering several health states and different computations of the PR, and not only its narrow use in the assessment of syncope.

Chapter 5

Real-Time Syncope Prediction with the Photoplethysmogram

This chapter concerns the study of an algorithm to predict impending NMS events, based on cardiovascular parameters computed only from PPG signals.

This study is based on all the considerations regarded throughout this document. It approaches a large number of directly and indirectly PPG-derived features, analyzing their effect on previously identified classification metrics. The conclusions of Chapter 4 are also taken into account in what refers to PRV features.

One of the main results of this chapter is, in fact, the careful evaluation and serialization of the most suitable features to predict impending syncope. Other influencing factors are also analyzed, such as different classification metrics and different PPG characteristic points. In this way, several setups of the algorithm are studied, based on different arrangements of the modified variables. Optimal solutions are proposed at the end.

The work in this chapter resulted on the writing of the scientific paper presented in Appendix B. This paper will be submitted to the joint conference of EMBEC'17 and NBC'17, in Tampere, Finland, on June 11-15, 2017.

5.1. Introduction

Several BP monitoring algorithms have been proposed to predict impending syncope in real time, as previously discussed.

However, they have some disadvantages regarding p-health settings. Some use cuff-based BP assessment, being invasive to the patient; others apply cuffless approaches, using ECG to compute surrogates of the BP (as PTT, a direct surrogate), but imply the use of expensive and uncomfortable hardware. On the other hand, approaches that are

more suitable for p-health settings, such as algorithms assembling only PPG are less reliable.

The aim of this work is to fulfill this gap, providing a fully PPG-based algorithm to predict impending syncope, with increased reliability, chosen between different setups.

The state-of-the-art algorithms on syncope prediction are discussed and compared in section 3.3. Table 10 summarizes the performed comparison.

Table 10 – Performance of state-of-the-art methods to predict impending syncope in real time. Adapted from [18].

Method	# Subjects	SE (%)	SP (%)	PTime (sec)	FPRh (h^{-1})	Modalities
Virag *et al.* [107]	1255	95	93	128±216	---	BP/ECG
Mereu *et al.* [108]	145	86.2	89.1	44.1±6.6	---	
Piccirillo *et al.* [109]	106	76%	99%	---	---	
Eickolt *et al.* [110]	44	81	85	203±227	---	ECG/PPG
Muehlsteff *et al.* [111]	43	90.48	83.33	77.71±71.78	---	
Couceiro *et al.* [19]		95.2	95.4	116.4±155.5	0.14	
Couceiro *et al.* [20]		93.3	100	56.1±36.8	0.00	
Couceiro *et al.* [21]		100	84.6	341.75±286.33	0.29	
Couceiro *et al.* [11]		65.3	94	82.6±44.9	0.14	PPG

5.2. Experimental Setup

5.2.1. Study Design

A scheduled HUTT test was performed in 55 patients with unexplained syncope. All the patients signed a written informed consent before taking part in the study (identifier of the ClinicalTrials.gov: NCT01262508).

The applied HUTT test's protocol consisted of four phases (Figure 30):

1. Initial resting period: the individual lies for at least 15 minutes in supine position;
2. Passive standing period: the patient stands in a degree of 70º for 20 minutes;
3. GTN administration: if no syncope occurs, the passive standing position is maintained for 15 min longer, and a minimum dose of 400 µg of glyceryl trinitrate (GTN) – a vasodilator agent [155] – is sublingually administrated in the subject;

4. Final recovery period: the patient is tilted back to the supine position, for recovery.

A technician registered the occurrence of prodromal symptoms (*e.g.* nausea, dizziness, sweating,…) during the protocol and, if the patient experienced syncope, he was immediately put back to the supine position.

The outcomes of the test were classified as positive (PO) or negative (NE) according to the guidelines of the European Society of Cardiology [2]. PO results were classified as the occurrence of a syncope event or pre-syncope symptoms, such as hypotension and bradycardia [19].

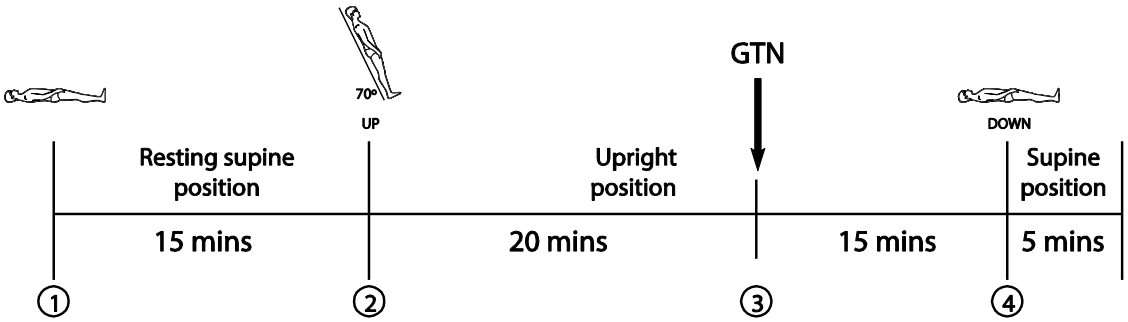

Figure 30 – Scheme of the protocol of the performed HUTT test. Kindly provided by R. Couceiro, PhD.

5.2.2. Collected Data

Several signals were recorded during the test. Using a Philips MP50 patient monitor extended with a data logger functionality, an ECG-II lead @500 Hz and a PPG @126 Hz were acquired. A "Taskforce Monitor" [156] was used to collect continuous noninvasive BP @50 Hz, two ECG leads @1000 Hz and other data. In this work, only the PPG signals were used, which were collected using a standard fingertip SpO_2 sensor.

Due to BP regulation failures not caused by syncope, arrhythmias and/or poor data quality in BP and PPG signals, 12 patients were not analyzed.

The biometric characteristics of the study population are described in Table 11.

Table 11 – Biometric characteristics of the study population (43 subjects).

Type	# Subjects	Gender (Male/Female)	Age (years)	Weight (kg)	BMI (kg/m^2)	GTN admin. (Yes/No)
PO	21	13/8	57±18	86±15	27.1±4.6	15/6
NE	22	10/12	63±17	74±13	26.0±5.0	15/7

5.3. Methods

5.3.1. Syncope Prediction

The studied algorithm is composed of four consecutive processing steps:

1. Detection of motion artifacts [55];
2. Collection and processing of hemodynamic parameters;
3. Feature extraction (with outliers' removal, as in [11] and [19]);
4. Prediction of syncope episodes.

The detection of motion artifacts was made according to the algorithm proposed by Couceiro *et al.* in [55], where a total of eight time and frequency domain characteristics of a PPG signal/section are used to classify it as being corrupted or clean. This is performed using a C-support vector classification with a radial basis function kernel [157].

The analyzed time domain characteristics are: pulse amplitude (height between the pulse peak and onset); trough depth difference (amplitude between the onset of consecutive pulses); pulse skewness (measure of the pulse's symmetry); pulse kurtosis (measure of the pulse's tails). The frequency domain characteristics, extracted using a discrete-time short-time Fourier transform [158], are: location of the spectrum second major spike; location of the spectrum third major spike; length of the spectrum third major spike; ratio between the area of the three major spikes and the area of the remaining spectrum [19, 55].

Before the computation of parameters (detailed in the following section 5.3.2), there is a removal of baseline fluctuations and HF noise from the PPG signal/section, using a band-pass filter in the range 0.23-18 Hz. Through the analysis of the first three derivatives of the data, each PPG pulse is detected. Then, it is normalized to the unit and the linear trend is removed. The systolic and diastolic phases are detected, and the desired parameters are extracted [19].

As specified in [19], there is the removal of outliers in each parameter based on a boxplot analysis of the data, compared to a reference that is calculated through a moving median average filter applied to the original parameter. The difference between

each value and the reference is $PD_i(t)$, referring to the i^{th} value of the series, in time *t*. The i^{th} value in time *t* is considered an outlier, if the following condition is satisfied:

$$PD_i(t) < Q_1 - 3.IQR \quad \vee \quad PD_i(t) > Q_3 + 3.IQR \tag{11}$$

where Q_1 is the lower quartile (25% of the values), Q_3 is the upper quartile (75% of the values) and IQR is the interquartile range ($IQR = Q_3 - Q_1$).

To end the post-processing step, each parameter is interpolated at 2 Hz and parsed with a Butterworth low-pass filter cut off on 0.05 Hz, to reduce HF noise [19].

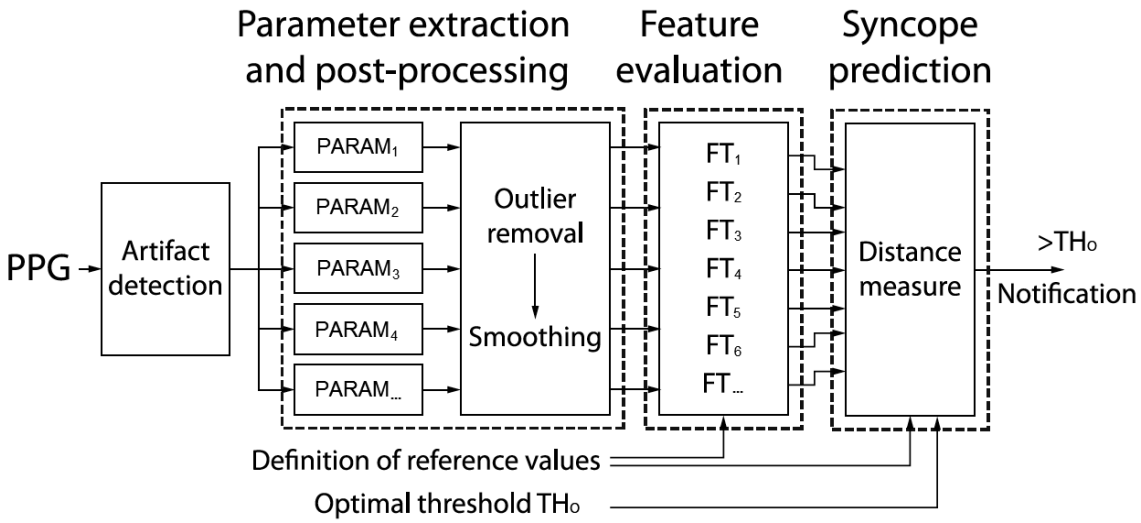

Figure 31 – Scheme of the algorithm structure. Adapted from [19]. Kindly provided by R. Couceiro, PhD. The modified variables between the different studied setups were the extracted parameters and evaluated features, the clipping of these features and the used distance metric.

For each patient, the algorithm analyzes 10-sec continuous windows of signal, returning a binary classification of the risk of impending syncope. This is originally based on a selected Minkowski distance metric with exponent $p=2^{-0.5}$, relatively to a stable orthostatic reference in the start of the standing period of the HUTT test. An impending syncope event is detected if the assessed distance (fed with the previously determined features) exceeds a predefined optimal threshold. This algorithmic approach was used by Couceiro *et al.* in several publications, such as [11], [19], [20] and [21].

Since distance metrics do not considerate the direction of the evolving trajectory of a signal, in [11], [19], [20] and [21], the features' variations known to be not associated with impending syncope were clipped using the following equation:

$$\begin{cases} Y(Y > ref) = ref, & if\ direction\ is\ negative \\ Y(Y < ref) = ref, & if\ direction\ is\ positive \end{cases} \tag{12}$$

where Y is the feature vector and ref is the reference value estimated at the onset of the standing position, used for clipping. This approach was tested by comparison, contrasting its results with the ones produced with unclipped features.

The performance of the several setups of the algorithm were assessed with a conventional three-way data split approach, with the study population being divided in two major subsets:

1. a train/validation subset with approximately 70% of the individuals (15 PO and 15 NE), used to select the best variation of the algorithm (the most suitable group of features and threshold);
2. a test subset with the remaining approximately 30% of subjects (6 PO and 7 NE), used to evaluate the actual performance of the solution.

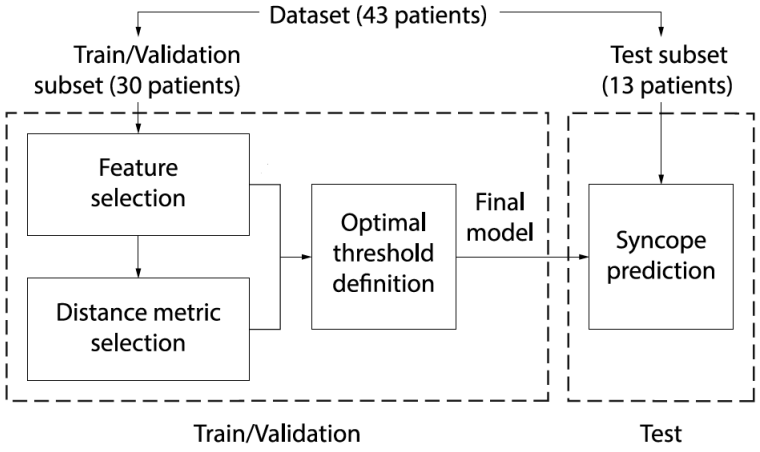

Figure 32 – Diagram of the followed three-way data split approach [19]. Kindly provided by R. Couceiro, PhD.

The optimal threshold computed in each studied setup of the algorithm was the result of the averaging of all thresholds produced by a 5-fold cross-validation scheme, with 20 repetitions. As stated in [19], this is transduced as:

$$TH_0 = \frac{1}{N}\sum_{n=1}^{N}\left(\frac{1}{K}\sum_{k=1}^{K} TH_{k,n}\right) \tag{13}$$

where TH_0 is the optimal threshold in calculation, N is the total number of repetitions, K is the total number of folds (iterations) and $TH_{k,n}$ is the computed threshold on the k^{th} fold of the n^{th} repetition.

5.3.2. Parameters, Features and Characteristic points

Several parameters were derived from the PPG signal of each patient. Each one of the extracted parameters (presented in the next five subsections) gave rise to four features to feed the classifier:

1. The normalized parameter itself;
2. The normalized change of the parameter over the previous 90 sec (identified with a Δ before the parameter's name) and;
3. Two features based on the ID of the normalized parameter – refer to 5.3.2.e).

The normalization of the parameter itself was performed according to:

$$FT_i(t) = {PR_i(t)}\Big/{PR_{ref_i}} \tag{14}$$

where $FT_i(t)$ is the i^{th} normalized feature in time t, $PR_i(t)$ is the i^{th} parameter in time t and PR_{ref_i} is the average of the i^{th} parameter during the 120 sec span (reference window) after tilting the patient back to the upright position, in the HUTT test. This reference window was chosen to ensure the orthostatic stabilization of the patient in that period (which typically occurs within less than 60 sec) [19, 159].

As for the normalization of the change of the parameter over the previous 90 sec, it was evaluated since it has been indicated as the minimum physiological response time in HUTT records [111]. It was defined as follows:

$$\Delta FT_i(t) = {PR_i(t) - PR_i(t - 90\ sec)}\Big/{PR_{ref_i}} \tag{15}$$

where $\Delta FT_i(t)$ is the i^{th} 90-sec normalized feature in time t and $PR_i(t - 90\ sec)$ is the value of the i^{th} parameter 90 sec before time t [19].

The direct parameters described in subsection 5.3.2.e) refer to PPG signal ID, hence, for these, only the first two features were calculated. The complete set of analyzed features in this chapter is enumerated in Table 25 of Appendix D.

5.3.2.a) Chronotropic/Inotropic changes, Vascular tone and Blood pressure

The parameters in this field comprise the PR, LVET, SI and RI, surrogating, respectively, the chronotropic and inotropic changes, and the vascular tone and BP, as stated in section 3.2.1.

Through the work in Chapter 4, it is concluded that the PPG characteristic point that presents more similarities between HRV and PRV parameters in patients with CVDs is the onset of the PPG pulse (PPG_{onset}). Because of this, PR was, here, computed with the time intervals between the onset of consecutive PPG pulses. Later in this chapter, the other characteristic points studied in Chapter 4 will also be evaluated, but only to compare to the previous option.

LVET was computed according to [160]. The systolic phase of each PPG pulse was modeled by a sum of three Gaussian functions, corresponding to the systolic model. The LVET value in each pulse was defined as the time interval between the systolic peak of the model's second derivative and the notch of the model's first derivative.

Based on the Gaussian modulation of the PPG pulse, SI and RI are computed as indicated in section 3.2.1.

5.3.2.b) Pulse rate variability

The PRV parameters evaluated in the algorithm were the same of Chapter 4. This includes six parameters in the time domain (*Mean*, SDNN, SDSD, RMSSD, NN50 and pNN50) and four in the frequency domain (aVL, aLF, aHF and RaLH).

Similarly to PR, these PRV parameters were firstly based on PPG_{onset}, and the other characteristic points were later evaluated just as comparison.

5.3.2.c) Second derivative of the PPG

Concerning this field, the highlighted parameters in section 3.2.3 were the ones evaluated as inputs to the classifier, consisting of: the ratios *b/a*, *c/a*, *d/a*, *e/a* and *f/a*, as well as the *aging index* SDPPG-AI.

5.3.2.d) Systolic rise of PPG pulse wave

Driven by the suggested association between the systolic amplitude of the PPG pulse with the pulsatile changes in blood volume, as well as the connection between the crest time and the susceptibility to CVDs (refer to section 3.2.4), two parameters of this field were evaluated.

The crest time (CT) was defined as the time interval between the onset of the PPG pulse (PPG_{onset}) and the time instant of its systolic peak (PPG_{peak}), as theoretically suggested. The velocity of rise (VR), based on these concepts, was specified as:

$$VR = \frac{amp\left(PPG_{peak}\right) - amp(PPG_{onset})}{CT} \quad (16)$$

where $amp\left(PPG_{peak}\right)$ is the amplitude of the PPG signal at the systolic peak and $amp(PPG_{onset})$ is the amplitude of the signal at the onset of the PPG pulse.

5.3.2.e) Information Dynamics

Based on the work of Faes *et al.* [13], three information-theoretic parameters were extracted from the PPG signal, as a univariate system (refer to section 3.2.5):

- System information (*SysInfor*), defined as the entropy of the system;
- Unexplained Information (*UnexpInf*), characterized by the conditional entropy of the system (given L lags of its past);
- Information storage (*InfStor*), corresponding to the mutual information of the system.

Besides being extracted as direct PPG-derived parameters, the first two attributes (*SysInfor* and *UnexpInf*) were also computed over the normalized parameters described in 5.3.2.a), 5.3.2.b), 5.3.2.c) and 5.3.2.d), producing indirect features to feed the classification model. These indirect features are identified with the suffixes $_{HY}$ and $_{UY}$, respectively, after the parameter's name.

5.3.3. Features' selection and Algorithm's evaluation

Given that a total of 94 features were evaluated in this work, only the most descriptive ones were introduced in the algorithm, based on a feature selection score (FSS) metric that combines their relevance and redundancy [12]:

$$FSS_i = AUC(FT_i) - \frac{|\sum_{FT_j \in S} RCC(FT_i, FT_j)|}{|S|} \quad (17)$$

where $AUC(FT_i)$ is the area under the receiver operating characteristic curve obtained with the i^{th} feature, $RCC(FT_i, FT_j)$ is the Spearman's rank correlation coefficient between the i^{th} and j^{th} features, S is the subset of selected features in each iteration and $|S|$ is its cardinality.

Each feature with FSS greater than 50% was selected, composing a set of X chosen features to evaluate in the prediction algorithm. Then, from this set, the algorithm was

fed and validated, iteratively, with $\{X,\ X-1,\ X-2, \ldots, 1\}$ features (from the least to the most descriptive one), allowing the comparison, not only between individual features (by their FSS), but also between combinations of them (through their conjugated impact on the syncope predictive classifier).

Among all the produced algorithm setups – varying in selected features and strategy of clipping (the studies were made with different clipped and unclipped features) –, the one with the best combination of f-measure (Fm), SE, SP and FPRh was picked. On this one, several distance metrics, as in [19], were applied, in order to verify if the most signifying option had been chosen.

5.4. Results and Discussion

Table 12, Table 13 and Table 14 compile the most significant results achieved, as well as Table 16, Table 17 and Table 18. The results in Table 12 were extracted from Table 26 of Appendix D. Table 27 and Table 28 of Appendix D give insight about the processes that led to the results in Table 14 and Table 18.

Table 12 shows the ranking order of the chosen features (with FSS>50%). Few features that were studied for the very first time (among this thesis and the works of Couceiro *et al.* [11, 19, 20]) fulfilled this condition. In fact, only $pNN50_{HY}$, PR_{HY}, *b/a* and $SDSD_{HY}$ were selected to Table 12 and none of them achieved even the five highest rated features.

Except for PR_{HY}, the mentioned PRV features ($pNN50_{HY}$ and $SDSD_{HY}$) achieved better scores than both their original normalized parameters (pNN50 and SDSD) and parameters' changes on 90 sec windows (ΔpNN50 and ΔSDSD), highlighting the importance of analyzing new features when studying new approaches to such an algorithm. In Chapter 4, it was denoted that the PPG signal's proneness to artifacts influences negatively the extraction of PRV indexes when comparing to HRV, especially in those related with higher frequencies. This may explain the lack of prediction capability of these features in the current system, in contrast with [20], where some HRV indexes enhanced the behavior of the algorithm (in [20], these indexes were based on ECG). PR direct features (PR and ΔPR) are the only PRV-related ones that

positively contribute to this algorithm with FSS>59%, following the conclusion of Chapter 4 that PR was the PRV index most similar to the one of HRV (the HR).

Besides showing that PR was a good surrogate of HR, Chapter 4 demonstrated that SDNN was one of the most accurate PRV indexes. In agreement with these findings, ΔPR, PR and SDNN were selected as suitable syncope predictors in 2nd, 4th and 6th places of the FSS list, as presented in Table 12.

Table 12 – Selected features to embed in the algorithm, ranked by their FSS, with FSS>50%.

Rank	Feature (FSS, %)	Rank	Feature (FSS, %)	Rank	Feature (FSS, %)
1	SI (91.8)	6	SDNN (56.9)	11	$SDSD_{HY}$ (51.7)
2	ΔPR (79.4)	7	$pNN50_{HY}$ (55.1)	12	ΔaVL (51.2)
3	ΔSI (60.0)	8	RI (55.0)		
4	PR (59.9)	9	PR_{HY} (53.6)	13	Δ*Mean* (51.1)
5	ΔLVET (57.5)	10	*b/a* (51.8)		

Table 13 – Features that were applied in the algorithm setups of Table 14. The trained threshold is also shown. The distance metric used for classification was Minkowski, $p=2^{-0.5}$.

n	Features Description	Threshold
1	SI (clipped), ΔPR, ΔSI, PR, ΔLVET, RI, LVET	4.405
2	SI, ΔPR, ΔSI	1.280
3	SI, ΔPR, ΔSI, PR, ΔLVET, RI, LVET	4.305
4	SI (clipped), ΔPR, ΔSI, PR, ΔLVET, RI	3.536
5	SI (clipped), ΔPR (clipped), ΔSI, PR, ΔLVET, RI	3.320
6	SI (clipped), ΔPR, ΔSI	1.165
7	SI, ΔPR, ΔSI, PR (all clipped)	1.412

Table 14 – Performance of the best scored algorithm setups. The applied features are described in Table 13.

	Test					Validation		
n	Fm (%)	SE (%)	SP (%)	FPRh (h^{-1})	PTime (sec)	SE (%)	SP (%)	FPRh (h^{-1})
1	86	100	85	1.9	242.3 ± 226.9	72.67 ± 2.98	93.67 ± 2.84	0.15 ± 0.11
2	86	100	85	2.05	360.0 ± 297.5	70.00 ± 7.01	77.67 ± 4.60	0.82 ± 0.22
3	80	100	77	2.2	368.8 ± 285.96	70.00 ± 3.42	89.83 ± 2.75	0.23 ± 0.06
4	80	100	77	2.34	345.8 ± 306.7	68.67 ± 4.88	82.17 ± 4.87	0.75 ± 0.31
5	80	100	77	2.64	210.7 ± 214.2	72.67 ± 4.27	81.33 ± 3.13	0.75 ± 0.22
6	80	100	77	2.93	363.1 ± 297.6	79.67 ± 4.03	77.50 ± 3.22	0.94 ± 0.15
7	80	100	77	1.46	190.9 ± 211.7	93.33 ± 0.00	80.17 ± 2.02	1.15 ± 0.17

As for the SDPPG features, *b/a* is the only one that exhibits FSS greater than 50%, which may be explained by its association with arterial elastic properties in aortic stiffness and in carotid and peripheral artery compliance [83].

CT and VR features, on their side, showed no major contribution to the prediction of syncope, exhibiting a low FSS. Nevertheless, these parameters are linearly derived from two PPG characteristic points, whose information is already embedded in some of the highest rated features, like the PR-related ones.

The ID framework revealed to be more useful when applied to calculated parameters than to the PPG signal itself, and the only ID function presented in Table 12 is the *SysInfor* applied to some parameters (corresponding to the entropy of the approached parameter). In physiological contexts, this framework has been used more in bivariate/multivariate systems, illustrating nuances between several interactions [13, 101, 103, 104, 102], which may have influenced these results (here, it was applied in a univariate setting, since the ID functions were computed over standalone features' series).

The signal window to derive these ID parameters may also play a role because of the captured dynamics. In fact, time windows of 10, 20, 30 and 40 sec were tested as possible choices, through the calculation of their correlation with the binary output of existence or non-existence of impending syncope. This operation (results in Table 15) proved that the 10-sec window interval achieved better correlation, being chosen to the algorithm.

Table 15 – SRC between ID features calculated in different time windows and the output of the HUTT test on impending syncope.

Window Size	**SysInfor** ***(p-value)***	**UnexpInf** ***(p-value)***	**InfStor** ***(p-value)***	**ΔSysInfor** ***(p-value)***	**ΔUnexpInf** ***(p-value)***	**ΔInfStor** ***(p-value)***
10 sec	-0,328 *(0.000)*	0,138 *(0.000)*	-0,381 *(0.000)*	-0,051 *(0.000)*	0,002 *(0.471)*	-0,050 *(0.000)*
20 sec	-0,172 *(0.000)*	0,117 *(0.000)*	-0,218 *(0.000)*	-0,050 *(0.000)*	0,008 *(0.011)*	-0,059 *(0.000)*
30 sec	-0,330 *(0.000)*	0,057 *(0.000)*	-0,342 *(0.000)*	-0,102 *(0.000)*	-0,028 *(0.000)*	-0,102 *(0.000)*
40 sec	-0,290 *(0.000)*	0,066 *(0.000)*	-0,336 *(0.000)*	-0,061 *(0.000)*	-0,036 *(0.000)*	-0,057 *(0.000)*

Getting back to the top 5 scored features, it is seen that the presented indexes are the same that were already identified as the studied potentially most valuable PPG-related predictors for syncope [11, 20]. But there is a notorious difference between the performance of the first two features and the rest of them. SI and ΔPR are actually the only indexes showing, respectively, FSS>90% and FSS>78%. All the other features exhibit FSS<61%.

Despite SI and ΔPR being, by far, the most important features for syncope prediction, expanding the set of evaluated features may improve the interpretability of the algorithm and its diagnostic value. Because of this, it must be noticed that the 13 selected features will eventually provide much more information than just the first two. Although the intervals of FSS are very similar between the 3^{rd}/4^{th} ranked features and the least ones (<10%), the bigger is the number of physiologically meaningful features, the bigger may be its diagnostic value.

Table 13 and Table 14 refer to the performance of some algorithm setups, listing the ones with better results (the others performed similarly or worse), in a decreasing order of the tests' Fm and in an increasing order of the validations' FPRh. The outcomes achieved here confirm the ones reported in [11], being unable to surpass the results of the ECG/PPG-based algorithm.

However, the PPG-based algorithm of [11] presents, in the validation phase, SE=65.3%, SP=94% and FPRh=0.14, and, in the test phase, SE=83.3%, SP=76.9%, FPRh=1.03 and PTime=238.6±185.1 sec. Through the comparison of these results with the ones in Table 14, it is seen that SE was highly increased, with SE=100% in the test phase of all the attempts and SE ∈ [68.67; 93.33] % in the validation phase. SP maintained similar values, with slight improvements and losses, considering the both phases: validation with [77.50; 93.67] % and test with [77; 85] %. PTime registered a range of [190.9; 368.8] sec, which contains the previous value of [11]. As for the FPRh values, only the first (n=1) measure presented in Table 14 was able to perform approximately as good as in [11], being 0.15 h^{-1} in the validation set and 1.9 h^{-1} in the test set. Except for the 7^{th} attempt (validation: FPRh=1.15 h^{-1}; test: FPRh=1.46 h^{-1}), all the others achieved FPRh<0.83 h^{-1} in the validation phase and underperformed in the test phase, always with FPRh>2 h^{-1}.

It seems that the enhancement of SE leads to some loss in FPRh, since these were the most divergent indicators between this study and the one in [11]. Furthermore, as the rate of true positives (SE) increases, it is normal that some false positives are also detected, diminishing the values of FPRh. This is an important balance to achieve, since the missing of a positive target in such a real-time classifier may lead to a potentially dangerous situation, but a high rate of frequent false positive alarms, in a daily life p-health system, is not desired, since it tends to reduce the user's compliance to the system.

The 2nd, 6th and 7th records, with only three and four embedded features, confirm the idea that just the parameters of SI and/or PR would often be sufficient to provide a decent syncope predictor, since all the features of these records are derived from them. The 7th record, only with four clipped features, is, in fact, the one with higher validation SE and SP, as well as lower test FPRh, in spite of presenting the worst values of PTime and validation FPRh. Records 2 and 6 only differ on the clipping of SI, but this revealed sufficient to increase the PTime in 3.1 sec and the validation SE in 9.67%, from the 2nd to the 6th register. Yet, the FPRh increased in 0.12 h^{-1} (validation) and 0.88 h^{-1} (test), in the opposite direction (from the 6th to the 2nd record).

Regarding the records 1, 3, 4 and 5, the first two use seven features, whereas the last two use six features. The only variables that change between them are the presence of the feature LVET and the features that are clipped. The 4th and 5th setups vary exclusively on the clipping of ΔPR, which was enough to decrease 135.1 sec in PTime and increase 0.30 h^{-1} in the test FPRh, but with an improvement of the validation SE in 4% (from 4th to 5th). The records 1 and 3, diverging merely on the clipping of SI, are the ones setting more features in and the ones with the lowest validation FPRh (1st: 0.15 h^{-1}; 3rd: 0.23 h^{-1}). Despite presenting less 126.5 sec of PTime, the 1st record has more interesting values of Fm, SE, SP and FPRh, in both the validation and test sets.

In a global perspective, the collected results indicate that the choice of features to embed in the algorithm is determinant, more than the clipping of values non-related to syncope. It is, therefore, expected that the improvement of its performance will depend mostly on the finding of other predictive features with FSS values similar to the ones of SI and ΔPR.

The feature LVET was included in the 1st record of Table 13 and Table 14, even though it was not one of the features suggested by the FSS ranking in Table 12. However, LVET illustrates myocardial contractility, being an important inotropic evaluator and indirectly associated with BP (although not following a linear relation with it). Moreover, its direct correlation with the training output was significant, leading us to embed it in some of the presented setups, despite the FSS ranking results. In fact, the 1st measure presented in Table 13 and Table 14, whose results were already highlighted, embeds LVET and is presented as the record that achieves a more interesting balance between the performance metrics, to be applied in a real-life system.

As suggested in the previous section 5.3, some of the features in Table 13 and Table 14 were clipped (SI, ΔPR and ΔSI). SI is, contrarily to the rest of the parameters, a direct estimator of the PTT and, consequently, of the BP (which explains its high FSS). To predict a syncope event, it is necessary to detect hypotension, which is illustrated by an increase in the SI curve. As distance metrics are symmetrical to the origin of the referential, the clipping of the decreasing points of the curve allows to focus on the increase of this feature, easing the distinguishing of impending syncope. Moreover, with the increase of BP, the detection of the characteristic points necessary to estimate SI can be severely compromised, leading to a higher uncertainty in the estimation of this parameter. Therefore, clipping lower SI values may also contribute to a better prediction capability of this feature. Concerning the PR, the prediction of a syncope is associated with a decrease in its signal, so, the clipped changes are the ones of increasing tendencies.

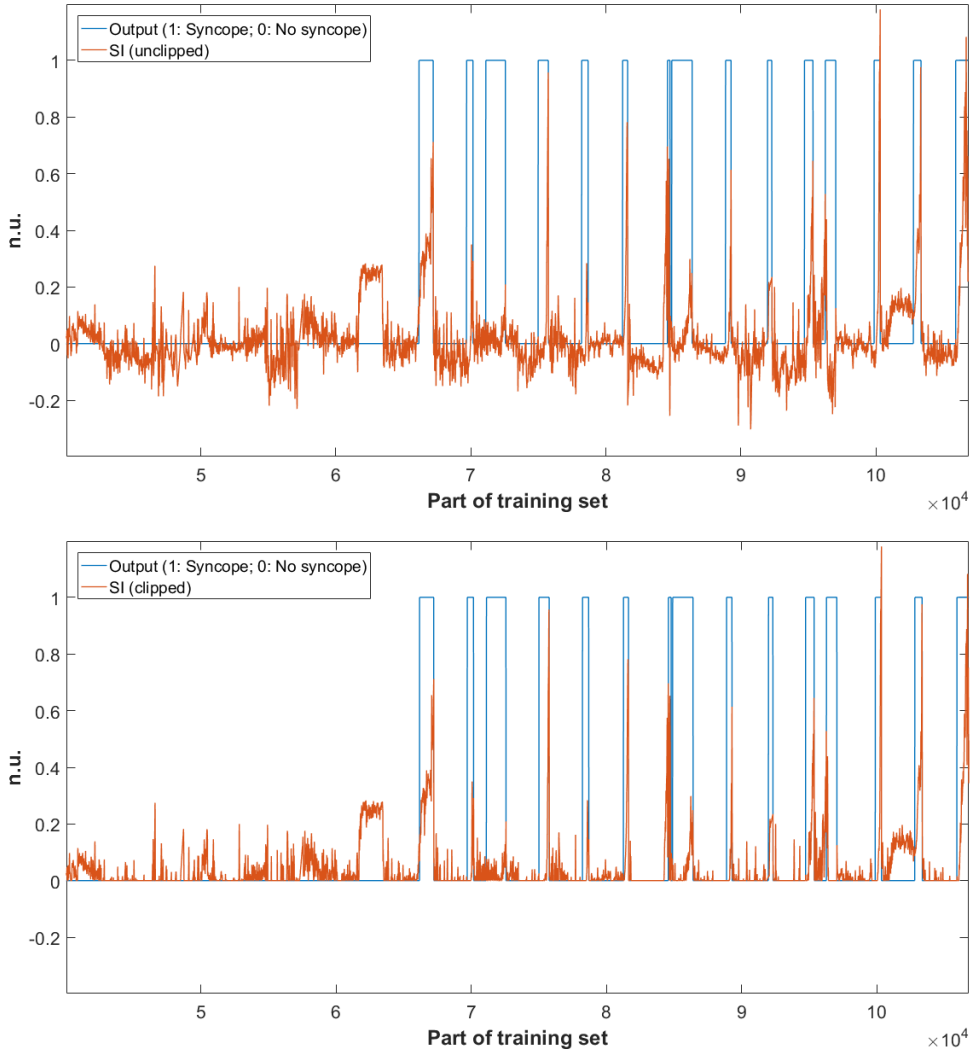

Figure 33 – Difference between unclipped SI (top) and clipped SI (bottom), and their relation with part of the training output (all the PO patients are presented, but some NE subjects were removed, for better visualization).

To verify that the Minkowski distance with exponent $p=2^{-0.5}$ kept being the most indicated classifier metric despite the proposed changes, all the distance metrics presented in [19] were applied to the 1st algorithm setup presented in Table 13 and Table 14. In fact, as in [19], considering Fm, SE and SP, any other distance metric performed as well as this one, as proven in Figure 34.

Other types of classifiers are not considered, since the focus of the task is to work on a simple classifier capable of achieving satisfying performances in p-health settings, not only in terms of the accuracy of the prediction, but also in terms of minimizing the consumption of time and resources to make the computation [14]. Distance metrics are, therefore, the ideal tool to apply.

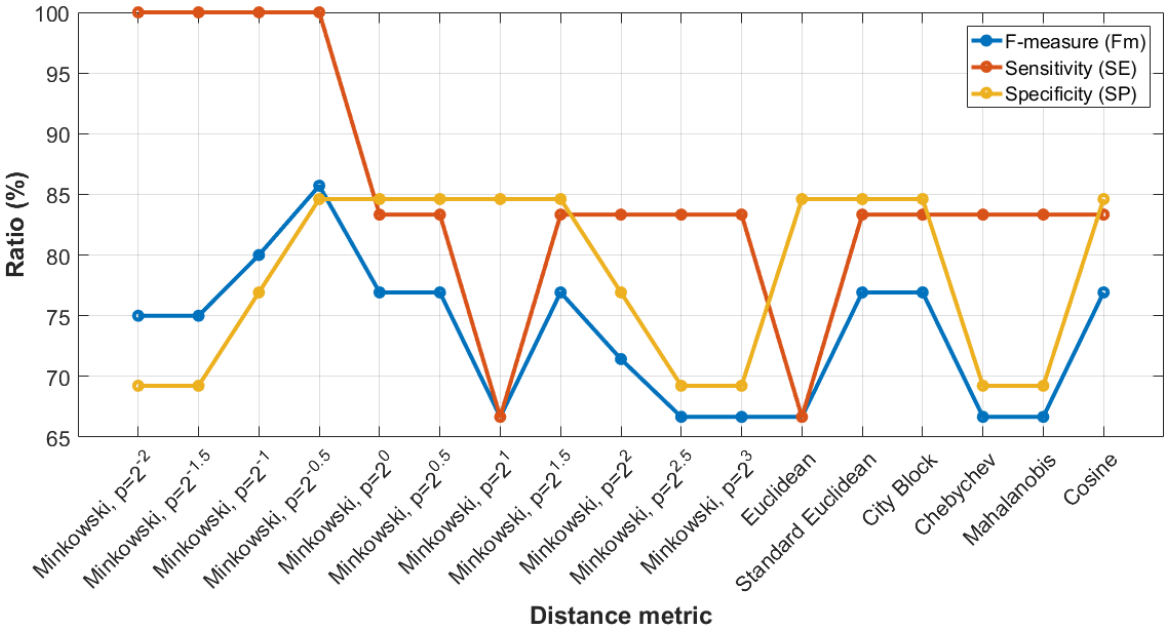

Figure 34 – Comparison of Fm, SE and SP between the evaluated distance metrics.

As mentioned in subsection 5.3.2.a), in order to undoubtedly verify that PPG_{onset} was the better option to derive PR and PRV parameters, the syncope prediction algorithm was also studied using other PPG characteristic points to extract these indexes. The approached characteristic intervals were the same of Chapter 4, as seen in Table 16.

Table 16 shows that the first six features with higher FSS are the same for every PPG characteristic points, slightly changing the order between themselves. Moreover, SI and ΔPR remain as the first two features with the best FSS, being the only indexes showing, correspondingly, FSS>90% and FSS>75%. Except for ΔSI in PPG_{der} (FSS=68.2%), all the other features have FSS<61%.

Table 16 – Comparison between the FSS-rank of the selected features, using different intervals of PPG characteristic points to derive PRV parameters. Only features with FSS>50% were selected (the ones here presented).

Rank	PPG_{onset} (FSS, %)	$PPG_{20\%}$ (FSS, %)	PPG_{der} (FSS, %)	$PPG_{50\%}$ (FSS, %)	$PPG_{80\%}$ (FSS, %)	PPG_{peak} (FSS, %)
1	SI (91.8)	SI (91.8)	SI (91.8)	SI (91.8)	SI (91.8)	SI (91.8)
2	ΔPR (79.4)	ΔPR (78.0)	ΔPR (77.3)	ΔPR (76.8)	ΔPR (79.5)	ΔPR (80.1)
3	ΔSI (60.0)	SDNN (60.7)	ΔSI (68.2)	SDNN (60.4)	ΔLVET (59.8)	ΔLVET (59.9)
4	PR (59.9)	PR (60.5)	PR (61.1)	PR (60.3)	PR (59.6)	ΔSI (59.9)
5	ΔLVET (57.5)	ΔSI (60.0)	SDNN (61.1)	ΔSI (60.0)	ΔSI (59.6)	PR (59.0)
6	SDNN (56.9)	ΔLVET (60)	ΔLVET (60.2)	ΔLVET (60.0)	SDNN (59.0)	SDNN (56.2)
7	$pNN50_{HY}$ (55.1)	RI (55.7)	$RMSSD_{HY}$ (55.1)	$RMSSD_{HY}$ (56.4)	$NN50_{HY}$ (55.8)	RI (54.6)
8	RI (55.0)	$pNN50_{HY}$ (52.6)	RI (54.9)	RI (55.2)	RI (54.8)	$SDSD_{HY}$ (53.4)
9	PR_{HY} (53.6)	*b/a* (50.9)	*b/a* (52.1)	*b/a* (51.0)	*b/a* (50.5)	*b/a* (51.5)
10	*b/a* (51.8)	---	---	---	---	---
11	$SDSD_{HY}$ (51.7)	---	---	---	---	---
12	ΔaVL (51.2)	---	---	---	---	---
13	Δ*Mean* (51.1)	---	---	---	---	---

Table 17 – Features and PPG intervals that were applied in the algorithm setups of Table 18. The trained threshold is also shown. The distance metric used for classification was Minkowski, $p=2^{-0.5}$.

n	PPG interval	Features Description	Threshold
1	$PPG_{80\%}$	SI, ΔPR, ΔSI, PR, ΔLVET, RI	3.652
2	$PPG_{80\%}$	SI, ΔPR, ΔSI (all clipped)	1.144
3	PPG_{peak}	SI, ΔPR, ΔSI (all clipped)	1.133
4	$PPG_{80\%}$	SI, ΔPR (all clipped)	0.606
5	PPG_{der}	SI, ΔPR, ΔSI (all clipped)	1.136
6	$PPG_{80\%}$	SI (clipped), ΔPR (clipped), ΔSI, PR, ΔLVET, RI	3.366

Table 18 – Performance of the best scored algorithm setups. The applied features are described in Table 17.

	Test					Validation		
n	Fm (%)	SE (%)	SP (%)	FPRh (h^{-1})	PTime (sec)	SE (%)	SP (%)	FPRh (h^{-1})
1	86	100	85	2.05	221.1 ± 236.3	78.00 ± 3.13	93.33 ± 0.00	0.40 ± 0.04
2	80	100	77	2.93	246.1 ± 209.3	90.00 ± 5.51	86.67 ± 0.00	0.37 ± 0.01
3	80	100	77	3.08	246.3 ± 209.8	91.00 ± 4.47	85.17 ± 1.70	0.39 ± 0.06
4	80	100	77	2.49	207.8 ± 212.5	88.33 ± 6.44	85.67 ± 1.90	0.57 ± 0.12
5	80	100	77	3.22	246.0 ± 209.2	90.67 ± 4.54	86.50 ± 0.75	0.61 ± 0.03
6	80	100	77	2.34	210.2 ± 214.4	80.00 ± 0.00	84.83 ± 2.29	0.62 ± 0.12

This fact also suggests that the operated PPG characteristic point has, to this end and with this evaluation method, a limited influence, even for clearly PR-related features. ΔPR shows a variation of less than 3% among all the characteristic intervals,

strengthening its position as the second best indicator for syncope. The discrepancy in PR is even smaller (~2%). For SDNN, the difference increases to ~5%. This also goes along with the conclusions of Chapter 4, pointing out PR as a truthful surrogate for HR, as well as SDNN as one of the most accurate PRV indexes (although in a less extent than PR).

Table 16 also leads to the observation that PPG_{onset} provides much more physiological information with the condition of FSS>50% (13 selected features) than the other characteristic points (9 features). This is a curious fact that remarks the importance of this comparative evaluation.

Concerning Table 17 and Table 18, it is seen that, although the performed analysis described in section 5.3.3 was repeated for all the listed characteristic points, $PPG_{20\%}$ and $PPG_{50\%}$ did not produce sufficiently satisfying results to be shown in this discussion. In fact, only examples using PPG_{der}, $PPG_{80\%}$ and PPG_{peak} are presented. In addition, the features that produced better classifiers (being clipped or unclipped) remain the same of PPG_{onset}, without any enhancement in any PRV index.

It is noticed that there are some records in Table 18 achieving better validation values than the records in Table 14, both in terms of SE, SP and FPRh. However, in the test phase, the FPRh and PTime of the records in Table 14 is generally better. Furthermore, the only record in Table 18 that achieves Fm=86% (as the 1^{st} and 2^{nd} measures of Table 14) is the 1^{st} one, and this underperformed in terms of FPRh, comparing to the 1^{st} setup of Table 14.

5.5. Conclusion

The work in this chapter proposes a PPG-based algorithm to predict impending syncope events in real time, in a p-health context.

Several parameters and their combinations were studied: PR, LVET, SI and RI, as well as parameters related with PRV, SDPPG, the systolic rise of PPG pulses and ID. The complete set of extracted parameters produced 94 features. The effects of applying a clipping operation to the features, as well as applying different distance metrics, were

also approached. The usage of different PPG characteristic points to derive PRV indexes was also evaluated.

In all the cases, the followed procedure was the same, in order to produce a valid comparison. The most relevant features to predict syncope were selected based on their FSS. The algorithm was fed and validated with the selected features, evaluating which combination of features was the most suitable one to predict syncope.

In each case, this assessment was made using a previous training/validation phase that produced an optimal threshold. This threshold was used as classifier, after applying the Minskowski distance ($p=2^{-0.5}$) with the chosen features. This method was confirmed as the most suitable distance metric to this end.

Despite the interesting number of evaluated records that produced interesting results (motivated by the numerous setups that were tested), PPG_{onset} was considered the best PPG characteristic point to extract PRV parameters to predict syncope.

Not having the ECG as a source and the consequent absence of PAT-related features weakens the PPG-based algorithm, and this drawback was not possible to overcome. However, our results had an overall positive evolution, comparing to the PPG-only suggestion in [11].

For application in a daily life scenario, at this point, we propose the use of any of the options shown in Table 14, but we emphasize the better results of the 1st record over the others, especially in its FPRh and for being one of the two listed options that use more features. This setup resorts on PPG_{onset} and on the Minskowski distance ($p=2^{-0.5}$), and uses the following features: SI (clipped), ΔPR, ΔSI, PR, ΔLVET, RI, LVET. Its optimal threshold is: ~4.236.

This work showed promising results on the PPG-based prediction of syncope, proving the importance of the careful investigation of features on the development of such algorithms. However, to be applied in a real-life scenario, this approach still requires some evolution. The detection of motion artifacts in the PPG signal is a key point in this, since the algorithm achieves such hopeful performances after an algorithmic noise detection that can be easily enhanced, for example, with the collection of a synchronized acceleration signal. Moreover, as this is a real-time algorithm and all its training, validation and test were done offline, an online approach is recommended, as well as the extent of the used dataset.

The use of another body site to acquire the PPG signal must also be a subject of investigation, since the fingertip does not provide a maximal comfort to the user, nor decreases the collection of motion noise. As seen in section 3.4, the wrist-worn devices that are widely distributed nowadays are a very interesting option.

In spite of all the considerations, the use of the proposed algorithm with a fingertip PPG sensor seems already reasonable in some specific p-health contexts, in which the fingers do not move much (avoiding motion artifacts and discomfort to the user). This concerns the monitoring, for example, of all sorts of drivers. In fact, an impending syncope prediction system can be very useful to all people that spend a lot of time travelling by car or motorcycle, and even more to public and merchandising drivers (in any kind of transportation), as well as to operators of heavy machinery and military drivers.

Moreover, the algorithm applied in systems for the elderly could prevent many cases of falls, which are, as demonstrated in Chapter 1, a major problem in such ages. This sort of application, however, requires a deeper work on the treatment of typical artifacts on the PPG signal, as suggested in Chapter 4.

Chapter 6

Concept Demo Application to Predict Syncope with Photoplethysmography

This chapter approaches the development of a software system as proof of concept that applies the knowledge described throughout this thesis, in order to predict impending syncope in real time and alert the user before an event. To that end, the algorithm setup emphasized in section 5.5 was applied in this system.

The need for such a system is easily justified with the number of losses of consciousness and falls that it could prevent in m-health contexts. In fact, as stated in section 3.3, some simple physical countermaneuvers (operated by the subject himself or by others) are known to avoid the oncoming occurrence of syncope, as well as to prevent falls (as the simple act of laying down). However, these maneuvers can only be successfully operated if the impending event is spotted early (which is often impossible to analyze only through visible symptoms).

Furthermore, the algorithm was developed over a set of subjects during HUTT tests, and the real-time acquisition was mimicked on the already saved signals. The development of this system provides an opportunity of getting signals from real-life scenarios, in true real-time conditions, which is more useful to the investigation of the algorithm.

6.1. Requirements' Analysis

This analysis comprises the description of the functional, non-functional and technological requirements to construct the system. The listed requirements in the sections below were prioritized using the MoSCoW method, which classifies each requirement in one of four categories [161]:

- Must have (M): the requirement has to be satisfied in the final acceptable solution;
- Should have (S): the condition shall be considered if possible, but workarounds are available since this is not a critical functionality;
- Could have (C): the requisite is desirable if allowed by time and available resources, but the final solution is fully accepted without it;
- Would have (W): the functionality is of the lowest level of priority, and its release can be postponed for latter attention.

6.1.1. Functional Requirements

The aim of this thesis concerns on the evaluation of data and algorithms related with PPG, and not on software engineering. Given this fact, this system serves only as a proof of concept with the basic functionalities for this purpose. Because of this, no further operational settings were specified, as stated in Table 19 (for example, the construction of supporting databases or the integration with other services).

This system is a concept demo final solution, so, it does not support the training of the algorithm, only applying the chosen setup of computation.

Table 19 – Identification and prioritization of the functional requirements mapped in Figure 35.

Identifier	Functional Requirement	Priority
FR.1	The system measures a PPG signal to detect impending syncope events.	M
FR.2	If a syncope episode is predicted, the system produces a warning/alert.	M
FR.3	The measurement is continuous and in real-time.	M
FR.4	If no syncope is detected, the system does not change any state by itself.	M
FR.5	The user decides when to start and stop the measurement.	M
FR.6	The data recorded by the system can be consulted after the measurement.	S
FR.7	All the values in the database are downloadable to a CSV file.	S
FR.8	The system shows graphical information about the performed measures.	C

6.1.3.a) Use case

The use of the system and its operational flow is also simple and easily understood, as shown in Figure 35. In fact, this sums up all the possible actions in the system.

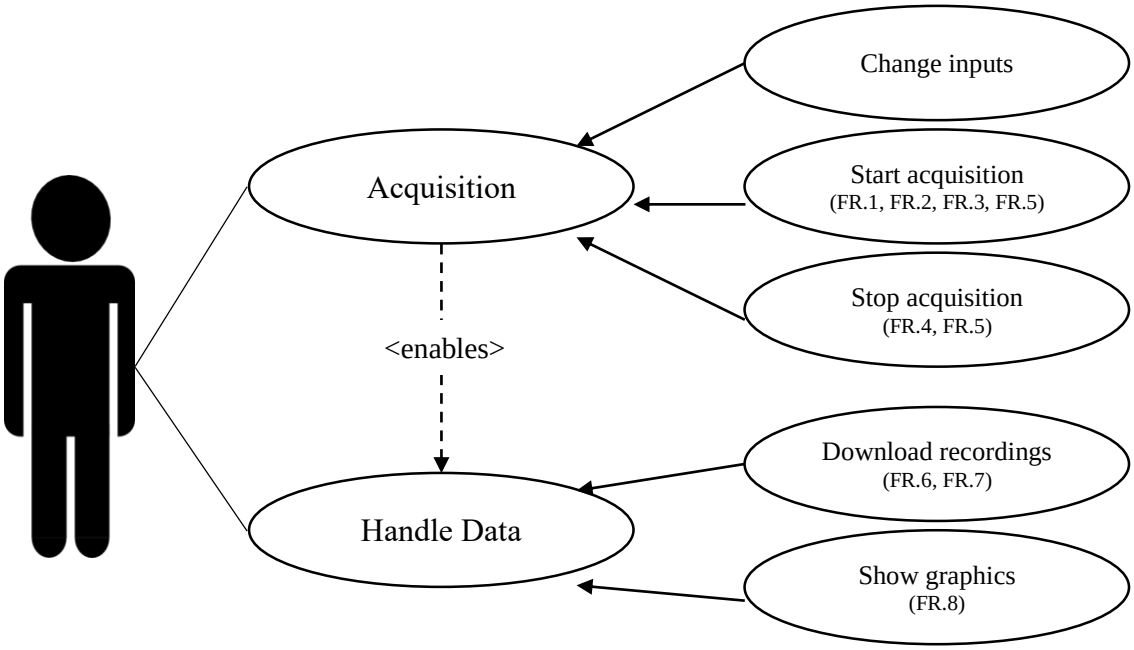

Figure 35 – Use case of the syncope prediction system, referencing the related functional requirements (Table 19).

6.1.2. Non-Functional Requirements

Despite the different priorities, the requirements in Table 20 were identified as the required ones to perform the necessary actions to demonstrate the functionality of a complete system. In this way, all these conditions were planned as milestones since the planning of this step of the project.

Table 20 – Identified and prioritized non-functional requirements.

Identifier	Non-Functional Requirement	Priority
NFR.1	The measurement of the PPG signal is made with a third-party p-health hardware device.	M
NFR.2	The processing of the signal is made in other hardware, more suited to processing information.	M
NFR.3	The user interface is of easy handling and self-explicative.	M
NFR.4	The warning/alert of impending syncope is given with a visual indication.	M
NFR.5	The binary indication of existing or non-existing danger of syncope is given, respectively, with a red and a green sign.	S
NFR.6	The acquiring/stopped states of the system are easily understood in the user interface.	S
NFR.7	The collection of data is performed since the user orders the beginning of an acquisition, until he manually stops it or a problem is detected (for example, absence of connection or a raw termination of the application).	M
NFR.8	Features' values are computed/updated in intervals of 10 seconds.	M
NFR.9	The system must be prepared for p-health settings.	M
NFR.10	System’s coding allows its simple adaptation and improvement.	S

6.1.3. Technological Requirements

The choice on the technologies to support the developed application – see below and in Table 21 – is based on the considerations from section 3.4.

To achieve the goal of the application, it is required to access the raw PPG signal acquired by the selected device. However, for technological protection, most of the devices only output the computed HR. In fact, from the highlighted devices, only Empatica E4® and biosignalsplux® provided the access to raw data, so, the choice of support hardware had to be between these two options. In spite of the motivation on studying a wrist PPG system like the E4®, the cost of biosignalsplux® was much more interesting (as well as the possibility of applying different sensors in future works beyond the scope of this thesis).

Table 21 – Identified and prioritized technological requirements.

Identifier	Technological Requirement	Priority
TR.1	The hardware used for PPG collection is the biosignalsplux®, consisting of a central hub with a plugged fingertip PPG sensor, by PLUX®.	M
TR.2	The processing station is compatible with a biosignalsplux® API, which comprises PCs running Microsoft Windows® and/or smartphones running Android®.	M
TR.3	The communication protocol between the processing station and the biosignalsplux® hub is Bluetooth Class II®.	M
TR.4	The processing station supports Bluetooth Class II® (either built-in or externally plugged).	M

Both PCs running Microsoft Windows® and smartphones running Android® were options as processing stations, since biosignalsplux® provides APIs compatible with these systems. However, despite the fact that the use of a smartphone would improve the m-health ability of the system, these devices are not prepared to run MATLAB® efficiently. For this reason, and since all the processing routines of the algorithm were implemented in MATLAB® (and given that a full adaptation to other language was not doable), the chosen processing platform was a Windows® PC, through Java® (which provides tools to interact both with MATLAB® and with biosignalsplux®).

6.2. Design

6.2.1. Architecture

Given the simplicity of the solution, its architecture is also easily understood, as depicted in Figure 36. It includes the Bluetooth® communication layer between both terminals (biosignalsplux® transmitting data to the PC). All the subsequent operations are done in the PC, and consist of a front-end Java® layer and a back-end MATLAB® layer. The first is responsible for communicating with biosignalsplux® (continuously asking for and receiving data and controlling the begin and end of the acquisitions) and interacting with the user (receiving inputs and showing outputs), working as a wrapper of the second one. The MATLAB® layer processes the received PPG signal, applying the algorithm to predict impending syncope (it returns a binary classification and all the computed features to produce it).

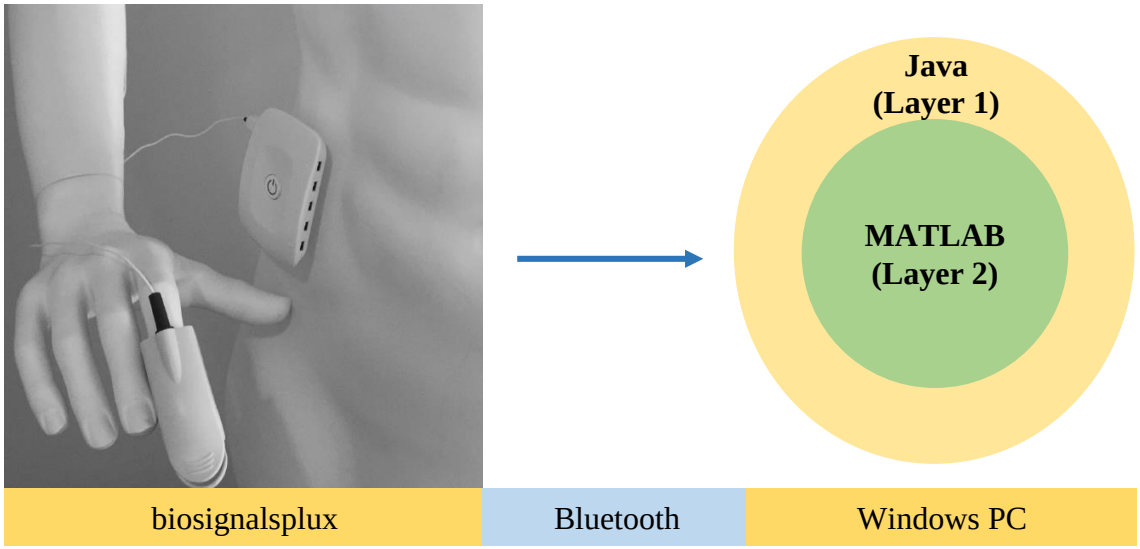

Figure 36 – Architecture of the real-time syncope prediction system. Image of biosignalsplux® in [162].

6.3. Implementation

6.3.1. Java® layer

The Java® layer of the created software in the processing station (the PC) establishes the front-end of the program and allows the integration of all the three

dynamics of the software: the acquisition device (biosignalsplux®) connected via Bluetooth®, the back-end layer on MATLAB® compiled to Java® and the user interface (built in Java®).

The main thread of the program corresponds to the user interface, which is opened when the software is run. This comprises a single window with two tabs: the first tab ("Detect your Syncope") allows all the user interaction (Figure 38), whereas the second one ("Help!") consists of a description concerning the system (Figure 37). The interface was partially designed in NetBeans® IDE 8.2. All the remaining Java® tasks were developed with Eclipse Mars®.

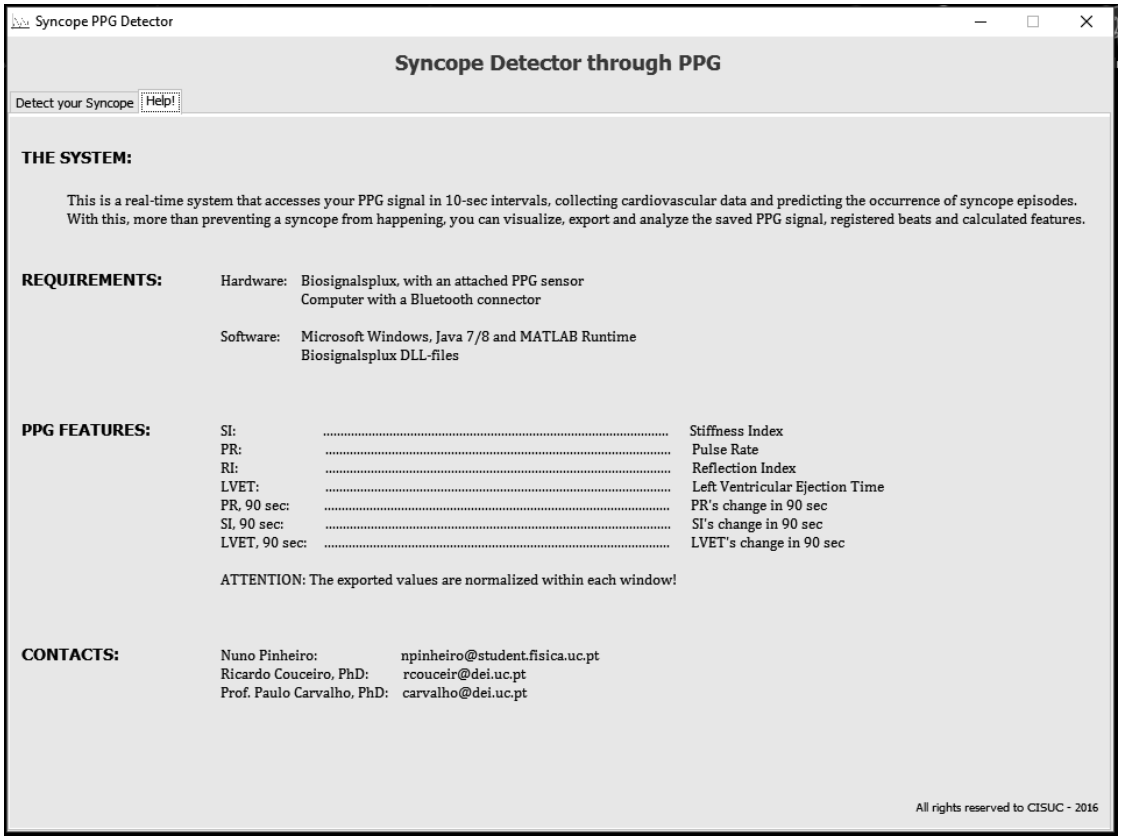

Figure 37 – "Help!" tab with the instructions of the application.

The "Detect your Syncope" tab enables the definition of all the inputs to the program: biosignalsplux® port, channel of the hub linked with a PPG sensor, sampling frequency of acquisition, number of bits and file names to export CSV files with performed measures. Moreover, it allows the viewing of graphical information about the extracted features and signals (in a separate window), and it retrieves all the output information (visual signs with the prediction of impending syncope and written messages about the system). It also allows the order of starting/stopping acquisitions, as well as exporting CSV records – Figure 39 and Figure 40. If any error occurs, it is

shown in the messages panel (except for user errors with inputs, which are shown in pop-up windows).

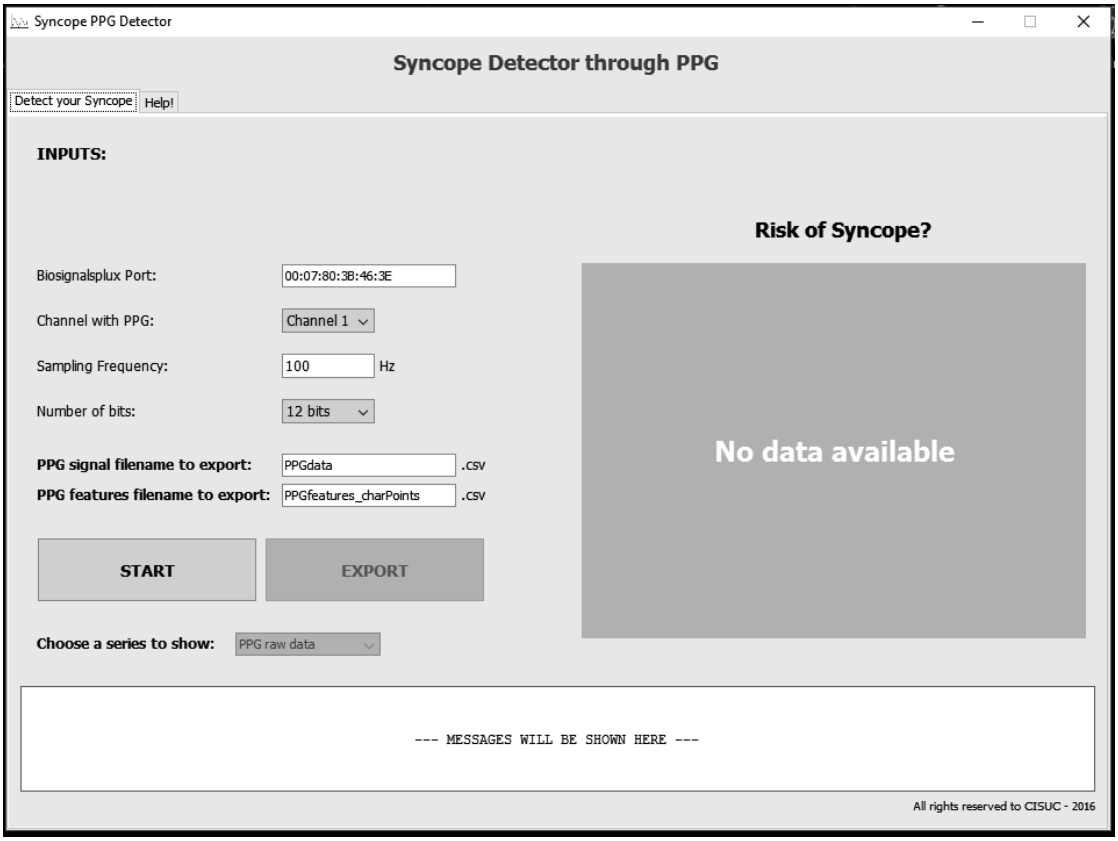

Figure 38 – Initial state of the "Detect your Syncope" tab, allowing the changing of inputs and the start of an acquisition.

The order to start an acquisition will open a parallel thread that firstly initiates the MATLAB® sources in back-end. This step takes some time and was a complicated issue to understand and solve during development, since the absence of such initialization puts a huge delay in the processing of the compiled MATLAB® functions, which is not compatible with a real-time system.

After the mentioned initialization, the thread proceeds to connect with the requested biosignalsplux® device. This is done with the creation of a new instance to an object Device, with the desired port identifier (defined by the user). Then, a real-time acquisition is started with the calling of the method *BeginAcq*, which opens a new thread that allows the communication of the measures performed by the device to the PC. These measures are saved in a temporary memory of the device's hub, and the PC fetches the desired amount of values (in this case, 10-sec windows of values) every time the method *Frame.GetFrames* is called. If there are not enough values in memory, the

system waits until its acquisition. All the mentioned structures belong to the biosignalsplux® Java® API (*plux.newdriver.bioplux*), embedded as a JAR file [163].

After the described acquisition, the PPG signal is passed into the MATLAB®, where it is fully processed to return a binary prediction of occurrence or non-occurrence of impending syncope (see next section 6.3.2). This loop is repeated until the user orders its stopping or until some fatal error occurs.

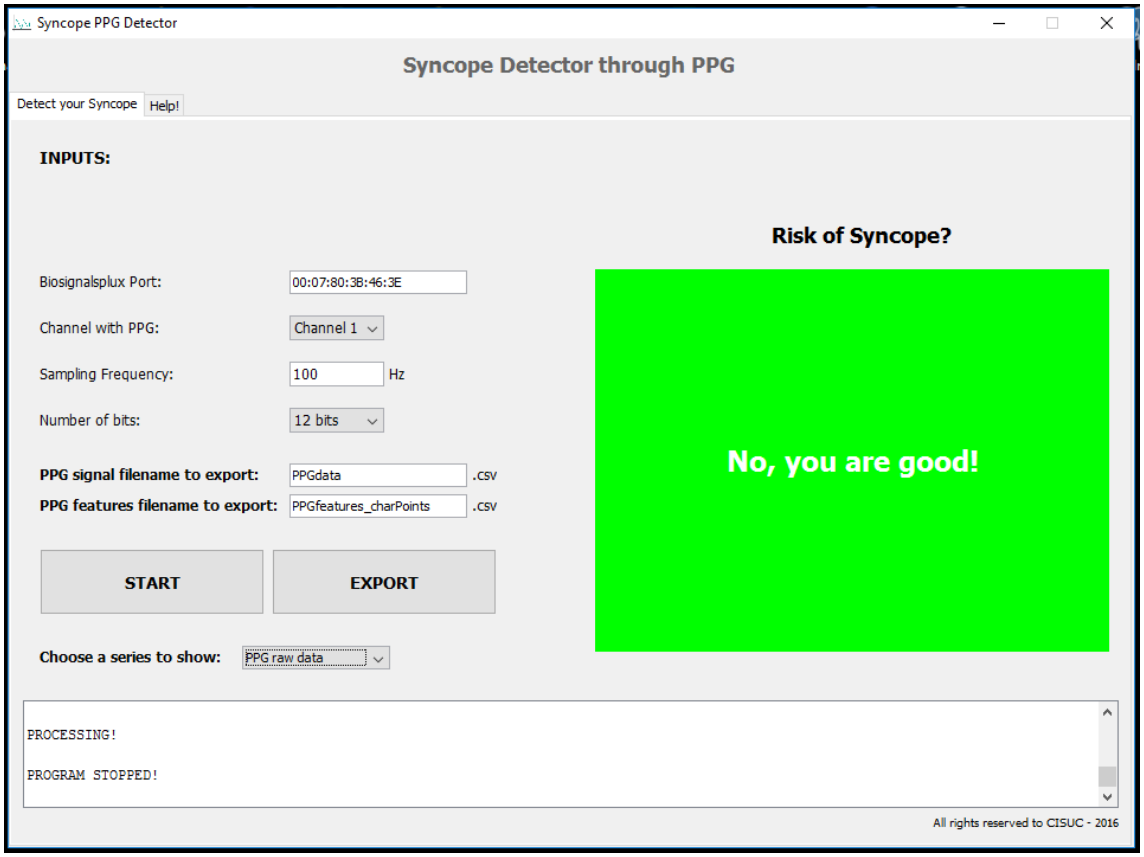

Figure 39 – Acquiring mode of the application, with the information of no impending syncope, allowing the options of exporting data and showing graphical information.

The specified dynamic requires much control in the flow of information between the biosignalsplux® hub and the processing station in the PC.

On one hand, the communication channel may fail to broadcast some measures (for example, if the Bluetooth® distance range is achieved). To face this issue, an extra Java® module was developed in the software, which verifies the identifier of each measure (each broadcasted measure has an identification) and detects if some is missing. In this case, a linear interpolation is performed between the neighbor values.

On the other hand, the compiled MATLAB® functions imply a long processing time. Because of this, if too many values are broadcasted, the processing time will be

much longer than the acquisition window (10 sec), leading to the corruption of the measures in the memory of the hub (more details in section 6.4.3) and/or to the inaccuracy of the predictions. This is the reason why the default sampling frequency displayed in the interface is 100 Hz, despite the maximum sampling frequency allowed by biosignalsplux® being 1000 Hz.

To ensure that no heartbeats are lost between the changing of windows, this layer also includes a verification step that prevents it. Based on the output of the MATLAB® layer that includes the record of the end of each heartbeat (PPG_{offset}), the program identifies the last PPG value of a complete cardiac cycle presented in that window. All the following values are temporarily stored and added to the next acquired measures (ensuring that a 10-sec window is fully acquired).

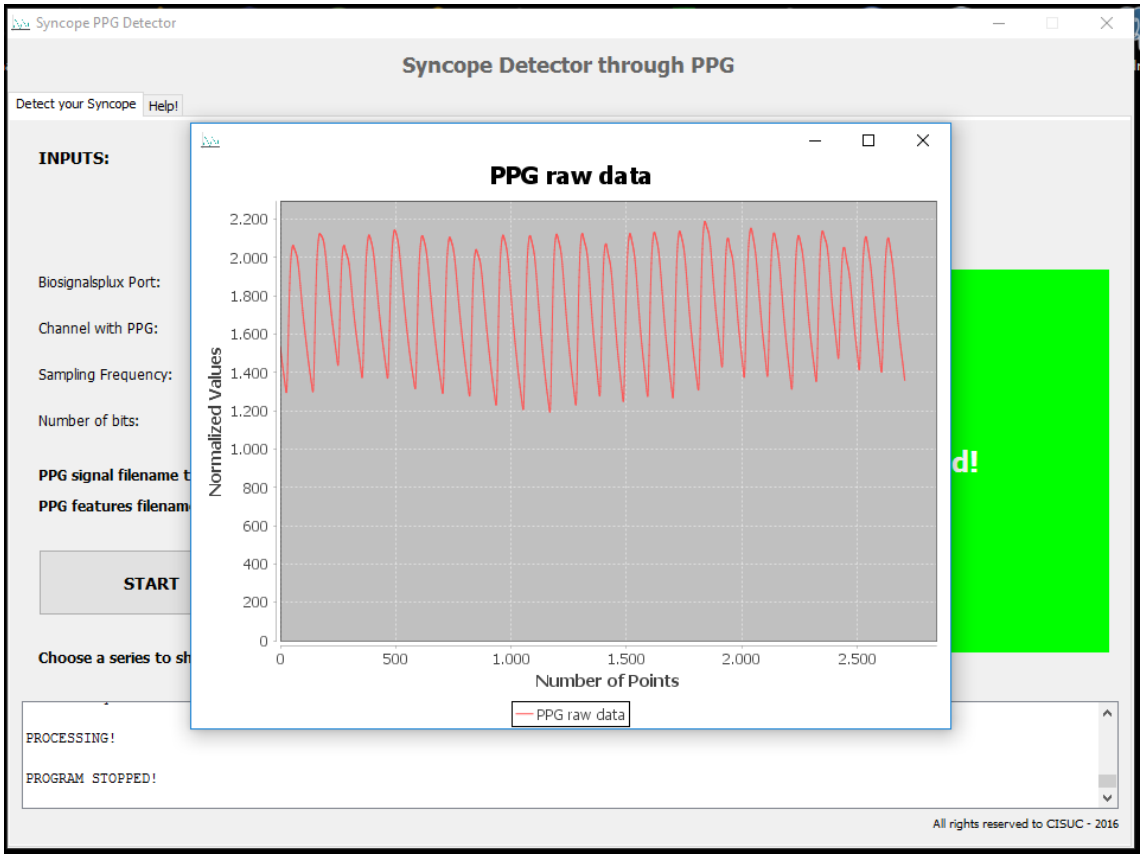

Figure 40 – Example of a graphical view, after an acquisition.

6.3.2. MATLAB® layer

The MATLAB® layer is the core back-end of the software. It is responsible for all the algorithmic component of the program, applying all the operations of signal

processing, extraction of features and prediction of syncope, resorting on continuous intervals of PPG signals with a length of 10 sec.

This layer only receives the PPG data, the sampling frequency of the signal and two other operational variables as inputs. With these components, it applies the algorithm described in Chapter 5, classifying the possible occurrence of syncope in accordance to the highlighted algorithmic setup in section 5.5. This setup resorts on PPG_{onset} and on the Minskowski distance ($p=2^{-0.5}$) with a threshold of ~4.236, using the features SI (clipped), ΔPR, ΔSI, PR, ΔLVET, RI and LVET.

The output of the layer is broadcasted to the Java® layer, corresponding to an object with 17 vectors of values: the SI, ΔPR, ΔSI, PR, ΔLVET, RI and LVET features, the records of PPG_{onset}, $PPG_{20\%}$, PPG_{der}, $PPG_{50\%}$, $PPG_{80\%}$, PPG_{peak} and PPG_{offset}, the registry of the calculated distance metrics and the correspondent binary classification of syncope/no syncope, as well as one operational variable. Each vector contains as many values as the number of detected heartbeats within each 10-sec window of signal.

To be embedded in the final software, the MATLAB® algorithm was compiled to Java® classes that wrap its operations, whose execution mandatorily requires the presence of the MATLAB Runtime® in the system. The compilation was made in a MATLAB R2016a® environment, using the tool MATLAB Compiler®.

The wrapping of MATLAB® functions with Java® classes allows the use of all the embedded functions by simply creating an instance of the Java® class and calling the desired methods. The interaction between MATLAB® and Java® values is enabled by the usage of MWArray structures (from *com.mathworks.toolbox.javabuilder*, added to Java® projects as a JAR file) to pass inputs to the MATLAB® component [164], which returns outputs of the type *java.lang.Object* [165].

6.4. Functional Tests

This section presents the various functional tests applied to the system, in order to simulate possible real-life behaviors. These tests were designed before the development of the system, to ensure that its results were as unbiased as possible. They were applied throughout the development for control and adaptation, and in its end, for registry.

The tests rely on five main areas described in the following subsections, which provide the definition and the output of each test.

6.4.1. Initializing/Stopping the system and acquisitions

6.4.1.a) Action: User starts the system.

Result: If the software and hardware are correctly set, the system starts normally. If something is wrong, an exception is thrown. There is an initialization delay before any acquisition, to start instances. The user has to start the system and an acquisition in separate actions (the system only acquires after being ordered).

6.4.1.b) Action: User stops the system.

Result: The system stops. When stopping an acquisition, there is a delay to stop the acquisition and the processing threads. This delay is variable, depending on the state of execution. To minimize this delay, several verifiers of the stop order were placed throughout the main thread.

6.4.2. Connection issues

6.4.2.a) Action: The distance range between the PC and the hub is in its limit.

Result: Some measured values may fail to be communicated between the terminals. Since each measure has an identifier, if a measure misses, a linear interpolation is made between the neighbors.

6.4.2.b) Action: The connection is lost.

Result: The connection may be uncontrolledly lost due to user mistakes, Bluetooth® errors, death of the hub's battery, surpassed distance range between terminals, etc. Any case leads to the same consequence: the acquisition thread stops and an exception is thrown, also leading to the stopping of the processing thread.

6.4.3. Input variables

6.4.3.a) Action: Changing input variables to impossible values.

Result: A warning is thrown and dependent operations are blocked until the correction of the issue.

6.4.3.b) Action: Using high sampling frequencies.

Result: Despite the hub allowing a top sampling frequency of 1000 Hz, sampling frequencies of orders higher than 10^1Hz produce an amount of values that lead to a processing time higher than the acquisition time. This eventually leads to the loss of communication between the PC and the hub, since the temporary memory of the hub becomes overwhelmed.

6.4.4. Usage of the PPG sensor

6.4.4.a) Action: The PPG sensor is acquiring, but it is not on the finger.

Result: This is users' responsibility and no warning is thrown. The acquisition carries on and the algorithm is applied to the acquired data.

6.4.4.b) Action: Other sensor, rather than the PPG one, is used to acquire signals.

Result: This is users' responsibility and no warning is thrown. The acquisition carries on and the algorithm is applied to the acquired data.

6.4.4.c) Action: The user specifies a sensor channel that is linked to other or to no sensor.

Result: This is users' responsibility and no warning is thrown. The acquisition carries on and the algorithm is applied to the acquired data. If no sensor is linked, the retrieved data consists of zeros only.

6.4.5. Data handling

6.4.5.a) Action: Saving of a CSV file and graphical visualization.

Result: This is allowed only when there is measured data in the system (of an already terminated measurement).

6.4.5.b) Action: Recover data from previous acquisitions.

Result: Since no database is used by the system, each new started acquisition overwrites the previous one. The closing of the application also deletes any previous measurements.

6.4.5.c) Action: Choosing a CSV export directory and filename already in use.

Result: The data is saved in the same file, after the previous records. In this way, no data is lost/overwritten.

6.5. Concluding Remarks

This chapter presents the development of a system to predict impending system in real time, using third-party hardware devices (biosignalsplux® with a PPG sensor and a Windows® PC).

The back-end of this system consists of one of the algorithm setups studied in Chapter 5 to process PPG data, extract cardiovascular features and predict syncope events. This back-end is written in MATLAB®, since it is the same implementation of the previous chapter. The extracted features are: SI (clipped), ΔPR, ΔSI, PR, ΔLVET, RI, LVET. The applied threshold is: ~4.236.

The front-end of the system is written in Java® and wraps the MATLAB® back-end. It also supports the real-time Bluetooth® communication between the terminals through windows of signal and interacts with the user through a customized interface.

This is a limited p-health system, since it depends on a PC, but it is already a satisfying proof of concept that provides a usable solution in some contexts, including the ones described in section 5.5: the elderly, drivers, machinery operators or, even, hospitalized patients. Furthermore, this system is built in a way that allows an easy

iterative work on it, either to change computed features, returned outputs, linked hardware or more operational details. This also enables a deeper work on the proper PPG-based syncope prediction algorithm, since it allows an actual (not mimicked) acquisition and analysis in real time.

Chapter 7

Conclusions and Future Work

Syncope refers to the temporary loss of consciousness caused by a decrease in the arterial systemic BP and global cerebral perfusion. Systemic BP depends on CO and SVR, which are influenced by the ANS. Any trigger that affects these conditions, disabling their capacity to remain in equilibrium, can lead to syncope. Some examples are orthostatic stress, emotions, physical exercise, etc. [1, 2, 3].

To health services, syncope implies a cost similar to that of HIV, asthma and chronic obstructive pulmonary disease [7], with its global annual cost rounding $1.7-$2 billion ($5000-$14000/inpatient [6, 7]). Since this condition is more presented in subjects older than 45 years [5], it is expected that the presented costs will tend to increase [7] with the aging of the populations in Europe and the USA.

The need to find ways of avoiding such large costs caused by syncope and related conditions (as CVDs and falls) gives rise to the investment in p-health and m-health preventive solutions. This fact motivated the conception of this thesis.

PPG sensors are hardware tools very suitable for p/m-health settings, since they are inexpensive, non-invasive, easy-to-use, comfortable and well-known diagnostic devices [16]. Because of their ability in producing cardiovascular analytical features, they present a tempting technique to apply in the prevention of syncope events. Its major drawback (especially, in fingertip PPG) is the easy introduction of motion artifacts during signal acquisitions [17], which decreases its reliability and accuracy.

Taking these ideas in mind, this project proposes de development of a PPG-based algorithm to accurately predict syncope episodes, in a real-time setting, supported by BP surrogating features. This main goal is divided in three large steps, as follows:

1. Comparison between PRV and HRV parameters, evaluating the reliability of the first ones in different life scenarios;
2. Construction of an algorithm to predict impending syncope in real time, solely based on PPG-derived features;

3. Development of a concept demo application to show the usefulness of such real-time algorithm.

The first objective consisted in a statistical comparison between ECG-derived HRV and PPG-derived PRV indexes, based on the analysis of the correlation, error and rank sum test. This comparison was performed between six different PPG characteristic points, in three different life scenarios: healthy subjects at rest, healthy subjects after light exercise and subjects with CVDs.

The results achieved confirm that the majority of PRV parameters may be used as surrogates for HRV ones in healthy subjects at rest, as in [17, 49, 50, 141]. Sufficiently accurate results were also observed in subjects after exercise, especially for aVL, aLF, HRV-PRV, *Mean* and SDNN. However, in CVD patients, a lower performance in the estimation of PRV features was found, with the exception of the mentioned features, which presented some acceptable results. Low agreement and/or high estimation errors was found for aHF (as well as for NN50 and pNN50), showing the propensity of the PPG signals to own HF-related artifacts.

The considered most suitable PPG characteristic point for healthy subjects at rest was PPG_{der}, while for healthy subjects after exercise was $PPG_{20\%}$ and for CVD patients was PPG_{onset}. This knowledge was used as an input to the algorithm presented in Chapter 5, where the computed PR-related features used to feed the syncope predictor were obtained using the PPG_{onset}.

The presented conclusions also provide insight on the potential usefulness of different HRV features derived from PPG, in general different physiological and operational contexts. This includes several health states, different applications (hospital/clinical settings, p/m-health, fitness,…) and different computations of the PR.

The second objective proposed the execution of a PPG-based algorithm to predict impending syncope events in real time, in a p-health context.

Several parameters and their combinations were studied: PR, left ventricular ejection time, stiffness index and reflection index, as well as parameters related with PRV, second derivative of the PPG, the systolic rise of PPG pulses and information dynamics. Furthermore, the application of a clipping operation to the features, the use of different PPG characteristic points in PRV and the application of different distance metrics were also approached.

The Minskowski distance with $p=2^{-0.5}$ was chosen as the most suitable distance metric, applied in a threshold-based classifier. Despite the numerous algorithm setups producing interesting results, PPG_{onset} was confirmed as the best PPG characteristic point to extract PRV parameters to predict syncope.

The computed results had an overall positive enhancement, comparing to the PPG-only state-of-the-art algorithm in [11]. However, the loss of PAT-related features derived from ECG lead to worse results than in [19]. In fact, to face all the real-life scenarios, this approach may still require some evolution, such as the incorporation of motion artifacts detection through sensor fusion approaches.

Nevertheless, its use is already acceptable in some specific p-health contexts, as the monitoring of the elderly, drivers, machinery operators or hospitalized patients. One setup that could be used resorts on PPG_{onset} and on the Minskowski distance ($p=2^{-0.5}$), and uses the following features: SI (clipped), ΔPR, ΔSI, PR, ΔLVET, RI, LVET. Its optimal threshold is: ~4.236.

The last objective concerns the development of a system to predict impending system in real time, using third-party hardware devices (biosignalsplux® with a PPG sensor and a Windows® PC).

The back-end of the system consists of the algorithm setup presented above, written in MATLAB®. The front-end of the system is written in Java® and performs three tasks: wrapping of MATLAB® back-end, real-time Bluetooth® communication between the terminals and interaction with the user through an interface.

This is a limited p-health system, since it depends on a PC, but it is already a satisfactory proof of concept that provides a usable solution in the mentioned contexts, as well as a valid research tool.

The presented thesis delivers a unified approach on the usability of the PPG technology in personal health contexts, not only to predict impending syncope episodes, but on a wide range of applications that concern monitoring of the cardiovascular and autonomic systems. It delineates a clear investigation path, starting with a wide scope subject (studying PRV parameters), applying its conclusions in a particular theme (prediction of syncope with cardiovascular features) and ending with the implementation of a proof of concept that employs all the considered knowledge.

Appendices

Appendix A

Can PPG be used for HRV analysis?

Scientific publication presented in the 2016 38th Annual International Conference of the Engineering in Medicine and Biology Society (EMBC'16) of the Institute for Electrical and Electronics Engineers (IEEE), in Orlando, Florida, the USA, on August 16-20, 2016. Its authors are: N. Pinheiro, R. Couceiro, J. Henriques, J. Muehlsteff, I. Quintal, L. Gonçalves and P. Carvalho.

Can PPG be used for HRV analysis?

N. Pinheiro, R. Couceiro, J. Henriques, J. Muehlsteff, I. Quintal, L. Gonçalves, P. Carvalho

Abstract— **Heart rate variability (HRV) represents one of the most promising markers of the autonomic nervous system (ANS) regulation. However, it requires the acquisition of the ECG signal in order to reliably detect the RR intervals, which is not always easily and comfortably available in personal health applications. Additionally, due to progress in single spot optical sensors, photoplethysmography (PPG) is an interesting alternative for heartbeat interval measurements, since it is a more convenient and a less intrusive measurement technique. Driven by the technological advances in such sensors, wrist-worn devices are becoming a commodity, and the interest in the assessment of HRV indexes from the PPG analysis (pulse rate variability – PRV) is rising.**

In this study, we investigate the hypothesis of using PRV features as surrogates for HRV indexes, in three different contexts: healthy subjects at rest, healthy subjects after physical exercise and subjects with cardiovascular diseases (CVD). Additionally, we also evaluate which are the characteristic points better suited for PRV analysis in these contexts, i.e. the PPG waveform characteristic points leading to the PRV features that present the best estimates of HRV (correlation and error analysis). The achieved results suggest that the PRV can be often used as an alternative for HRV analysis in healthy subjects, with significant correlations above 82%, for both time and frequency features. Contrarily, in the post-exercise and CVD subjects, time and (most importantly) frequency domain features shall be used with caution (mean correlations ranging from 68% to 88%).

I. Introduction

Heart rate variability (HRV) parameters quantify the change of time periods between consecutive cardiac cycles. It has been proven to be a valuable tool to characterize and understand the regulation of the cardiovascular system by the autonomic nervous system (ANS) [1]. In HRV analysis, the RR intervals obtained from the ECG are required [2]. Nevertheless, in principle, any signal providing accurate inter-beat heartbeat intervals could be used instead. A promising alternative technology is PPG, which can potentially provide similar results compared to a HRV analysis. However, since pulse signals are used, it shall be called pulse rate variability (PRV) instead [3]. Due to its technological and practical advantages, PPG is becoming increasingly popular in wrist-worn devices for pulse rate detection [3, 4], driving the interest for PRV analysis (rather than HRV) in different physiological, demographic and biometric circumstances. The PRV may achieve better estimates than HRV under some circumstances, such as when the ECG is subject to ECG-specific electrical artifacts, e.g., during clinical interventions [4].

Recent research has shown a sufficient accuracy of PRV compared to HRV in healthy mostly young subjects at rest [3], with high correlations (r) of both time and frequency domain parameters ($r > 0.94$, p-value < 0.0001) [5], and suitable limits of agreement: from [-0.1, 0.1] min^{-1} (in heart rate – HR) to [-7.0; 19.8] % (in pNN50) and from [-1.38; 0.9] n.u. (in low/high frequency ratio – LF/HF) to [-202; 343] ms^2 (in low frequencies – LF) [6]. In non-stationary conditions, like the tilt table test, similar results were found [7].

It has also been shown that PRV-derived parameters tend to overestimate HRV values representing physiological processes related with short-term variability [3], but without impairing the evaluation of ANS in individuals at rest: absolute differences from 0.0±0.7 min^{-1} (in HR) to 6.4±0.8% (in pNN50), and from 0.31±0.21 n.u. (in LF/HF) to 54±44 ms^2 (in HF) [6]. A major challenge for using PPG in HRV analysis is its sensitivity to motion artifacts [3, 5]. Suppression of these artifacts by improved algorithms is a popular research topic [8]. A complementary strategy for artifact suppression deals with acquisition from other body sites, like the earlobe [5, 6] or inside the auditory canal [9]. Often, an acceleration signal is synchronously acquired as well [5, 8], enhancing the deletion of motion artifacts using sensor fusion approaches.

Rauh *et al.* [6] achieved appropriate limits of agreement between the ECG-derived HR and the PPG-derived pulse rate (PR) in healthy subjects for paced breathing. However, worse ranges were observed for some parameters (from [-0.4, 0.5] min^{-1} – HR – to [-10.2; 21.3] % – pNN50 – in the time domain, and from [-4.56; 3.31] n.u. – LF/HF – to [-715; 1260] ms^2 – LF – in the frequency domain), which was interpreted as a higher influence of breathing effects on the PPG compared to the ECG. Similar results were reported during obstructive sleep apnea events [10]. Furthermore, Han *et al.* [11] found that different breathing patterns lead to unequally altered characteristics of HRV and PRV. Breathing frequency had a higher impact than breathing volume. It was also demonstrated that the agreement between HRV and PRV-derived frequency features diminishes (e.g., a decrease of 28% in HF) during the Stroop Color-Word Test, when compared to resting conditions [12].

Since moderate physical or mental stress has been associated with a compromised agreement between PRV and HRV [3], the aim of this study is to extend these observations and to compare the HRV and PRV parameters, extracted using a time-variant analysis, in three experimental settings:

This work was supported in part by the LINK (H2020 - 692023) and HeartCycle (FP7 – 216695) projects.

N. Pinheiro, R. Couceiro, J. Henriques and P. Carvalho are with the University of Coimbra, Department of Informatics Engineering, Science and Technology Faculty of the University of Coimbra, Pólo II, Coimbra, Portugal (e-mail: npinheiro@student.fisica.uc.pt, {rcouceir, carvalho, jh}@dei.uc.pt).

I. Quintal and L. Gonçalves are with the Hospital and Universitary Centre of Coimbra – General Hospital, Coimbra, Portugal (email: isabelquintal@chc.minsaude.pt, dir.cardiologia@chc.min-saude.pt).

J. Muehlsteff is with Philips Research Laboratories Europe, Eindhoven, Netherlands, (e-mail: {Jens.Muehlsteff}@philips.com).

978-1-4577-0220-4/16/$31.00 ©2016 IEEE

healthy subjects at rest, healthy subjects after physical exercise and subjects with cardiovascular diseases (CVD).

II. Collected Data

Three datasets were collected at the "Centro Hospitalar de Coimbra" covering different populations and circumstances: case 1) 33 healthy subjects at rest; case 2) same subjects as in case 1, after moderate physical exercise on a treadmill and; case 3) 35 subjects with CVD (such as hypertension, acute infarction, heart failure and coronary artery disease) at rest in supine position. Our datasets comprise ECG and PPG signals collected from all enrolled individuals using a HP-CMS monitor extended with a data logger functionality. The PPG signal (@125Hz) was recorded from the tip of the index finger using an infrared transmission finger probe, while the ECG waveform (MLII lead) was digitized at 500Hz. The biometric characteristics of the enrolled subjects (51 male and 17 female) are:

- **Cases 1 and 2 -** Age: 29.72±8.54 years; BMI: 24.48±2.41 kg/m^2;
- **Case 3 -** Age: 58.97±17.22 years; BMI: 25.38±3.10 kg/m^2.

Since our data analysis is based on a sliding window of 180 sec. with increments of 5 secs., the minimum length of the analyzed signals must be at least 185 secs. to retrieve two data points. This requirement could not be achieved for some subjects, which had to be excluded from the analysis: case 1) Patient 19; case 2) Patients 3, 4 and 5; case 3) Patients 4 and 34.

III. Methods

A. Assessment of Heart Rate obtained from ECG R-peaks and Pulse Rate from different PPG characteristic points

In HRV and PRV analysis, it is essential to first extract the HR and the PR. HR was calculated from detected consecutive R-peaks in the ECG signal, while PR was inferred as the time span between the characteristic points of two consecutive PPG pulses.

Characteristic points for PRs were as follows: 1) the onset of the PPG pulse – PPG_{onset}; 2) time instant corresponding to 20% of the PPG pulse's total amplitude, at the systolic rise – $PPG_{20\%}$; 3) time instant corresponding to the local maxima of the PPG pulse's first derivative – PPG_{deriv}; 4) time instant corresponding to 50% of the PPG pulse's total amplitude, at the systolic rise – $PPG_{50\%}$; 5) time instant corresponding to 80% of the PPG pulse's total amplitude, at the systolic rise – $PPG_{80\%}$ and; 6) the peak of the PPG pulse – PPG_{peak}.

B. HRV and PRV analysis

Using a 180 sec. sliding window, shifted by 5 sec. increments, time and frequency domain HRV and PRV features were extracted using the same algorithm. Noisy segments and signal artifacts in the ECG and PPG signals were carefully removed from the analysis.

We analyzed the following six time domain features: Mean – mean of the time intervals within the sliding window; SDNN – standard deviation of normal-to-normal (NN) intervals; SDSD – standard deviation of successive differences between adjacent NN intervals; RMSSD – square root of the mean squared differences between adjacent NN intervals; NN50 – number of interval differences of successive NN intervals greater than 50ms; pNN50 – ratio between NN50 and the total number of NN intervals [3].

Additionally, four frequency domain parameters were extracted from the analysis of the estimated spectra (Burg's method [13]): aVL – normalized area of the spectrum of very low frequency (VLF) band (0.003-0.04 Hz); aLF – normalized area of the spectrum of low frequency (LF) band (0.04-0.15 Hz); aHF – normalized area of the spectrum of high frequency (HF) band (0.15-0.4 Hz); RaLH – ratio between aLF and aHF [3]. While the HF component is widely accepted as a marker of parasympathetic activity (and influenced by the respiratory activity), the LF component is thought to be the result of both sympathetic and parasympathetic activities [1, 14]. RaLH is commonly defined as a marker of sympatho-vagal balance [14].

C. Statistical Evaluation Methods

In this study, we evaluate the accuracy of the extracted PRV features (in the time and frequency domains, extracted from different characteristic intervals) by comparing them to the reference HRV features, extracted from the analysis of the ECG signal. Data were synchronized in time, ensuring the correct correspondence between the analyzed features. This comparison was performed using the Spearman's rank correlation (SRC), the normalized root mean squared error (NRMSE) and the Wilcoxon's rank sum test (WRST). MATLAB R2014b® was used for signal processing and subsequent data analysis.

First, a one-sample unequal-tailed Kolmogorov-Smirnov test (KST) was performed in each set of parameters' values to test if the data belong to a standard normal distribution (at the 5% significance level). The results show that almost none of our data fulfilled this criterion. Exceptions were observed in cases: 1) patient 20 / feature pNN50 (p-value = 0); 2) patients 1, 2, 17 and 30 / feature pNN50 (p-value = 0), and patient 2 / feature RaLH (p-value ∈ [0.0482, 0.1565]). Therefore, non-parametric methods were used to assess the agreement between the extracted features and to test the hypothesis that those features came from the same distribution.

Using a two-tailed SRC we aim to assess the agreement between the HRV and PRV features, i.e. the existence of a monotonic relationship between them. The normalized error between each PRV feature and its homologous HRV feature was assessed using the NRMSE, defined as:

$$NRMSE = \frac{\sqrt{\frac{1}{N}\sum_{m=1}^{N}(PRV_{feat_i}^{j}[m] - HRV_{feat_i}[m])^2}}{\overline{HRV_{feat}}}, \quad (1)$$

where HRV_{feat_i} is the i^{th} extracted feature (e.g.: aVL,…, pNN50) from the ECG analysis, $PRV_{feat_i}^{j}$ is the i^{th} extracted feature from the analysis of the j^{th} PPG interval (e.g.: PPG_{onset},…, PPG_{peak}) and $\overline{HRV_{feat}}$ is the mean of the values of the HRV-derived feature. To test if the HRV and PRV features came from the same population, i.e. could be classified as samples from continuous distributions with equal medians (p-value < 0.05), a two-sided WRST was performed.

IV. Results and Discussion

Our results are summarized in Figure 1 and Figure 2, which present the average of the results (SRC and NRMSE) presented TABLE I and TABLE II of the APPENDIX, obtained for each feature category (time and frequency domains) and according to the different PPG characteristic points and to the different datasets.

Almost all correlation values were statistically significant (p-value < 0.05), except for those found to belong to a standard normal distribution (the KST exceptions discussed in section III C. Statistical Evaluation Methods).

From Figure 1, it is possible to observe that under ideal conditions, i.e. healthy patients at rest (case 1), the agreement between the features extracted from HRV and PRV analysis is high (SRC ∈ [82.4±17.1; 90.6±6.2] %) in the majority of the analyzed parameters. Exceptions were found for NN50 and pNN50 (see TABLE I). Contrarily, in cases 2 and 3, the agreement between the analyzed features decreases drastically (SRC ∈ [68±9.7; 80.6±16.2] %). An exception was found for the frequency domain features in case 2, which range from 81.9±13.4 % to 88±8.4 %. It is also shown that the agreement between PRV and HRV features tend to decrease from case 1 to case 3, and that the achieved correlations within frequency domain features present higher values when compared to the time domain features (except for case 3).

Regarding the estimation error of the PRV features, it is possible to observe from Figure 2 that the time domain features extracted from PRV analysis achieved the lowest estimation errors (comparing to frequency features), in each of the three cases (NRMSE ∈ [5.3±3.9; 15.6±18.3] %), being the case 2 where the worst estimates were achieved (NRMSE ∈ [13.7±14.6; 15.6±18.3]). As for the frequency features, it is shown that there is a drastic increase in the estimation error from case 1 (NRMSE ∈ [14.7±5.3; 17.4±6.4] %) to case 3 (NRMSE ∈ [38.9±8.5; 47.1±13.2] %).

From the analysis of each specific feature in the time domain, one observes in TABLE I and TABLE II that the direct comparison between HRV and PRV signals (specified as HRV-PRV) returns excellent estimation errors (NRMSE ∈ [1.3±0.6; 2.8±2.6] %), followed by high correlations (SRC ∈ [88.6±16; 98.3±2.1] %) in the three cases under study. This observation shows a close agreement and high similarity between the estimated PRV and HRV signals under different physiological conditions. It is also noticed that the features presenting better accuracy (i.e. lowest NRMSE) are the mean (NMRSE ∈ [0.1±0.1; 0.4±0.6] %) and SDNN (NMRSE ∈ [2.6±2; 8.7±8.2] %).

It shall be noticed that the NN50/pNN50 features present a very low agreement in all the three cases, ranging from 36.2±46.2% to 69.1±30.6% (see TABLE I.), representing one of the main contributes to the decrease in the global correlation of the time domain features depicted in Figure 1. Nevertheless, these two features presented a good estimation error (NRMSE ∈ [5.7±3.6; 10.6±7.7] %). In order to investigate the reason for such observations, a histogram of the error ($HRV_{feat_i} - PRV^{j}_{feat_i}$) for each feature of each PRV interval was calculated, showing an overestimation of the

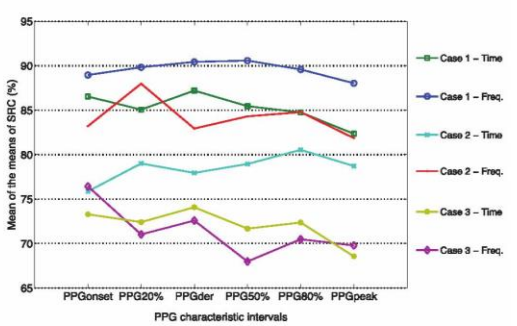

Figure 1. Mean of the Means of SRC (%) between ECG-derived and each PPG interval-derived features, in time and frequency (freq.) domains.

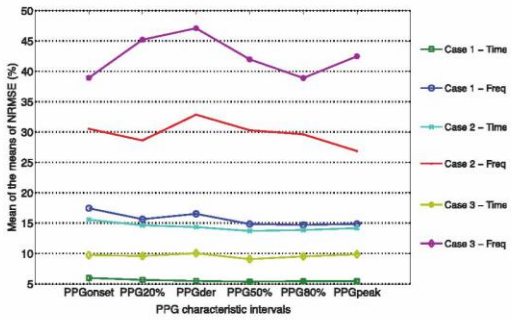

Figure 2. Mean of the Means of NRMSE (%) between ECG-derived and each PPG interval-derived features, in time and frequency (freq.) domains.

PRV features, as mentioned in the literature [3, 6], but not for NN50 and pNN50. Moreover, the tails of their histograms are longer, with more widespread values. One possible reason for the low correlation within these two features relies on the fact that they are based on the counting of interval differences among a very short amount of time (50 ms), which is approximately 5% of the RR interval (considering an HR of 60 min^{-1}). Therefore, it is expected that even the smallest estimation error produces a highly negative impact on the agreement of these features with their reference.

Regarding the frequency domain features, the RaLH presented a more complex behavior, since the accuracy in the estimation of this feature is highly dependent on the estimation errors of both aLF and aHF, a high uncertainty in the estimation of one of these features results in a dramatic increase in the estimation error of the RaLH. It is also shown in TABLE I that the agreement between the frequency features and their reference decreases from VLF (aVL) to HF (aHF). This trend is also clear when inspecting the estimation error, with a special emphasis to the aHF, where the NRMSE is clearly higher in all the three cases.

Issues for HF-related features have been previously found already [3, 4, 12]. Many PPG artifacts (e.g. motion artifacts) influence the HF component, as well as stronger breathing patterns induced by exercise or mental stress (such as in case 2), which induce higher uncertainty in the estimation of this feature. Similarly, in case 3 subjects (older subjects and with CVD), abnormal patterns in breathing and in the Frank-

Starling mechanism (which cause stronger fluctuations in HR/PR) [3, 6], as well as the existence of a poorer blood perfusion and a lower compliance (stiffer arteries), can represent an obstacle to the correct detection of the PPG characteristic points. Moreover, elderly subjects are known to have distinct skin characteristics that prevent the reflectance/ transmittance of light to the photo-detector (mimicking a low-pass filter behavior), which can also prevent the correct characterization of the PPG pulse. These aspects increase the uncertainty in the calculation of the heartbeat intervals and consequently have a negative impact on the agreement between aHF estimated from PRV and the reference HRV.

Analyzing the characteristic points that achieved the best results, it is possible to observe, from Figure 1 and Figure 2, a small variation in the correlation and NRMSE values (ap. < 3%), for the various PPG characteristic points of case 1. The only exception was observed in the correlation of time domain features for the PPG_{peak}. As for the cases 2 and 3, although the NRMSE within time domain features increases when compared to case 1, it is shown in Figure 2 that it remains with a low range of values ([9±5.9; 15.6±18.3] %). A lower agreement within these features was observed, being the best values achieved for $PPG_{80\%}$ (after-exercise individuals) and for PPG_{deriv} (subjects with CVD). In these cases, a higher range of correlation values was also seen for the frequency domain features (SRC ∈ [68±9.7; 88±8.4] %), suggesting that the selection of a suitable PPG characteristic interval is much more important in these sets, than in healthy individuals.

The characteristic points exhibiting the best estimation error (NRMSE) were, in general, the $PPG_{50\%}$, $PPG_{80\%}$ and PPG_{peak}, while the agreement between features did not follow a consistent pattern, depending on the context and analyzed feature category. However, there is more accordance between the intervals with best correlation and with best NRMSE in case 1 subjects, rather than in the remaining cases.

PPG_{peak} underperformed in almost all cases. One plausible reason for this is the change in the characteristics of the PPG pulse, leading to a very broad maximum of the PPG pulse and preventing the correct estimation of PR intervals and, consequently, the derived PRV features. Effects such as breathing are reported to have a strong influence on PR detection accuracy [6, 11].

Finally, one must notice that in cases 1 and 2, the WRST of PRV and HRV features always stated that the tested features came from continuous distributions with equal medians. In case 3, the same results were observed, with an exception to 3 subjects and a marked decrease in the performed tests' p-value.

The spread between the least and the most accurate values suggest that the choice of the best characteristic point is dependent on the physiological condition of the subject and on the analysis' context, which highlights the need for an automatic decision-making algorithm to select the most suitable PPG intervals. To our knowledge, in such a system, the SRC may provide better guidelines, since the trend between HRV and PRV features can be corrected through algebraic means.

V. Conclusion

This study focuses on the evaluation of commonly used HRV features calculated from PR signals, both in frequency and time domains. This was achieved by comparing HRV and PRV-derived parameters (including HR and PR) using the Spearman's rank correlation (SRC), the normalized rout mean square error (NRMSE) and Wilcoxon's rank sum test (WRST).

Our results confirm that the majority of PRV indexes may be used as surrogates for ECG-based HRV in healthy subjects at rest, as reported in the literature [3, 5, 6, 7]. Accurate results can be observed in subjects after exercise, especially for aVL, aLF, HRV-PRV, Mean and SDNN. However, in CVD patients, we found a lower performance in the estimation of PRV features, with an exception to the abovementioned features, where some acceptable results were achieved. Low agreement and/or high estimation errors within aHF, NN50 and pNN50 were identified and justified.

In general, time domain features present a mean NRMSE below 15% in the three case studies, whereas frequency domain features show such a result in healthy subjects at rest only. As for the achieved correlation values, the features extracted from CVD patients are the only ones with results below 75%. Therefore, time domain features may be used for PRV analysis covering the three presented protocols, whereas frequency domain features require more caution.

Our results show that, for healthy subjects at rest the most suitable characteristic point (highest agreement with the reference) is PPG_{deriv}, while for healthy subjects after exercise the best characteristic point is $PPG_{20\%}$. As for the subjects with CVD, the characteristic point achieving the highest agreement was the PPG_{onset}.

Summing up, this study provides a ranking of PRV parameters, which might be used depending on the obtained PPG characteristic interval and analyzed context.

Future work will focus on the adaptation of our previous algorithm for syncope prediction [15] to resort only on PPG analysis including PRV, which will benefit from our findings in this study.

Appendix

TABLE I. Spearman's Rank Correlation (%) between ECG-Derived Features and each PPG Interval-Derived Features

Feature	**Intervals between characteristic PPG points**					
	PPG_{onset}	$PPG_{20\%}$	PPG_{deriv}	$PPG_{50\%}$	$PPG_{80\%}$	PPG_{peak}
Dataset: Case 1						
aVL	97.1±4.6	96.5±9.7	95.2±18.6	97.9±3	96.4±8.1	97.7±3.4
aLF	95.6±7.8	96.2±4.9	95.3±10.6	95.5±8.6	96.4±7.2	92±17.4
aHF	81.3±31.7	83.9±20.2	87.1±19.9	83.9±23.1	84.9±21.7	81.2±23
RaLH	81.8±22.6	82.7±21.8	84.1±20.7	85±19.9	80.6±29.4	81.2±29.2
HRV-PRV	98.2±2	98.1±2.4	98.1±2.2	98.3±2.1	98.1±2.4	97.9±2.4
Mean	99.3±2	98.8±4.3	99.5±1	99.4±1.8	99.2±2.6	98.6±4
SDNN	93.6±21.1	93.4±18.8	93.2±23.4	91.8±23.3	93.2±17.4	93.6±17.3
SDSD†	89.3±13.9	90.6±13	90.7±11.2	87.9±18	90.9±12.1	87±15.2
NN50*	68±22.7	61.9±32.1	69.1±30.6	66.4±30.6	60.4±34.2	56.1±37.5

Dataset: Case 2						
aVL	98.5±2.3	98.6±2.3	98.6±2.2	99.1±1.5	98.9±1.9	98.9±1.8
aLF	86.5±34.5	88.9±28.9	87.1±30.9	86.8±30.1	86.7±29.2	84.4±38.8
aHF	79.7±27.6	89.3±16.2	77.2±30.8	86.4±19	83±38.9	82.8±24.5
RaLH	68.1±34.4	75.1±27	68.8±34.9	64.9±40.4	70.5±37.5	61.3±46.5
HRV-PRV	97.5±2.2	97.5±2.3	97.6±2.4	97.5±2.5	97.4±2.6	97.2±3.1
Mean	99.9±0.4	99.8±0.5	99.7±1	99.7±1	99.7±1	99.6±1.1
SDNN	98.8±4	97.5±7.7	99±3.9	97.3±9	98.8±4	97.5±7.7
SDSD†	62±54.3	72.6±41.4	63.5±49.4	66.7±46.6	72.5±43.3	72.6±40.8
NN50*	55.3±40.5	56.5±36.6	60.7±30.3	62.4±40.4	61.8±30.3	55.7±39.7
Dataset: Case 3						
aVL	85.1±21.2	81.1±35.5	83.9±30.8	78.8±37	84.4±28.7	85.1±28.8
aLF	81.5±27.3	79.3±35.8	78.3±37.9	76.5±41	74.5±43	70.6±51.1
aHF	71.3±42.1	56.7±53.9	62.2±51.2	57.5±53	55±56.8	56.3±56.3
RaLH	67.8±37.9	67±36.1	65.9±38.9	59.1±42.9	68±38.8	67.1±38.5
HRV-PRV	89.1±15.6	89.5±15.9	89±15.7	89.3±15.7	89.4±16.1	88.6±16
Mean	96±6.8	95.7±9.4	95.2±9.1	95.2±8.9	96.2±6.7	94.9±7.9
SDNN	92.9±9.4	90.4±14.6	87.4±22.4	87.3±21	85.7±26.3	87.6±23.7
SDSD†	73.9±35.7	75.8±26.7	75±29.4	73.1±31.1	72.6±32.7	68.2±42.7
NN50*	43.6±42.8	39.8±42.6	48.4±38.4	41.9±49.2	45±44.3	36.2±46.2

*and pNN50; †and RMSSD

TABLE II. NRMSE (%) BETWEEN ECG-DERIVED FEATURES AND EACH PPG INTERVAL-DERIVED FEATURES

Feature	Intervals between characteristic PPG points					
	PPG_{onset}	$PPG_{20\%}$	PPG_{deriv}	$PPG_{50\%}$	$PPG_{80\%}$	PPG_{peak}
Dataset: Case 1						
aVL	11.3±10.9	11.3±9.9	10.5±13.4	10.1±8.3	9.1±5.5	13.2±14.2
aLF	11.5±10.6	9.7±5.8	10.1±6.5	10.3±7.4	10.4±8.1	11.6±10.8
aHF	26.4±21.5	23±20.6	24.9±19.1	21.1±11.7	22.2±13.8	18.1±11.1
RaLH	20.6±9.6	18.6±10.2	20.6±11.4	17.9±8.9	17.1±10	16.6±7.9
HRV-PRV	1.3±0.8	1.3±0.9	1.3±0.9	1.3±0.9	1.3±0.9	1.4±0.9
Mean	0.1±0.1	0.1±0.1	0.1±0.1	0.1±0.1	0.1±0.1	0.1±0.1
SDNN	3±2.5	2.6±2	2.7±1.8	2.7±1.8	2.7±1.9	2.6±2.1
SDSD†	12.6±6.7	11.4±7.5	11.4±6	10.5±6.3	10.4±6.2	10.7±7
NN50*	6.1±3.6	6.4±3.4	5.7±3.6	6.2±3.7	6.6±3.8	6.3±3.6
Dataset: Case 2						
aVL	15.5±16.7	17.3±39.1	21.9±63.5	24.2±68.8	22.5±65	22.3±73.3
aLF	13.4±10.5	12.9±9.2	21.9±50.7	14.3±17.1	13.8±11.8	14.5±13.5
aHF	63.2±65.7	57.8±63.8	60.4±64.8	54.7±48.9	55.6±71.4	44.3±41.3
RaLH	30±20.3	26.5±19.5	27.3±20.2	28±19.5	26.6±20.3	26.4±18.1
HRV-PRV	1.3±0.6	1.4±0.9	1.3±0.8	1.4±0.8	1.4±0.9	1.4±1
Mean	0.1±0.1	0.1±0.1	0.1±0.1	0.1±0.2	0.1±0.1	0.1±0.1
SDNN	3.1±2.9	3.1±3.6	4.4±10.5	3.8±7.2	3.7±6	3.6±7.4
SDSD†	44.1±42.8	40.1±40.4	37.8±34.6	36.3±34.7	36.2±34.8	37±37.1
NN50*	8.2±5.3	8.9±5.3	9.6±5.5	9.1±5.5	9.8±5.9	10.1±5.5
Dataset: Case 3						
aVL	28.8±33.4	36.4±40.9	38.8±43.2	33.5±33.6	32.6±34.1	30.9±29.7
aLF	27±24	31.6±41.3	33.2±31.6	31.4±36.3	29.5±31.9	39.8±44.8
aHF	55.4±57	67.2±112.7	67.8±93.7	50.2±39.1	50.9±42.3	54.7±66.2
RaLH	44.5±31.4	45.6±37.6	48.6±37.9	52.8±48.1	42.6±32.6	44.5±37.1
HRV-PRV	2.6±2.5	2.7±2.5	2.8±2.6	2.6±2.4	2.6±2.3	2.8±2.5
Mean	0.2±0.3	0.2±0.3	0.4±0.6	0.3±0.4	0.3±0.5	0.3±0.3
SDNN	6.6±4.9	7±5.8	8.6±7.7	7.4±6.4	7.5±7	8.7±8.2
SDSD†	20.1±18	19.3±16.1	20.5±16.7	16.9±12.6	17.8±13.6	18±16.1
NN50*	9.3±6	9.3±5.9	8.7±5.7	9.7±6.9	10.3±7	10.6±7.7

*and pNN50; †and RMSSD

REFERENCES

[1] U. R. Acharya, K. P. Joseph, N. Kannathal, C. M. Lim, and J. S. Suri, "Heart rate variability: a review," *Medical and biological engineering and computing*, vol. 44, no. 12, pp. 1031–1051, 2006.

[2] D. Bansal, M. Khan, and A. K. Salhan. "A review of measurement and analysis of heart rate variability," *Computer and Automation Engineering, 2009. ICCAE'09. International Conference on*, pp. 243-246, IEEE, March 2009.

[3] A. Schäfer, and J. Vagedes, "How accurate is pulse rate variability as an estimate of heart rate variability?: A review on studies comparing photoplethysmographic technology with an electrocardiogram," *International journal of cardiology*, vol. 166, no. 1, pp. 15–29, 2013.

[4] M. Bolanos, H. Nazeran, and E. Haltiwanger, "Comparison of heart rate variability signal features derived from electrocardiography and photoplethysmography in healthy individuals," *Engineering in Medicine and Biology Society, 2006. EMBS'06. 28th Annual International Conference of the IEEE*, pp. 4289-4294, IEEE, 2006.

[5] G. Lu, F. Yang, J. A. Taylor, and J. F. Stein, "A comparison of photoplethysmography and ECG recording to analyse heart rate variability in healthy subjects," *Journal of medical engineering and technology*, vol. 33, no. 8, pp. 634–641, 2009.

[6] R. Rauh, R. Limley, R. D. Bauer, M. Radespiel-Troger, and M. Mueck-Weymann, "Comparison of heart rate variability and pulse rate variability detected with photoplethysmography," *Saratov Fall Meeting 2003: Optical Technologies in Biophysics and Medicine V*, pp. 115–126, International Society for Optics and Photonics, 2004.

[7] E. Gil, M. Orini, R. Bailón, J. M. Vergara, L. Mainardi, and P. Laguna, "Photoplethysmography pulse rate variability as a surrogate measurement of heart rate variability during non-stationary conditions," *Physiological Measurement*, vol. 31, no. 9, p. 1271, 2010.

[8] H. Han, M. J. Kim, and J. Kim, "Development of real-time motion artifact reduction algorithm for a wearable photoplethysmography," *Engineering in Medicine and Biology Society, 2007. EMBS 2007. 29th Annual International Conference of the IEEE*, pp. 1538–1541, IEEE, 2007.

[9] S. Vogel, S. Leonhardt, M. Hulsbusch, and D. Starke, "In-ear heart rate monitoring using a micro-optic reflective sensor," *Engineering in Medicine and Biology Society, 2007. EMBS 2007. 29th Annual International Conference of the IEEE*, pp. 1375–1378, IEEE, 2007.

[10] A. H. Khandoker, C. K. Karmakar, and M. Palaniswami, "Comparison of pulse rate variability with heart rate variability during obstructive sleep apnea," *Medical engineering and physics*, vol. 33, no. 2, pp. 204–209, 2014.

[11] Y. Han, W. C. Lin, S. C. Huang, C. L. Tsai, and K. P. Lin, "Comparison of Heart Rate Variability and Pulse Rate Variability of Respiratory Control," submitted for publication.

[12] N. D. Giardino, P. M. Lehrer, and R. Edelberg, "Comparison of finger plethysmograph to ECG in the measurement of heart rate variability," *Psychophysiology*, vol. 39, no. 2, pp. 246–253, 2002.

[13] T. J. Ulrych, and T. N. Bishop, "Maximum entropy spectral analysis and autoregressive decomposition," *Reviews of Geophysics*, vol. 13, no. 1, pp. 183–200, 1975.

[14] M. Malik, "Heart rate variability: Standards of measurement, physiological interpretation and clinical use," *European Heart Journal*, vol. 17, pp. 354–381, 1996.

[15] R. Couceiro, P. Carvalho, R. P. Paiva, J. Muehlsteff, J. Henriques, C. Eickholt, and C. Meyer, "Real Time Prediction of Neurally Mediated Syncope," 2015.

Appendix B

PPG-based Feature Evaluation for Syncope Prediction

Scientific publication submitted for presentation in the 2017 joint event of the European Medical and Biological Engineering Conference (EMBEC'17) and the Nordic-Baltic Conference on Biomedical Engineering and Medical Physics (NBC'17), in Tampere, Finland, on June 11-15, 2017. Its authors are: N. Pinheiro, R. Couceiro, J. Muehlsteff, C. Eickholt, J. Henriques and P. Carvalho.

PPG-based Feature Evaluation for Syncope Prediction

N. Pinheiro[1], R. Couceiro[1], J. Muehlsteff[2], C. Eickholt[3], J. Henriques[1], and P. Carvalho[1]

[1]Department of Informatics Engineering, FCTUC, University of Coimbra, Coimbra, Portugal
[2]Philips Research Laboratories Europe, Eindhoven, Netherlands
[3] Department of Cardiology, Pneumology and Vascular Medicine, Heinrich-Heine University Hospital, Düsseldorf, Germany

Abstract— **Blood pressure (BP) monitoring algorithms have been proposed to predict impending syncope in real time. Some use cuff-based BP or electrocardiogram, being expensive and uncomfortable. However, algorithms more suitable for p-health settings, *e.g.* based on photoplethysmogram (PPG), are less reliable. The aim of this work is to provide a PPG-based algorithm to predict impending syncope, with increased reliability. A threshold-based classification model was used, applying the Minkowski distance metric with exponent $p=2^{-0.5}$ (proved as the best tested metric). Numerous parameters were evaluated to feed the algorithm: pulse rate (PR) – chronotropic evaluator –, left ventricular ejection time (LVET) – inotropic evaluator –, stiffness index (SI), reflection index (RI) – BP and volume tone surrogates –, as well as several indexes related with the pulse rate variability (PRV), the second derivative of the PPG, the PPG wave's systolic rise and information dynamics. The onsets of the PPG pulses were used to assess PR and PRV related attributes. From all the parameters, a total of 94 different features was computed. The most relevant were selected and ranked with a proper score system and, with these, different algorithm setups were assessed. The most promising are shown, highlighting the one tested with Fm=86%, SE=100%, SP=85%, FPRh=1.9h^{-1} and PT= 242.3±226.9 sec. This embeds features derived from SI, PR, LVET and RI.**

Keywords— **Syncope, photoplethysmogram, blood pressure regulation.**

I. Introduction

Noninvasive techniques to estimate blood pressure (BP) have been used to predict syncope in real time, using data collected on head-up tilt table (HUTT) tests [1]. Couceiro *et al.* [1] developed an algorithm based on electrocardiogram (ECG) and photoplethysmogram (PPG), with validation results of 95.2% of sensibility (SE), 95.4% of specificity (SP), 116.4±155.5 sec of prediction time (PT) and a false positive rate per hour (FPRh) of 0.14 h^{-1}. In this algorithm, threshold-based classifier yielded better results than Support Vector Machines [2]. Heart rate variability (HRV) indexes [3] improved the performance of the algorithm in [1]. Despite BP and ECG being recommended for syncope diagnoses, in a p-health context, PPG, for its cheapness and easiness-to-use, is more interesting. In [4], Couceiro *et al.* compared the algorithm in [1] with a fully PPG-based version. This performed worse, since the best scored parameter of the original algorithm is the ECG and PPG-based pulse arrival time (PAT). This work extends [4], integrating new BP surrogates in the algorithm, increasing its performance and providing a more consistent predictive value, through the study of new attributes and combinations. Furthermore, in [5], it was suggested that the optimal PPG characteristic point (PPG_{CP}) to derive parameters in these conditions is the onset of the PPG pulse (PPG_{onset}). In this work, all the PR-related features were computed using this reference point.

II. Methods

The dataset used herein is the same of [1-4], using one PPG signal/patient. 21 patients registered syncope events (positives, PO). 22 patients did not (negatives, NE).

A. Syncope Prediction

The algorithm concerns: detection of motion artifacts (refer to [1]), collection/processing of hemodynamic parameters, feature extraction (with outliers' removal [1, 4]) and prediction of syncope. A threshold-based binary classification of syncope prediction is applied on 10-sec continuous windows of signal, using the Minkowski distance metric with exponent $p=2^{-0.5}$ [1].

In [1], features' variations not linked with syncope were clipped to a reference. This approach was also tested, being compared to the use of unclipped features.

The performance of the algorithm was assessed with a three-way data split. The optimal threshold of each setup of the algorithm was the average of all thresholds of a 5-fold cross-validation with 20 repetitions.

B. Parameters, Features and Characteristic Points

Each of the PPG-derived parameters (see next four subsections) gave rise to four features to feed the system: *1)* the normalized parameter itself; *2)* the normalized change of the parameter over the previous 90 sec (identified with a Δ before the parameter's name); *3)* two features based on the information dynamics (ID) of the normalized parameter.

The parameters described in subsection *e)* refer to PPG's ID, hence, for them, only features 1) and 2) were calculated.

a) Chronotropy/inotropy, vascular tone and blood pressure:

These comprise the PR derived from PPG_{onset}, the left ventricular ejection period (LVET), the stiffness index (SI) and the reflection index (RI), surrogating, the chronotropic and inotropic changes, and the vascular tone and BP [4].

b) Pulse rate variability:

Concerning pulse rate variability (PRV), six time domain parameters (*mean*, SDNN, SDSD, RMSSD, NN50 and pNN50) and four in the frequency domain (aVL, aLF, aHF and RaLH) were extracted [5]. High frequencies (aHF) are related to parasympathetic activity and are influenced by respiration, while low frequencies (aVL, aLF) are thought to link with sympathetic and parasympathetic activities [6].

c) Second derivative of the photoplethysmogram:

The 2nd derivative of the PPG (SDPPG) provides an accurate detection of PPG_{CP}, distinguishing five waves (*a*, *b*, *c*, *d*, *e*). The relative heights (*b/a*, *c/a*, *d/a* and *e/a*) relate to dynamics of the vascular system: age, arterial BP, stiffness, drugs and atherosclerosis. An "aging index" (SDPPG-AI) was defined: *(b-c-d-e)/a* [7]. For these reasons, the four ratios and the SDPPG-AI were studied as parameters.

d) PPG pulse wave's systolic rise:

The systolic rise of the PPG pulse relates with the rise of the pulse pressure wave, illustrating the increase of blood flow from the heart to the aorta. To assess these dynamics, two parameters were specified: the crest time (CT) – the time interval between PPG_{onset} and the time instant of the systolic peak (PPG_{peak}) –; and the velocity of rise (VR):

$$VR = (PPG_{peak} - PPG_{onset})/CT. \quad (1)$$

e) Information dynamics:

Based on the work of Faes *et al.* [8], three information-theoretic parameters were extracted from the PPG, as a univariate system: 1. *SysInfor*, defining the system's entropy; 2. *UnexpInf*, or conditional entropy (given *L* lags of its past); 3. information storage (*InfStor*) – system's mutual information. The first two attributes were also computed over the normalized parameters described in subsections *a)*, *b)*, *c)* and *d)*, producing indirect features to feed the classification model.

C. Features' Selection and Algorithm's Evaluation

Given that 94 features were evaluated in this work, only the most descriptive were introduced in the algorithm, based on a feature selection score (FSS) metric [1]. Each feature with FSS greater than 50% was selected, composing a set of *X* chosen features. Then, from these, the algorithm was fed and validated with {*X*, *X*-1, *X*-2, …, 1} features (from the least to the most descriptive one). Among all the produced algorithm setups (varying in selected features and strategy of values' clipping – the studies were made with different clipped and unclipped features), the one with the best combination of f-measure (Fm), SE, SP and FPRh was picked to test several distance metrics, as in [1].

III. Results and Discussion

Table 1 Selected features to embed in the algorithm, ranked by their FSS

Rank	Feature (FSS, %)	Rank	Feature (FSS, %)	Rank	Feature (FSS, %)
1	SI (91.8)	6	SDNN (56.9)	11	$SDSD_{HY}$ (51.7)
2	ΔPR (79.4)	7	$pNN50_{HY}$ (55.1)	12	ΔaVL (51.2)
3	ΔSI (60.0)	8	RI (55.0)		
4	PR (59.9)	9	PR_{HY} (53.6)	13	*Δmean* (51.1)
5	ΔLVET (57.5)	10	*b/a* (51.8)		

Table 2 Performance of the best scored algorithm setups

n	Test					Validation		
	Fm (%)	SE (%)	SP (%)	FPRh (h^{-1})	PT (sec)	SE (%)	SP (%)	FPRh (n.u.)
1	86	100	85	1.9	242.3 ±226.9	72.67 ±2.98	93.67 ±2.84	0.15 ±0.11
2	86	100	85	2.05	360.0 ±297.5	70.00 ±7.01	77.67 ±4.60	0.82 ±0.22
3	80	100	77	2.2	368.8 ±285.96	70.00 ±3.42	89.83 ±2.75	0.23 ±0.06
4	80	100	77	2.34	345.8 ±306.7	68.67 ±4.88	82.17 ±4.87	0.75 ±0.31
5	80	100	77	2.64	210.7 ±214.2	72.67 ±4.27	81.33 ±3.13	0.75 ±0.22
6	80	100	77	2.93	363.1 ±297.6	79.67 ±4.03	77.50 ±3.22	0.94 ±0.15
7	80	100	77	1.46	190.9 ±211.7	93.33 ±0.00	80.17 ±2.02	1.15 ±0.17

Table 3 Applied features in the algorithm setups of Table 2

n	Features Description
1	SI (clipped), ΔPR, ΔSI, PR, ΔLVET, RI, LVET
2	SI, ΔPR, ΔSI
3	SI, ΔPR, ΔSI, PR, ΔLVET, RI, LVET
4	SI (clipped), ΔPR, ΔSI, PR, ΔLVET, RI
5	SI (clipped), ΔPR (clipped), ΔSI, PR, ΔLVET, RI
6	SI (clipped), ΔPR, ΔSI
7	SI, ΔPR, ΔSI, PR (all clipped)

Tables 1-3 compile the most important results achieved. Table 1 shows the ranking order of the chosen features (with FSS>50%). Few features studied for the very first time fulfilled this condition. In fact, only $pNN50_{HY}$, PR_{HY}, *b/a* and $SDSD_{HY}$ were selected to Table 1 and none of them achieved even the top 5 of highest rated features. Except for PR_{HY}, the mentioned PRV features ($pNN50_{HY}$ and $SDSD_{HY}$)

achieved better scores than both their original normalized parameters and parameters' changes on 90 sec windows, highlighting the importance of analyzing new features when studying new approaches to such an algorithm. In [5], it was denoted that the PPG signal's proneness to artifacts influences negatively the extraction of PRV indexes when comparing to HRV, especially in those related to higher frequencies. This may explain the lack of prediction capability of these features in the current system, contrasting with [3], where some ECG-based HRV indexes enhanced the behavior of the algorithm. PR features are the only PRV-related that positively contribute to this algorithm, following the conclusion that PR was the PRV index most similar to the one of HRV (the heart rate – HR). As observed in [5], PR showed to be a good surrogate of HR and SDNN as one of the most accurate PRV indexes. In accordance, ΔPR, PR and SDNN were selected in 2nd, 4th and 6th places (Table 1).

As for the SDPPG features, *b/a* is the only that exhibits FSS greater than 50%, which may be explained by its relation with arterial elastic properties in aortic stiffness and in carotid and peripheral artery compliance [7].

CT and VR features, on their side, showed no major contribution to the prediction of syncope, exhibiting a low FSS. Nevertheless, these parameters are linearly derived from two PPG_{CP}, whose information is already embedded in PR-related features. The ID framework revealed to be more useful when applied to calculated parameters than to the PPG signal itself, and the only ID function presented in Table 1 is the *SysInfor* applied to some parameters.

The 5 best scored features concern indexes already identified as some of the potentially most valuable PPG-related predictors for syncope [3, 4]. However, the first two features (SI and ΔPR) are the only ones showing, respectively, FSS>90% and FSS>78%. The others exhibit FSS<61%.

Despite SI and ΔPR being the most promising features for syncope prediction, expanding the set of evaluated features improves the interpretability of the algorithm. Although the intervals of FSS between the remaining features being less than 10%, the increase of their number may increase the diagnostic value of the algorithm. This justifies our analysis on combinations of all the features in Table 1.

Tables 2-3 refer to the performance of the algorithm setups with better results (the others performed similarly or worse), in a decreasing order of test-phase Fm and in an increasing order of validation-phase FPRh. The achieved outcomes are unable to surpass the results of the ECG/PPG-based algorithm, as in [4]. However, the PPG-based algorithm of [4] presents, in the validation phase, SE=65.3%, SP=94% and FPRh=0.14, and, in the test phase, SE=83.3%, SP=76.9%, FPRh=1.03 h^{-1} and PT=238.6±185.1 sec. Comparing these results with the ones in Table 2, SE was highly increased, with SE=100% in the test phase of all the attempts and SE ∈ [68.67; 93.33] % in the validation phase. SP maintained similar values, with slight improvements: validation with [77.50; 93.67] % and test with [77; 85] %. PT registered a range that contains the previous value: [190.9; 368.8] sec. As for the FPRh values, only the first (n=1) measure in Table 2 was able to perform near the reference, being 0.15 h^{-1} (validation) and 1.9 h^{-1} (test). Except for the 7th attempt (validation FPRh=1.15; test FPRh=1.46), all the others achieved FPRh<0.83 in the validation phase and underperformed in the test phase, always with FPRh>2.

It is suggested that the enhancement of SE leads to some loss in FPRh, since these were the most divergent indicators between this study and [4]. Furthermore, as the rate of true positives (SE) increases, it is normal that some false positives are also detected, diminishing the values of FPRh. This is an important balance to achieve, since the missing of a positive target in such a real-time classifier may lead to a potentially dangerous situation, but a high rate of frequent false positive alarms, in a daily life p-health system, is not desired (it reduces the user's compliance to the system).

The 2nd, 6th and 7th records, with only three and four embedded features, confirm the idea that just the parameters of SI and/or PR would often provide a decent syncope predictor (all the features of these records are derived from them). The 7th record, only with four clipped features, is, in fact, the one with higher validation SE and SP, as well as lower test FPRh, in spite of presenting the worst values of PT and validation FPRh. Records 2 and 6 only differ on the clipping of SI, which was enough to increase PT in 3.1 sec and the validation SE in 9.67%, from the 2nd to the 6th register. Yet, FPRh increased in 0.12 (validation) and 0.88 (test).

The 1st and 3rd records also diverge merely on the clipping of SI, being the ones setting more features in and with the lowest validation FPRh (1st: 0.15; 3rd: 0.23). Despite with less 126.5 sec of PT, the 1st record has more interesting values of Fm, SE, SP and FPRh (both validation and test).

In a global perspective, the collected results indicate that the choice of features to embed in the algorithm is more determinant than the clipping of values non-related to syncope. It is, therefore, expected that the improvement of its performance will depend on the finding of other predictive features with FSS values similar to the ones of SI and ΔPR.

LVET was included in the 1st setup of Tables 2-3, even though it was not one of the features suggested by the FSS ranking in Table 1. However, LVET illustrates myocardial contractility, being an important inotropic evaluator. Moreover, its direct correlation with the training output was significant, leading us to embed it in some of the presented setups, despite the FSS ranking results.

As suggested in the previous section, some of the features in Tables 2-3 were clipped (SI, ΔPR and ΔSI). SI is, contrarily to the rest of the parameters, a direct estimator of

the pulse transit time (PTT) and, consequently, of the BP (explaining its high FSS). To predict syncope event, it is necessary to detect hypotension, illustrated by an increase in the SI curve. As distance metrics are symmetrical to the origin of the referential, the clipping of the decreasing points of the curve allows the focus on the increase of the signal, easing the distinguishing of impending syncope. With the increase of BP, the detection of the PPG_{CP} needed to estimate SI can be severely compromised, increasing the uncertainty in the estimation of the parameter. Therefore, clipping lower SI values also contributes to its better prediction capability. As for the PR, the prediction of a syncope is associated with a decrease in its signal, so, the clipped changes are the ones of increasing tendencies.

To verify that the Minkowski distance with $p=2^{-0.5}$ kept being the most indicated classifier metric despite the proposed changes, all the distance metrics presented in [1] were applied to the 1st algorithm setup presented in Tables 2-3. As in [1], no distance metric performed as well as this one.

IV. Conclusions

This work proposes a PPG-based algorithm to predict impending syncope in real time, in a p-health context. Several parameters and their combinations were studied, producing a total set of 94 features. The application of a clipping operation to the features, as well as applying different distance metrics, was also approached. In this way, the most relevant features to predict syncope were selected, based on their FSS. The algorithm was fed and validated with the selected features, evaluating which combination of features was the most suitable one to predict syncope. This assessment was made using a trained threshold as classifier, after applying the Minskowski distance ($p=2^{-0.5}$) (which was confirmed as the most suitable distance metric to this end).

The absence of PAT-related features weakens the PPG-based algorithm (this drawback was not possible to overcome). However, our results had an overall positive evolution over the PPG-only suggestion in [4]. At this point, we do not propose the use of any of the options shown in Tables 2-3 in a daily life scenario, but we emphasize the better results of the 1st setup over the others, especially in its FPRh. It resorts to the PPG_{onset} and the Minskowski distance ($p=2^{-0.5}$), using: SI (clipped), ΔPR, ΔSI, PR, ΔLVET, RI and LVET. Its optimal threshold is: ~4.236.

Acknowledgment

This work was supported in part by the LINK (H2020 – 692023) and HeartCycle (FP7 – 216695) projects.

Conflict of Interest

The authors declare that they have no conflict of interest.

References

[1] Couceiro R, Carvalho P, Paiva RP et al., "Real-Time Prediction of Neurally Mediated Syncope," *IEEE journal of biomedical and health informatics,* vol. 20, no. 2, pp. 508-520, 2016.

[2] Couceiro R, Carvalho P, Paiva RP et al., "Neurally mediated syncope prediction based on changes of cardiovascular performance surrogates: Algorithms comparison," *7th International Conf on Biomedical Engineering and Informatics,* pp. 358-362, 2014.

[3] Couceiro R, Carvalho P, Paiva RP et al., "Algorithm for real-time prediction of neurally mediated syncope integrating indexes of autonomic modulation," *Comput in Cardiol Conf (CinC),* pp. 685-688, 2015.

[4] Couceiro R, Carvalho P, Paiva RP et al., "Evaluation of a PPG-based algorithm for prediction of neurally mediated syncope," *2016 IEEE-EMBS International Conference on Biomedical and Health Informatics (BHI),* pp. 434-436, 2016.

[5] Pinheiro N, Couceiro R, Henriques J et al., "Can PPG be used for HRV analysis?," *Engineering in Medicine and Biology Society (EMBC), 2016 IEEE 38th Annual International Conference of the,* pp. 2945-2949, 2016.

[6] Malik M, "Heart rate variability: Standards of measurement, physiological interpretation and clinical use," *Eur Heart J,* vol. 17, p. 354–381, 1996.

[7] Qawqzeh YK, Uldis R, Alharbi M, "Photoplethysmogram second derivative review: Analysis and applications," *Scientific Research and Essays,* vol. 10, no. 21, pp. 633-639, 2015.

[8] Faes L, Porta A, "Conditional entropy-based evaluation of information dynamics in physiological systems," *Directed information measures in neuroscience,* pp. 61-86, 2014.

Enter the information of the corresponding author:

Author:
Institute:
Street:
City:
Country:
Email:

Appendix C

Materials related with Chapter 4

This appendix comprises detailed data that was computed to produce the analysis in Chapter 4.

Table 22 – Means of SRC (%) between the ECG-derived and each PPG interval-derived features.

Feature	**Intervals between PPG characteristic points**					
	PPG$_{onset}$	***PPG$_{20\%}$***	***PPG$_{der}$***	***PPG$_{50\%}$***	***PPG$_{80\%}$***	***PPG$_{peak}$***
Dataset: Case 1						
aVL	97.1±4.6	96.5±9.7	95.2±18.6	97.9±3	96.4±8.1	97.7±3.4
aLF	95.6±7.8	96.2±4.9	95.3±10.6	95.5±8.6	96.4±7.2	92±17.4
aHF	81.3±31.7	83.9±20.2	87.1±19.9	83.9±23.1	84.9±21.7	81.2±23
RaLH	81.8±22.6	82.7±21.8	84.1±20.7	85±19.9	80.6±29.4	81.2±29.2
HRV-PRV	98.2±2	98.1±2.4	98.1±2.2	98.3±2.1	98.1±2.4	97.9±2.4
Mean	99.3±2	98.8±4.3	99.5±1	99.4±1.8	99.2±2.6	98.6±4
SDNN	93.6±21.1	93.4±18.8	93.2±23.4	91.8±23.3	93.2±17.4	93.6±17.3
SDSD	89.3±13.9	90.6±13	90.7±11.2	87.9±18	90.9±12.1	87±15.2
RMSSD	89.3±14.1	90.7±12.9	90.7±11.4	87.9±18	91±12	87.1±15
NN50	68±22.7	61.9±32.1	69.1±30.6	66.4±30.6	60.4±34.2	56.1±37.5
pNN50	68±22.7	61.9±32.1	69.1±30.6	66.4±30.6	60.4±34.2	56.1±37.5
Dataset: Case 2						
aVL	98.5±2.3	98.6±2.3	98.6±2.2	99.1±1.5	98.9±1.9	98.9±1.8
aLF	86.5±34.5	88.9±28.9	87.1±30.9	86.8±30.1	86.7±29.2	84.4±38.8
aHF	79.7±27.6	89.3±16.2	77.2±30.8	86.4±19	83±38.9	82.8±24.5
RaLH	68.1±34.4	75.1±27	68.8±34.9	64.9±40.4	70.5±37.5	61.3±46.5
HRV-PRV	97.5±2.2	97.5±2.3	97.6±2.4	97.5±2.5	97.4±2.6	97.2±3.1
Mean	99.9±0.4	99.8±0.5	99.7±1	99.7±1	99.7±1	99.6±1.1
SDNN	98.8±4	97.5±7.7	99±3.9	97.3±9	98.8±4	97.5±7.7
SDSD	62±54.3	72.6±41.4	63.5±49.4	66.7±46.6	72.5±43.3	72.6±40.8
RMSSD	62.2±54.6	72.6±41.6	64.4±48.6	66.6±46.7	71.7±44	72.7±41.1
NN50	55.3±40.5	56.5±36.6	60.7±30.3	62.4±40.4	61.8±30.3	55.7±39.7
pNN50	55.3±40.5	56.5±36.6	60.7±30.3	62.4±40.4	61.8±30.3	55.7±39.7
Dataset: Case 3						
aVL	85.1±21.2	81.1±35.5	83.9±30.8	78.8±37	84.4±28.7	85.1±28.8
aLF	81.5±27.3	79.3±35.8	78.3±37.9	76.5±41	74.5±43	70.6±51.1
aHF	71.3±42.1	56.7±53.9	62.2±51.2	57.5±53	55±56.8	56.3±56.3
RaLH	67.8±37.9	67±36.1	65.9±38.9	59.1±42.9	68±38.8	67.1±38.5
HRV-PRV	89.1±15.6	89.5±15.9	89±15.7	89.3±15.7	89.4±16.1	88.6±16
Mean	96±6.8	95.7±9.4	95.2±9.1	95.2±8.9	96.2±6.7	94.9±7.9
SDNN	92.9±9.4	90.4±14.6	87.4±22.4	87.3±21	85.7±26.3	87.6±23.7
SDSD	73.9±35.7	75.8±26.7	75±29.4	73.1±31.1	72.6±32.7	68.2±42.7
RMSSD	73.9±35.7	75.8±26.8	75.1±29.5	73±30.9	72.6±32.7	68.2±42.7
NN50	43.6±42.8	39.8±42.6	48.4±38.4	41.9±49.2	45±44.3	36.2±46.2
pNN50	43.6±42.8	39.8±42.6	48.4±38.4	41.9±49.2	45±44.3	36.2±46.2

Table 23 – Means of NRMSE (%) between the ECG-derived and each PPG interval-derived features.

Feature	**Intervals between PPG characteristic points**					
	PPG$_{onset}$	***PPG$_{20\%}$***	***PPG$_{der}$***	***PPG$_{50\%}$***	***PPG$_{80\%}$***	***PPG$_{peak}$***
Dataset: Case 1						
aVL	11.3±10.9	11.3±9.9	10.5±13.4	10.1±8.3	9.1±5.5	13.2±14.2
aLF	11.5±10.6	9.7±5.8	10.1±6.5	10.3±7.4	10.4±8.1	11.6±10.8
aHF	26.4±21.5	23±20.6	24.9±19.1	21.1±11.7	22.2±13.8	18.1±11.1
RaLH	20.6±9.6	18.6±10.2	20.6±11.4	17.9±8.9	17.1±10	16.6±7.9
HRV-PRV	1.3±0.8	1.3±0.9	1.3±0.9	1.3±0.9	1.3±0.9	1.4±0.9
Mean	0.1±0.1	0.1±0.1	0.1±0.1	0.1±0.1	0.1±0.1	0.1±0.1
SDNN	3±2.5	2.6±2	2.7±1.8	2.7±1.8	2.7±1.9	2.6±2.1
SDSD	12.6±6.7	11.4±7.5	11.4±6	10.5±6.3	10.4±6.2	10.7±7
RMSSD	12.6±6.7	11.4±7.5	11.4±6	10.5±6.3	10.4±6.2	10.7±7
NN50	6.1±3.6	6.4±3.4	5.7±3.6	6.2±3.7	6.6±3.8	6.3±3.6
pNN50	6.1±3.6	6.4±3.4	5.7±3.6	6.2±3.7	6.6±3.8	6.3±3.6
Dataset: Case 2						
aVL	15.5±16.7	17.3±39.1	21.9±63.5	24.2±68.8	22.5±65	22.3±73.3
aLF	13.4±10.5	12.9±9.2	21.9±50.7	14.3±17.1	13.8±11.8	14.5±13.5
aHF	63.2±65.7	57.8±63.8	60.4±64.8	54.7±48.9	55.6±71.4	44.3±41.3
RaLH	30±20.3	26.5±19.5	27.3±20.2	28±19.5	26.6±20.3	26.4±18.1
HRV-PRV	1.3±0.6	1.4±0.9	1.3±0.8	1.4±0.8	1.4±0.9	1.4±1
Mean	0.1±0.1	0.1±0.1	0.1±0.1	0.1±0.2	0.1±0.1	0.1±0.1
SDNN	3.1±2.9	3.1±3.6	4.4±10.5	3.8±7.2	3.7±6	3.6±7.4
SDSD	44.1±42.8	40.1±40.4	37.8±34.6	36.3±34.7	36.2±34.8	37±37.1
RMSSD	44±42.6	40±40.2	37.7±34.5	36.2±34.5	36.1±34.6	36.9±36.9
NN50	8.2±5.3	8.9±5.3	9.6±5.5	9.1±5.5	9.8±5.9	10.1±5.5
pNN50	8.2±5.3	8.9±5.3	9.6±5.5	9.1±5.5	9.8±5.9	10.1±5.5
Dataset: Case 3						
aVL	28.8±33.4	36.4±40.9	38.8±43.2	33.5±33.6	32.6±34.1	30.9±29.7
aLF	27±24	31.6±41.3	33.2±31.6	31.4±36.3	29.5±31.9	39.8±44.8
aHF	55.4±57	67.2±112.7	67.8±93.7	50.2±39.1	50.9±42.3	54.7±66.2
RaLH	44.5±31.4	45.6±37.6	48.6±37.9	52.8±48.1	42.6±32.6	44.5±37.1
HRV-PRV	2.6±2.5	2.7±2.5	2.8±2.6	2.6±2.4	2.6±2.3	2.8±2.5
Mean	0.2±0.3	0.2±0.3	0.4±0.6	0.3±0.4	0.3±0.5	0.3±0.3
SDNN	6.6±4.9	7±5.8	8.6±7.7	7.4±6.4	7.5±7	8.7±8.2
SDSD	20.1±18	19.3±16.1	20.5±16.7	16.9±12.6	17.8±13.6	18±16.1
RMSSD	20.1±18	19.3±16.1	20.5±16.7	16.9±12.6	17.8±13.6	18±16.1
NN50	9.3±6	9.3±5.9	8.7±5.7	9.7±6.9	10.3±7	10.6±7.7
pNN50	9.3±6	9.3±5.9	8.7±5.7	9.7±6.9	10.3±7	10.6±7.7

Table 24 – Mean p-values (plus STD) between HRV and PRV features, produced with the WRST.

Feature	**Intervals between PPG characteristic points**					
	PPG$_{onset}$	***PPG$_{20\%}$***	***PPG$_{der}$***	***PPG$_{50\%}$***	***PPG$_{80\%}$***	***PPG$_{peak}$***
Dataset: Case 1						
aVL	0.674±0.246	0.690±0.000	0.636±0.246	0.628±0.296	0.713±0.000	0.640±0.246
aLF	0.416±0.336	0.466±0.246	0.409±0.296	0.465±0.246	0.447±0.177	0.492±0.246
aHF	0.135±0.499	0.174±0.507	0.125±0.492	0.142±0.507	0.165±0.508	0.271±0.504
RaLH	0.221±0.499	0.281±0.457	0.193±0.483	0.312±0.44	0.366±0.42	0.418±0.397
HRV-PRV	0.842±0.000	0.845±0.000	0.845±0.000	0.894±0.000	0.838±0.000	0.822±0.000
Mean	0.697±0.000	0.641±0.000	0.628±0.000	0.742±0.000	0.703±0.000	0.717±0.000
SDNN	0.297±0.440	0.317±0.397	0.250±0.440	0.244±0.457	0.278±0.44	0.346±0.296
SDSD	0.073±0.369	0.056±0.369	0.068±0.296	0.057±0.296	0.035±0.296	0.094±0.471
RMSSD	0.073±0.369	0.056±0.369	0.069±0.296	0.057±0.296	0.034±0.296	0.094±0.471
NN50	0.063±0.397	0.033±0.369	0.049±0.369	0.062±0.336	0.063±0.336	0.023±0.336
pNN50	0.063±0.397	0.033±0.369	0.049±0.369	0.062±0.336	0.063±0.336	0.023±0.336
Dataset: Case 2						
aVL	0.571±0.251	0.632±0.263	0.607±0.284	0.628±0.296	0.609±0.274	0.607±0.304
aLF	0.386±0.341	0.371±0.274	0.337±0.290	0.430±0.343	0.380±0.293	0.374±0.291
aHF	0.150±0.265	0.188±0.278	0.192±0.279	0.170±0.271	0.204±0.238	0.290±0.337
RaLH	0.190±0.314	0.249±0.327	0.239±0.267	0.244±0.300	0.295±0.352	0.241±0.269
HRV-PRV	0.898±0.070	0.889±0.099	0.897±0.083	0.884±0.129	0.876±0.137	0.864±0.119
Mean	0.717±0.130	0.707±0.142	0.711±0.150	0.707±0.172	0.704±0.135	0.713±0.174
SDNN	0.410±0.270	0.429±0.292	0.413±0.275	0.433±0.292	0.445±0.296	0.503±0.317
SDSD	0.040±0.099	0.041±0.094	0.034±0.086	0.037±0.091	0.039±0.089	0.062±0.137
RMSSD	0.040±0.099	0.041±0.094	0.034±0.087	0.037±0.091	0.039±0.089	0.060±0.129
NN50	0.062±0.143	0.066±0.191	0.101±0.240	0.059±0.156	0.030±0.086	0.033±0.087
pNN50	0.062±0.143	0.066±0.191	0.101±0.240	0.059±0.156	0.030±0.086	0.033±0.087
Dataset: Case 3						
aVL	0.413±0.325	0.470±0.368	0.370±0.344	0.460±0.364	0.456±0.355	0.429±0.320
aLF	0.406±0.282	0.463±0.311	0.444±0.315	0.446±0.305	0.462±0.335	0.393±0.339
aHF	0.184±0.285	0.180±0.297	0.129±0.215	0.195±0.305	0.145±0.284	0.193±0.296
RaLH	0.162±0.255	0.192±0.265	0.190±0.256	0.198±0.244	0.222±0.307	0.196±0.265
HRV-PRV	0.661±0.266	0.672±0.296	0.691±0.300	0.677±0.297	0.697±0.305	0.680±0.291
Mean	0.519±0.348	0.460±0.369	0.490±0.394	0.481±0.365	0.522±0.356	0.452±0.372
SDNN	0.231±0.309	0.174±0.253	0.198±0.259	0.202±0.299	0.245±0.307	0.161±0.270
SDSD	0.072±0.158	0.073±0.135	0.119±0.231	0.056±0.131	0.126±0.247	0.089±0.212
RMSSD	0.072±0.158	0.073±0.135	0.119±0.231	0.056±0.131	0.126±0.247	0.089±0.212
NN50	0.048±0.140	0.011±0.039	0.023±0.079	0.054±0.199	0.012±0.047	0.053±0.159
pNN50	0.048±0.140	0.011±0.039	0.023±0.079	0.054±0.199	0.012±0.047	0.053±0.159

Appendix D

Materials related with Chapter 5

This appendix comprises detailed data that was computed to produce the analysis in Chapter 5.

Table 25 – Analyzed features to embed in the syncope prediction algorithm, listed and numbered by type.

Direct Features				**Indirect Features**			
#	**Norm. Param.**	**#**	**90-sec Norm. Param.**	**#**	**Param. *SysInfor***	**#**	**Param. *UnexpInf***
1	PR	26	ΔPR	51	PR_{HY}	73	PR_{UY}
2	LVET	27	ΔLVET	52	$LVET_{HY}$	74	$LVET_{UY}$
3	SI	28	ΔSI	53	SI_{HY}	75	SI_{UY}
4	RI	29	ΔRI	54	RI_{HY}	76	RI_{UY}
5	*Mean*	30	Δ*Mean*	55	$Mean_{HY}$	77	$Mean_{UY}$
6	SDNN	31	ΔSDNN	56	$SDNN_{HY}$	78	$SDNN_{UY}$
7	SDSD	32	ΔSDSD	57	$SDSD_{HY}$	79	$SDSD_{UY}$
8	RMSSD	33	ΔRMSSD	58	$RMSSD_{HY}$	80	$RMSSD_{UY}$
9	NN50	34	ΔNN50	59	$NN50_{HY}$	81	$NN50_{UY}$
10	pNN50	35	ΔpNN50	60	$pNN50_{HY}$	82	$pNN50_{UY}$
11	aVL	36	ΔaVL	61	aVL_{HY}	83	aVL_{UY}
12	aLF	37	ΔaLF	62	aLF_{HY}	84	aLF_{UY}
13	aHF	38	ΔaHF	63	aHF_{HY}	85	aHF_{UY}
14	RaLH	39	ΔRaLH	64	$RaLH_{HY}$	86	$RaLH_{UY}$
15	*b/a*	40	Δ*b/a*	65	b/a_{HY}	87	b/a_{UY}
16	*c/a*	41	Δ*c/a*	66	c/a_{HY}	88	c/a_{UY}
17	*d/a*	42	Δ*d/a*	67	d/a_{HY}	89	d/a_{UY}
18	*e/a*	43	Δ*e/a*	68	e/a_{HY}	90	e/a_{UY}
19	*f/a*	44	Δ*f/a*	69	f/a_{HY}	91	f/a_{UY}
20	SDPPG-AI	45	ΔSDPPG-AI	70	$SDPPG\text{-}AI_{HY}$	92	$SDPPG\text{-}AI_{UY}$
21	CT	46	ΔCT	71	CT_{HY}	93	CT_{UY}
22	VR	47	ΔVR	72	VR_{HY}	94	VR_{UY}
23	*SysInfor*	48	Δ*SysInfor*	--	-----	--	-----
24	*UnexpInf*	49	Δ*UnexpInf*	--	-----	--	-----
25	*InfStor*	50	Δ*InfStor*	--	-----	--	-----

Table 26 – Ranking of all the evaluated features by their FSS to predict impending syncope. The PR and PRV-related features were computed with PPG_{onset}. This ranking was made for each PPG characteristic point, but they are not shown here, due to much volume of information.

Rank	Feature	FSS (%)	Rank	Feature	FSS (%)	Rank	Feature	FSS (%)
1	SI	91.78	33	aVL_{UY}	41.86	64	b/a_{HY}	28.45
2	ΔPR	79.43	34	$NN50_{UY}$	41.32	65	RMSSD	28.28
3	SI	60.00	35	$RMSSD_{UY}$	40.99	66	*e/a*	28.05
4	PR	59.94	36	Δ*UnexpInf*	40.85	67	RaLH	27.84
5	ΔLVET	57.52	37	$Mean_{HY}$	40.58	68	VR	27.51
6	SDNN	56.91	38	Δ*f/a*	40.52	69	ΔaHF	27.20
7	$pNN50_{HY}$	55.08	39	pNN50	40.12	70	c/a_{HY}	27.04
8	RI	55.01	40	SI_{UY}	40.08	71	ΔaLF	26.95
9	PR_{HY}	53.57	41	ΔpNN50	39.09	72	*f/a*	26.90
10	Δ*b/a*	51.84	42	$SDNN_{HY}$	39.08	73	aLF_{HY}	26.70
11	$SDSD_{HY}$	51.70	43	Δ*c/a*	38.88	74	*b/a*	25.84
12	ΔaVL	51.21	44	$RaLH_{HY}$	38.42	75	d/a_{HY}	25.78
13	Δ*Mean*	51.15	45	$Mean_{UY}$	38.12	76	aLF_{UY}	25.51
14	LVET	48.83	46	*SysInfor*	37.88	77	*c/a*	25.14
15	$LVET_{HY}$	48.53	47	CT_{HY}	37.59	78	ΔSDSD	25.05
16	PR_{UY}	47.26	48	ΔNN50	37.50	79	aLF	24.99
17	ΔSDPPG-AI	46.62	49	$SDNN_{UY}$	37.37	80	e/a_{HY}	24.68
18	$SDSD_{UY}$	46.29	50	$RaLH_{UY}$	36.57	81	ΔCT	24.65
19	aVL	45.71	51	*InfStor*	35.91	82	*d/a*	24.53
20	aVL_{HY}	45.63	52	CT_{UY}	35.82	83	ΔRMSSD	24.11
21	$pNN50_{UY}$	45.61	53	*UnexpInf*	35.33	84	SDPPG-AI	23.83
22	VR_{HY}	45.25	54	Δ*InfStor*	33.94	85	f/a_{HY}	23.68
23	$LVET_{UY}$	44.01	55	RI_{HY}	33.18	86	aHF	22.80
24	ΔSDNN	43.99	56	CT	32.27	87	$SDPPG\text{-}AI_{HY}$	22.70
25	Δ*e/a*	43.83	57	aHF_{HY}	32.14	88	b/a_{UY}	21.64
26	SI_{HY}	43.01	58	RI_{UY}	31.60	89	c/a_{UY}	20.60
27	$NN50_{HY}$	42.97	59	Δ*SysInfor*	31.56	90	d/a_{UY}	19.59
28	*Mean*	42.37	60	aHF_{UY}	30.86	91	e/a_{UY}	18.59
29	NN50	42.20	61	ΔRI	30.79	92	f/a_{UY}	17.62
30	$RMSSD_{HY}$	42.20	62	ΔRaLH	30.68	93	$SDPPG\text{-}AI_{UY}$	16.67
31	Δ*d/a*	42.10	63	ΔVR	29.66	---	---	---
32	VR_{UY}	41.94	64	SDSD	29.58	---	---	---

Table 27 – Numbered list of all the different features' sets used to feed the algorithm. These setups were tested following the order of decreased FSS, for each PPG interval. They were also tested in unclipped and clipped versions. The achieved results are not shown, due to much information volume and lack of interest (the best results are indicated in Chapter 5).

n	PPG interval	Features Description	n	PPG interval	Features Description
1	PPG_{onset}	SI, ΔPR, ΔSI, PR, ΔLVET, SDNN, $pNN50_{HY}$, RI, PR_{HY}, Δ*b/a*, $SDSD_{HY}$, ΔaVL, Δ*Mean*	28	$PPG_{50\%}$	SI, ΔPR, ΔSI
2		SI, ΔPR, ΔSI, PR, ΔLVET, SDNN, $pNN50_{HY}$, RI, PR_{HY}, Δ*b/a*, $SDSD_{HY}$, ΔaVL	29		SI, ΔPR
3		SI, ΔPR, ΔSI, PR, ΔLVET, SDNN, $pNN50_{HY}$, RI, PR_{HY}, Δ*b/a*, $SDSD_{HY}$	30		SI, ΔPR, SDNN, PR, ΔSI, ΔLVET, $RMSSD_{HY}$, RI, Δ*b/a*
4		SI, ΔPR, ΔSI, PR, ΔLVET, SDNN, $pNN50_{HY}$, RI, PR_{HY}, Δ*b/a*	31		SI, ΔPR, SDNN, PR, ΔSI, ΔLVET, $RMSSD_{HY}$, RI
5		SI, ΔPR, ΔSI, PR, ΔLVET, SDNN, $pNN50_{HY}$, RI, PR_{HY}	32		SI, ΔPR, SDNN, PR, ΔSI, ΔLVET, $RMSSD_{HY}$
6		SI, ΔPR, ΔSI, PR, ΔLVET, SDNN, $pNN50_{HY}$, RI	33		SI, ΔPR, SDNN, PR, ΔSI, ΔLVET
7		SI, ΔPR, ΔSI, PR, ΔLVET, SDNN, $pNN50_{HY}$	34		SI, ΔPR, SDNN, PR, ΔSI
8		SI, ΔPR, ΔSI, PR, ΔLVET, SDNN	35		SI, ΔPR, SDNN, PR
9		SI, ΔPR, ΔSI, PR, ΔLVET	36		SI, ΔPR, SDNN
10		SI, ΔPR, ΔSI, PR	37		SI, ΔPR
11		SI, ΔPR, ΔSI	38	$PPG_{80\%}$	SI, ΔPR, ΔLVET, PR, ΔSI, SDNN, $NN50_{HY}$, RI, Δ*b/a*
12		SI, ΔPR	39		SI, ΔPR, ΔLVET, PR, ΔSI, SDNN, $NN50_{HY}$, RI
13		SI	40		SI, ΔPR, ΔLVET, PR, ΔSI, SDNN, $NN50_{HY}$
14	$PPG_{20\%}$	SI, ΔPR, SDNN, PR, ΔSI, ΔLVET, RI, $pNN50_{HY}$, Δ*b/a*	41		SI, ΔPR, ΔLVET, PR, ΔSI, SDNN
15		SI, ΔPR, SDNN, PR, ΔSI, ΔLVET, RI, $pNN50_{HY}$	42		SI, ΔPR, ΔLVET, PR, ΔSI
16		SI, ΔPR, SDNN, PR, ΔSI, ΔLVET, RI	43		SI, ΔPR, ΔLVET, PR
17		SI, ΔPR, SDNN, PR, ΔSI, ΔLVET	44		SI, ΔPR, ΔLVET
18		SI, ΔPR, SDNN, PR, ΔSI	45		SI, ΔPR
19		SI, ΔPR, SDNN, PR	46	PPG_{peak}	SI, ΔPR, ΔLVET, ΔSI, PR, SDNN, RI, $SDSD_{HY}$, Δ*b/a*
20		SI, ΔPR, SDNN	47		SI, ΔPR, ΔLVET, ΔSI, PR, SDNN, RI, $SDSD_{HY}$
21		SI, ΔPR	48		SI, ΔPR, ΔLVET, ΔSI, PR, SDNN, RI
22	PPG_{der}	SI, ΔPR, ΔSI, PR, SDNN, ΔLVET, $RMSSD_{HY}$, RI, Δ*b/a*	49		SI, ΔPR, ΔLVET, ΔSI, PR, SDNN
23		SI, ΔPR, ΔSI, PR, SDNN, ΔLVET, $RMSSD_{HY}$, RI	50		SI, ΔPR, ΔLVET, ΔSI, PR
24		SI, ΔPR, ΔSI, PR, SDNN, ΔLVET, $RMSSD_{HY}$	51		SI, ΔPR, ΔLVET, ΔSI
25		SI, ΔPR, ΔSI, PR, SDNN, ΔLVET	52		SI, ΔPR, ΔLVET
26		SI, ΔPR, ΔSI, PR, SDNN	53		SI, ΔPR
27		SI, ΔPR, ΔSI, PR	-----		

Table 28 - Tested sets of features that include LVET in the first record for each PPG interval, not following the ranking of FSS. They were also tested in unclipped and clipped versions. The achieved results are not shown, due to much information volume and lack of interest (the best results are indicated in Chapter 5).

n	PPG interval	Features Description
1	PPG_{onset}	SI, ΔPR, ΔSI, PR, ΔLVET, RI, LVET
2		SI, ΔPR, ΔSI, PR, ΔLVET, RI
3		SI, ΔPR, ΔSI, PR, ΔLVET
4		SI, ΔPR, ΔSI, PR
5		SI, ΔPR, ΔSI
6	$PPG_{20\%}$	SI, ΔPR, ΔSI, PR, ΔLVET, RI, LVET
7		SI, ΔPR, ΔSI, PR, ΔLVET, RI
8		SI, ΔPR, ΔSI, PR, ΔLVET
9		SI, ΔPR, ΔSI, PR
10		SI, ΔPR, ΔSI
11	PPG_{der}	SI, ΔPR, ΔSI, PR, ΔLVET, RI, LVET
12		SI, ΔPR, ΔSI, PR, ΔLVET, RI
13		SI, ΔPR, ΔSI, PR, ΔLVET
14		SI, ΔPR, ΔSI, PR
15		SI, ΔPR, ΔSI
16	$PPG_{50\%}$	SI, ΔPR, ΔSI, PR, ΔLVET, RI, LVET
17		SI, ΔPR, ΔSI, PR, ΔLVET, RI
18		SI, ΔPR, ΔSI, PR, ΔLVET
19		SI, ΔPR, ΔSI, PR
20		SI, ΔPR, ΔSI
21	$PPG_{80\%}$	SI, ΔPR, ΔSI, PR, ΔLVET, RI, LVET
22		SI, ΔPR, ΔSI, PR, ΔLVET, RI
23		SI, ΔPR, ΔSI, PR, ΔLVET
24		SI, ΔPR, ΔSI, PR
25		SI, ΔPR, ΔSI
26	PPG_{peak}	SI, ΔPR, ΔSI, PR, ΔLVET, RI, LVET
27		SI, ΔPR, ΔSI, PR, ΔLVET, RI
28		SI, ΔPR, ΔSI, PR, ΔLVET
29		SI, ΔPR, ΔSI, PR
30		SI, ΔPR, ΔSI

References

[1] J. G. van Djik, and R. Sheldon, "Is there any point to vasovagal syncope?," *Clinical Autonomic Research,* vol. 18, no. 4, pp. 167-169, 2008.

[2] A. Moya, R. Sutton, F. Ammirati, J. J. Blanc, M. Brignole, J. B. Dahm, et al., "Guidelines for the diagnosis and management of syncope (version 2009)," *European heart journal,* vol. 30, no. 21, pp. 2631-2671, 2009.

[3] D. G. Benditt, J. J. Blanc, M. Brignole, and R. S. Sutton, The evaluation and treatment of syncope. A handbook for clinical practice, Blackwell Publishing, 2006.

[4] N. Colman, K. Nahm, K. S. Ganzeboom, W. K. Shen, J. Reitsma, M. Linzer, et al., "Epidemiology of reflex syncope," *Clinical Autonomic Research,* vol. 14, no. 1, pp. i9-i17, 2004.

[5] D. M. Lemonick, "Evaluation of Syncope in the emergency department," *American Journal of Clinical Medicine,* vol. 14, no. 1, pp. 11-9, 2010.

[6] A. Alshekhlee, W. K. Shen, J. Mackall, and T. C. Chelimsky, "Incidence and mortality rates of syncope in the United States," *The American journal of medicine,* vol. 122, no. 2, pp. 181-188, 2009.

[7] C. Kessler, J. M. Tristano, R. De Lorenzo, "The emergency department approach to syncope: evidence-based guidelines and prediction rules," *Emergency medicine clinics of North America,* vol. 28, no. 3, pp. 487-500, 2010.

[8] H. Snooks, W. Y. Cheung, J. Close, J. Dale, S. Gaze, I. Humphreys, et al., "Support and Assessment for Fall Emergency Referrals (SAFER 1) trial protocol. Computerised on-scene decision support for emergency ambulance staff to assess and plan care for older people who have fallen: evaluation of costs and benefits using a pragmatic," *BMC Emergency Medicine,* vol. 10, no. 1, p. 1, 2010.

[9] M. P. Tan, and R. A. Kenny, "Cardiovascular assessment of falls in older people," *Clinical interventions in aging,* vol. 1, no. 1, p. 57, 2006.

[10] J. Stephenson, Fits and Faints, Cambridge University Press, 1991, pp. 41-57.

[11] R. Couceiro, P. Carvalho, R. P. Paiva, J. Muehlsteff, J. Henriques, S. Willems, et al., "Evaluation of a PPG-based algorithm for prediction of neurally mediated syncope," *2016 IEEE-EMBS International Conference on Biomedical and Health Informatics (BHI),* pp. 434-436, 2016.

[12] U. R. Acharya, K. P. Joseph, N. Kannathal, C. M. Lim, and J. S. Suri, "Heart rate variability: a review," *Medical and biological engineering and computing,* vol. 44, no. 12, pp. 1031-1051, 2006.

[13] L. Faes, and A. Porta, "Conditional entropy-based evaluation of information dynamics in physiological systems," *Directed information measures in neuroscience,* pp. 61-86, 2014.

[14] X. F. Teng, Y. T. Zhang, C. C. Poon, and P. Bonato, "Wearable medical systems for p-health," *IEEE reviews in Biomedical engineering,* vol. 1, pp. 62-74, 2008.

[15] C. C. Poon, Y. M. Wong, and Y. T. Zhang, "M-health: the development of cuff-less and wearable blood pressure meters for use in body sensor networks," *2006 IEEE/NLM Life Science Systems and Applications Workshop,* pp. 1-2, 2006.

[16] M. Elgendi, "On the analysis of fingertip photoplethysmogram signals," *Current cardiology reviews,* vol. 8, no. 1, pp. 14-25, 2012.

[17] A. Schäfer, and J. Vagedes, "How accurate is pulse rate variability as an estimate of heart rate variability?: A review on studies comparing photoplethysmographic technology with an electrocardiogram," *International journal of cardiology,* vol. 166, no. 1, p. 15–29, 2013.

[18] R. Couceiro, "PhD Thesis: Cardiovascular Performance Assessment for p-Health Applications," University of Coimbra, Coimbra, 2014.

[19] R. Couceiro, P. Carvalho, R. P. Paiva, J. Muehlsteff, J. Henriques, C. Eickholt, et al., "Real-Time Prediction of Neurally Mediated Syncope," *IEEE journal of*

biomedical and health informatics, vol. 20, no. 2, pp. 508-520, 2016.

[20] R. Couceiro, P. Carvalho, R. P. Paiva, J. Muehlsteff, J. Henriques, S. Willems, et al., "Algorithm for real-time prediction of neurally mediated syncope integrating indexes of autonomic modulation," *2015 Computing in Cardiology Conference (CinC),* pp. 685-688, 2015.

[21] R. Couceiro, P. Carvalho, R. P. Paiva, J. Henriques, J. Muehlsteff, C. Eickholt, et al., "Neurally mediated syncope prediction based on changes of cardiovascular performance surrogates: Algorithms comparison," *2014 7th International Conference on Biomedical Engineering and Informatics,* pp. 358-362, 2014.

[22] N. Pinheiro, R. Couceiro, J. Henriques, J. Muehlsteff, I. Quintal, L. Gonçalves, and P. Carvalho, "Can PPG be used for HRV analysis?," *Engineering in Medicine and Biology Society (EMBC), 2016 IEEE 38th Annual International Conference of the,* pp. 2945-2949, 2016.

[23] R. Klabunde, Cardiovascular physiology concepts, Lippincott Williams & Wilkins, 2011.

[24] J. R. Levick, An introduction to cardiovascular physiology, Butterworth-Heinemann, 2013.

[25] C B Munjewar, "Structure of the Heart & Circulation," The Fit Heart, 2016. [Online]. Available: http://www.www.thefitheart.in/structure-of-heart. [Accessed 13 December 2016].

[26] G. R. Doyle, and J. A. McCutcheon, "Clinical Procedures for Safer Patient Care, Chapter 2. Patient Assessment, 2.7 Focused Assessments," British Columbia Institute of Technology (BCIT), 2015. [Online]. Available: https://opentextbc.ca/clinicalskills/chapter/2-5-focussed-respiratory-assessment/. [Accessed 13 December 2016].

[27] Practice Learning Resources, "Cardiology Teaching Package - Cardiac Conduction System," School of Health Sciences, University of Nottingham, [Online]. Available: http://www.nottingham.ac.uk/nursing/practice/resources/cardiology/function/condu

ction.php. [Accessed 13 December 2016].

[28] G. Gabella, "Autonomic Nervous System: Introductory article," in *Encyclopedia of Life Sciences*, John Wiley & Sons, 2001, pp. 1-7.

[29] P. Low, "MSD Manuals: Overview of the Autonomic Nervous System," Merck Sharp & Dohme Corp., 2016. [Online]. Available: http://www.msdmanuals.com/home/brain,-spinal-cord,-and-nerve-disorders/autonomic-nervous-system-disorders/overview-of-the-autonomic-nervous-system. [Accessed 19 12 2016].

[30] R. Klabunde, "Cardiovascular Physiology Concepts: Regulation of Stroke Volume," Richard E. Klabunde, 07 03 2015. [Online]. Available: http://cvphysiology.com/Cardiac%20Function/CF002. [Accessed 19 12 2016].

[31] R. Klabunde, "Cardiovascular Physiology Concepts: Cardiac Preload," Richard E. Klabunde, 07 07 2015. [Online]. Available: http://cvphysiology.com/Cardiac%20Function/CF002. [Accessed 19 12 2016].

[32] R. Klabunde, "Cardiovascular Physiology Concepts: Cardiac Afterload," Richard E. Klabunde, 07 07 2015. [Online]. Available: http://cvphysiology.com/Cardiac%20Function/CF008. [Accessed 19 12 2016].

[33] Transonic Systems Inc., "Scisense PV Technical Note - Understanding Contractility: Cardiac Inotropy," 2016. [Online]. Available: http://www.transonic.com/resources/research/understanding-contractility-cardiac-intropy/. [Accessed 19 12 2016].

[34] S. Iwase, N. Nishimura, and T. Mano, "Role of sympathetic nerve activity in the process of fainting," *Frontiers in physiology*, vol. 5, p. 343, 2014.

[35] C. A. Swenne, "Baroreflex sensitivity: mechanisms and measurement," *Netherlands Heart Journal*, vol. 21, no. 2, pp. 58-60, 2013.

[36] G. L. Pierce, S. A. Harris, D. R. Seals, D. P. Casey, P. B. Barlow, et al., "Estimated aortic stiffness is independently associated with cardiac baroreflex sensitivity in humans: role of ageing and habitual endurance exercise," *Journal of human*

hypertension, 2016.

[37] M. C. Baruch, D. E. Warburton, S. S. Bredin, A. Cote, D. W. Gerdt, and C. M. Adkins, "Pulse Decomposition Analysis of the digital arterial pulse during hemorrhage simulation," *Nonlinear biomedical physics*, vol. 5, no. 1, p. 1, 2011.

[38] WA Hoefnagels, GW Padberg, J Overweg, EA Velde, RA Roos, "Transient loss of consciousness: the value of the history for distinguishing seizure from syncope," *J Neurol*, vol. 238, pp. 39-43, 1991.

[39] M. Brignole, A. Ungar, A. Bartoletti, I. Ponassi, A. Lagi, C. Mussi, et al., "Standardized-care pathway vs. usual management of syncope patients presenting as emergencies at general hospitals," *Europace*, vol. 8, no. 8, pp. 644-650, 2006.

[40] E. S. Soteriades, J. C. Evans, M. G. Larson, M. H. Chen, L. Chen, E. J. Benjamin, and D. Levy, "Incidence and prognosis of syncope," *N Engl J Med*, vol. 347, pp. 878-885, 2002.

[41] L. Olde Nordkamp, N. van Dijk, K. S. Ganzeboom, J. Reitsma, J. Luitse, L. Dekker, et al., "Syncope prevalence in the ED compared to that in the general practice and population: a strong selection process," *Am J Emerg Med*, vol. 27, pp. 271-279, 2009.

[42] J. J. Blanc, C. L'Her, A. Touiza, B. Garo, E. L'Her, J. Mansourati, "Prospective evaluation and outcome of patients admitted for syncope over a 1 year period," *Eur Heart J*, vol. 23, pp. 815-820, 2002.

[43] F. Ammirati, R. Colaceci, A. Cesario, S. Strano, A. Della Scala, I. Colangelo, et al., "Management of syncope: clinical and economic impact of a Syncope Unit," *Europace*, vol. 10, pp. 471-476, 2008.

[44] W. K. Shen, W. W. Decker, P. A. Smars, D. G. Goyal, A. E. Walker, D. O. Hodge, et al., "Syncope Evaluation in the Emergency Department Study (SEEDS): a multidisciplinary approach to syncope management," *Circulation*, vol. 110, pp. 3636-3645, 2004.

[45] A. L. Mark, "The Bezold-Jarisch reflex revisited: clinical implications of inhibitory

reflexes originating in the heart," *Journal of the American College of Cardiology,* vol. 1, no. 1, pp. 90-102, 1983.

[46] J. Allen, "Photoplethysmography and its application in clinical physiological measurement," *Physiological measurement,* vol. 28, no. 3, p. R1, 2007.

[47] A. Reisner, P. A. Shaltis, D. McCombie, and H. H. Asada, "Utility of the photoplethysmogram in circulatory monitoring," *The Journal of the American Society of Anesthesiologists,* vol. 108, no. 5, pp. 950-958, 2008.

[48] G. Lu, and F. Yang, "Limitations of oximetry to measure heart rate variability measures," *Cardiovascular Engineering,* vol. 9, no. 3, pp. 119-125, 2009.

[49] G. Lu, F. Yang, J. A. Taylor, and J. F. Stein, "A comparison of photoplethysmography and ECG recording to analyse heart rate variability in healthy subjects," *Journal of medical engineering and technology,* vol. 33, no. 8, pp. 634-641, 2009.

[50] R. Rauh, R. Limley, R. D. Bauer, M. Radespiel-Troger, and M. Mueck-Weymann, "Comparison of heart rate variability and pulse rate variability detected with photoplethysmography," *Saratov Fall Meeting 2003: Optical Technologies in Biophysics and Medicine V,* p. 115–126, 2004.

[51] S. Vogel, S. Leonhardt, M. Hulsbusch, and D. Starke, "In-ear heart rate monitoring using a micro-optic reflective sensor," *Engineering in Medicine and Biology Society, 2007. EMBS 2007. 29th Annual International Conference of the IEEE,* p. 1375–1378, 2007.

[52] T. Haydon, "The ABCs of Pulse Oximetry," HomeCare - The Leading Business Maganize for HME Professionals, 2011. [Online]. Available: http://www.homecaremag.com/senior-care-products/abcs-pulse-oximetry. [Accessed 21 12 2016].

[53] C. R. Marques, A. A. Martin, C. J. Lima, L. A. Conrado, F. L. Silveira, and M. V. Carvalho, "The use of hyperbaric oxygen therapy and LED therapy in diabetic foot," *Biomedical Optics 2004,* pp. 47-53, 2004.

[54] A. M. Smith, M. C. Mancini, and S. Nie, "Second window for in vivo imaging," *Nature nanotechnology*, vol. 4, no. 11, p. 710, 2009.

[55] R. Couceiro, P. Carvalho, R. P. Paiva, J. Henriques, and J. Muehlsteff, "Detection of motion artifact patterns in photoplethysmographic signals based on time and period domain analysis," *Physiological measurement*, vol. 35, no. 12, p. 2369, 2014.

[56] PulseOximeter.org, "CMS-50F Wristband Pulse Oximeter with Software & Bluetooth," PulseOximeter.org, 2016. [Online]. Available: http://www.pulseoximeter.org/cms50f.html. [Accessed 21 12 2016].

[57] L. Asare, E. Kviesis-Kipge, A. Grabovskis, U. Rubins, J. Spigulis, and R. Erts, "Multi-spectral photoplethysmography biosensor," *SPIE Optics+ Optoelectronics*, pp. 80731Z-80731Z, 2011.

[58] Y. Maeda, M. Sekine, T. Tamura, and K. Mizutani, "The effect of contact pressure to the photoplethysmographic sensor during walking," *生体医工学*, vol. 51, no. Supplement, pp. R-307, 2013.

[59] M. Bolanos, H. Nazeran, and E. Haltiwanger, "Comparison of heart rate variability signal features derived from electrocardiography and photoplethysmography in healthy individuals," *Engineering in Medicine and Biology Society, 2006. EMBS'06. 28th Annual International Conference of the IEEE,* pp. 4289-4294, 2006.

[60] Mayo Clinic Staff, "Premature ventricular contractions (PVCs)," Mayo Clinic, 26 04 2014. [Online]. Available: http://www.mayoclinic.org/diseases-conditions/premature-ventricular-contractions/basics/definition/con-20030205. [Accessed 21 12 2016].

[61] F. Orso, S. Baldasseroni, and A. P. Maggioni, "Heart rate in coronary syndromes and heart failure," *Progress in cardiovascular diseases*, vol. 52, no. 1, pp. 38-45, 2009.

[62] P. H. Brubaker, and D. W. Kitzman, "Chronotropic incompetence causes, consequences, and management," *Circulation*, vol. 123, no. 9, pp. 1010-1020,

2011.

[63] W. B. Kannel, "New perspectives on cardiovascular risk factors," *American heart journal*, vol. 114, no. 1, pp. 213-219, 1987.

[64] J. C. Tardif, "Heart rate as a treatable cardiovascular risk factor," *British medical bulletin*, vol. 90, no. 1, pp. 71-84, 2009.

[65] M. Ortiz, "A Brief History of Biosignal-Driven Art - FROM BIOFEEDBACK TO BIOPHYSICAL PERFORMANCE," eContact!, July 2012. [Online]. Available: http://econtact.ca/14_2/ortiz_biofeedback.html. [Accessed 28 12 2016].

[66] R. Couceiro, P. Carvalho, R. P. Paiva, J. Henriques, I. Quintal, et al., "Assessment of cardiovascular function from multi-Gaussian fitting of a finger photoplethysmogram," *Physiological measurement*, vol. 36, no. 9, p. 1801, 2015.

[67] G. S. Chan, P. M. Middleton, B. G. Celler, L. Wang, L., and N. H. Lovell, "Automatic detection of left ventricular ejection time from a finger photoplethysmographic pulse oximetry waveform: comparison with Doppler aortic measurement," *Physiological measurement*, vol. 28, no. 4, p. 439, 2007.

[68] F. Van de Werf, J. Piessens, H. Kesteloot, and H. De Geest, "A comparison of systolic time intervals derived from the central aortic pressure and from the external carotid pulse tracing," *Circulation*, vol. 51, no. 2, pp. 310-316, 1975.

[69] A. M. Weissler, W. S. Harris, and C. D. Schoenfeld, "Systolic time intervals in heart failure in man," *Circulation*, vol. 37, no. 2, pp. 149-159, 1968.

[70] T. Geeraerts, P. Albaladejo, A. D. Declère, J. Duranteau, J. P. Sales, and D. Benhamou, "Decrease in left ventricular ejection time on digital arterial waveform during simulated hypovolemia in normal humans," *J. Trauma Acute Care Surg.*, vol. 56, pp. 845-849, 2004.

[71] B. Sztrymf, S. Gažnther, E. Artaud-Macari, L. Savale, X. JaaƆs, O. Sitbon, et al., "Left ventricular ejection time in acute heart failure complicating precapillary pulmonary hypertension," *CHEST Journal*, vol. 144, no. 5, pp. 1512-1520, 2013.

[72] L. Afonso, J. Pradhan, V. Veeranna, A. Niraj, and S. Jacob, "Global and regional left ventricular contractile impairment in patients with Wolff-Parkinson-White syndrome," *Indian pacing and electrophysiology journal*, vol. 9, no. 4, p. 195, 2009.

[73] S. C. Millasseau, R. P. Kelly, J. M. Ritter, and P. J. Chowienczyk, "Determination of age-related increases in large artery stiffness by digital pulse contour analysis," *Clinical science*, vol. 103, no. 4, pp. 371-377, 2002.

[74] S. S. DeLoach, and R. R. Townsend, "Vascular stiffness: its measurement and significance for epidemiologic and outcome studies," *Clinical Journal of the American Society of Nephrology*, vol. 3, no. 1, pp. 184-192, 2008.

[75] P. J. Chowienczyk, R. P. Kelly, H. MacCallum, S. C. Millasseau, T. L. Andersson, and R. G. Gosling, "Photoplethysmographic assessment of pulse wave reflection: blunted response to endothelium-dependent beta2-adrenergic vasodilation in type II diabetes mellitus," *Journal of the American College of Cardiology*, vol. 34, no. 7, pp. 2007-2014, 1999.

[76] A. Laucevičius, L. Ryliškyte, and Ž. Petrulioniene, "First experience with salbutamol–induced changes in the photoplethysmographic digital volume pulse," *Kardiologijos Seminarai*, vol. 8, no. 1, pp. 87-93, 2002.

[77] D. Bansal, M. Khan, and A. K. Salhan, "A review of measurement and analysis of heart rate variability," *Computer and Automation Engineering, 2009. ICCAE'09. International Conference on*, pp. 243-246, 2009.

[78] Task Force of the European Society of Cardiology, "Heart rate variability standards of measurement, physiological interpretation, and clinical use," *Eur Heart J*, vol. 17, pp. 354-381, 1996.

[79] HeartMath Institute, "Science of the Heart - Heart Rate Variability: An Indicator of Self-Regulatory Capacity, Autonomic Function and Health," HeartMath Institute, 2016. [Online]. Available: https://www.heartmath.org/research/science-of-the-heart/heart-rate-variability/. [Accessed 28 12 2016].

[80] J. H. Tulen, and F. Boomsma, "Cardiovascular control and plasma catecholamines

during rest and mental stress: effects of posture," *Clinical Science,* vol. 96, no. 6, pp. 567-576, 1999.

[81] D. Verlinde, F. Beckers, D. Ramaekers, and A. E. Aubert, "Wavelet decomposition analysis of heart rate variability in aerobic athletes," *Autonomic Neuroscience,* vol. 90, no. 1, pp. 138-141, 2001.

[82] T. J. Leipzig, and R. I. Lowensohn, "Heart rate variability in neurosurgical patients," *Neurosurgery,* vol. 19, no. 3, pp. 356-362, 1986.

[83] Y. K. Qawqzeh, R. Uldis, and M. Alharbi, "Photoplethysmogram second derivative review: Analysis and applications," *Scientific Research and Essays,* vol. 10, no. 21, pp. 633-639, 2015.

[84] K. Takazawa, Y. Kiyoshi, T. Sakai, T. Kobayashi, K. Maeda, et al., "Clinical usefulness of the second derivative of a plethysmogram (acceleration plethysmogram)," *Cardiology,* vol. 23, pp. 207-217, 1993.

[85] K. Takazawa, M. Fujita, O. Matsuoka, T. Saiki, M. Aikawa, S. Tamura, and C. Ibukiyama, "Assessment of vasocative agents and vascular aging by the second derivative of photoplethysmogram waveform," *Hypertension,* vol. 32, pp. 365-370, 1998.

[86] H. J. Baek, J. S. Kim, Y. S. Kim, H. B. Lee, K. S. Park, "Second Derivative of Photoplethysmography for Estimating Vascular Aging," *The 6th International Special Topic Conference on Information Technology Applications in Biomedicine,* pp. 70-72, 2007.

[87] I. Imanaga, H. Hara, S. Koyanagi, K. Tanaka, "Correlation between wave components of the second derivative of plethysmogram and arterial distensibility," *Jpn Heart J,* vol. 39, pp. 775-784, 1998.

[88] T. Otsuka, T. Kawada, M. Katsumata, and C. Ibuki, "Utility of second derivative of the finger photoplethysmogram for the estimation of the risk of coronary heart disease in the general population," *Circ J,* vol. 70, pp. 304-310, 2006.

[89] N. Nousou, S. Urase, Y. Maniwa, K. Fujimura, Y. Fukui, "Classification of

Acceleration Plethysmogram Using Self-Organizing Map," *Intelligent Signal Processing and Communications, 2006 ISPACS '06 International Symposium on,* pp. 681-684, 2006.

[90] K. Atsushi, M. Masaaki, I. Yoko, and S. Kazuna, "Responses of the second derivative of the finger photoplethysmogram indices and hemodynamic parameters to anesthesia induction," *Hypertens. Res.,* vol. 35, no. 2, pp. 166-172, 2012.

[91] R. Blazek, and C. Lee, "Multi-resolution Linear Model Comparison for Detection of Dicrotic Notch and Peak in Blood Volume Pulse Signals," in *Biosignal 2010,* Czech Republic, 2010.

[92] L. Antonelli, W. Ohley, and R. Khamlach, "Dicrotic notch detection using wavelet transform analysis," *Proceedings of the 16th Annual International Conference of the IEEE Engineering in Medicine and Biology Society, Engineering Advances: New Opportunities for Biomedical Engineers,* 1994.

[93] Y. Kimura, K. Takamatsu, A. Fujii, M. Suzuki, N. Chikada, R. Tanada, et al., "Kampo therapy for premenstrual syndrome: efficacy of Kamishoyosan quantified using the second derivative of the fingertip photoplethysmogram," *Journal of Obstetrics and Gynaecology Research,* vol. 33, no. 3, pp. 325-332, 2007.

[94] H. Asada, P. Shaltis, A. Reisner, R. Sokwoo, R. C. Hutchinson, "Mobile monitoring with wearable photoplethysmographic biosensors," *IEEE Engineering in Medicine and Biology Magazine,* vol. 22, no. 3, pp. 28-40, 2003.

[95] C. P. Chua, and C. Heneghan, "Continuous Blood Pressure Monitoring using ECG and Finger Photoplethysmogram," *The 28th Annual International Conference of the IEEE Engineering in Medicine and Biology Society,* 2006.

[96] W. Murray, and P. Foster, "The peripheral pulse wave: information overlooked," *Journal of Clinical Monitoring and Computing,* vol. 12, pp. 365-377, 1996.

[97] E. Chua, S. Redmond, G. McDarby, C. Heneghan, "Towards using photo-plethysmogram amplitude to measure blood pressure during sleep," *Annals of Biomedical Engineering,* vol. 38, no. 3, pp. 945-954, 2010.

[98] J. Dorlas, and J. Nijboer, "Photo-electric plethysmography as a monitoring device in anaesthesia. Application and interpretation," *British Journal of Anaesthesia,* vol. 57, pp. 524-530, 1985.

[99] S. R. Alty, N. Angarita-Jaimes, S. C. Millasseau, and P. J. Chowienczyk, "Predicting Arterial Stiffness From the Digital Volume Pulse Waveform," *IEEE Transactions on Biomedical Engineering,* vol. 54, no. 12, pp. 2268-2275, 2007.

[100] A. Bashan, R. P. Bartsch, J. W. Kantelhardt, S. Havlin, and P. C. Ivanov, "Network physiology reveals relations between network topology and physiological function," *Nature communications,* vol. 3, p. 702, 2012.

[101] L. Faes, M. Javorka, and G. Nollo, "Information-Theoretic Assessment of Cardiovascular Variability During Postural and Mental Stress," *XIV Mediterranean Conference on Medical and Biological Engineering and Computing 2016,* pp. 67-70, 2016.

[102] L. Faes, G. Nollo, and A. Porta, "Mechanisms of causal interaction between short-term RR interval and systolic arterial pressure oscillations during orthostatic challenge," *Journal of Applied Physiology,* vol. 114, no. 12, pp. 1657-1667, 2013.

[103] L. Faes, A. Porta, G. Rossato, A. Adami, D. Tonon, A. Corica, and G. Nollo, "Investigating the mechanisms of cardiovascular and cerebrovascular regulation in orthostatic syncope through an information decomposition strategy," *Autonomic Neuroscience,* vol. 178, no. 1, pp. 76-82, 2013.

[104] L. Faes, D. Marinazzo, F. Jurysta, and G. Nollo, "Linear and non-linear brain–heart and brain–brain interactions during sleep," *Physiological measurement,* vol. 36, no. 4, p. 683, 2015.

[105] J. Beckerman, "Heart Disease and the Head-Up Tilt Table Test," WebMD, 17 10 2016. [Online]. Available: http://www.webmd.com/heart-disease/guide/tilt-table-test#2-4. [Accessed 30 12 2016].

[106] P. A. Low, and W. Singer, "Management of neurogenic orthostatic hypotension: an update," *The Lancet Neurology,* vol. 7, no. 5, pp. 451-458, 2008.

[107] N. Virag, R. Sutton, R. Vetter, T. Markowitz, and M. Erickson, "Prediction of vasovagal syncope from heart rate and blood pressure trend and variability: experience in 1,155 patients," *Heart Rhythm,* vol. 4, no. 11, pp. 1375-1382, 2007.

[108] R. Mereu, G. De Barbieri, T. Perrone, A. Mugellini, A. Di Toro, and L. Bernardi, "Heart rate/blood pressure ratio as predictor of neuromediated syncope," *International journal of cardiology,* vol. 167, no. 4, pp. 1170-1175, 2013.

[109] G. Piccirillo, N. Camilla, A. Moisè, M. Lionetti, M. Nocco, S. Di Carlo, et al., "Heart rate and blood pressure variability in subjects with vasovagal syncope," *Clinical Science,* vol. 107, no. 1, pp. 55-61, 2004.

[110] C. Eickholt, T. Drexel, J. Muehlsteff, A. Ritz, M. Siekiera, K. Kirmanoglou, et al., "Neurally mediated syncope prediction based on heart rate and pulse arrival time," *European Heart Journal,* vol. 34, no. suppl 1, p. 796, 2013.

[111] J. Muehlsteff, T. Correia, R. Couceiro, P. Carvalho, A. Ritz, C. Eickholt, et al., "Detection of hemodynamic adaptations during impending syncope: Implementation of a robust algorithm based on pulse arrival time measurements only," *2013 35th Annual International Conference of the IEEE Engineering in Medicine and Biology Society (EMBC),* pp. 2291-2294, 2013.

[112] G. B. del Pozo, "Deliverable D4.1 State of the Art – Wearable Sensors," DAPHNE - Data-as-a-service platform for healthy lifestyle and preventive medicine, 2014.

[113] plux | wireless biosignals, "biosignalsplux | wearable body sensing platform," plux | wireless biosignals, 2015-2016. [Online]. Available: http://biosignalsplux.com/index.php/en/. [Accessed 2015-2016].

[114] F. El-Amrawy, and M. I. Nounou, "Are currently available wearable devices for activity tracking and heart rate monitoring accurate, precise, and medically beneficial?," *Healthcare informatics research,* vol. 21, no. 4, pp. 315-320, 2015.

[115] Empatica Inc., "E4 wristband," Empatica Inc., 2016. [Online]. [Accessed March 2016].

[116] T. J. Bruno, D. N. Paris, CRC Handbook of Fundamental Spectroscopic Correlation

Charts, CRC Press, 2005.

[117] Apple Inc., "Your heart rate. What it means, and where on Apple Watch you'll find it.," Apple Inc., 2015. [Online]. Available: https://support.apple.com/en-us/HT204666. [Accessed 4 10 2015].

[118] A. Haavikko, "MSc Thesis: Evaluation of an optical heart rate sensor," Tampere University of Technology, 2014.

[119] SAMSUNG, "Welcome to Simband," SAMSUNG, 2015. [Online]. Available: https://www.simband.io/. [Accessed 2015 10 10].

[120] CBS Interactive Inc., "Samsung's second-gen Simband wearable features more robust sensors and sweatproofing," CBS Interactive Inc., 12 11 2014. [Online]. Available: https://www.cnet.com/products/samsung-simband/preview/. [Accessed 10 10 2015].

[121] M. James, "Microsoft Band Gets An SDK," i-programmer.info, 24 2 2015. [Online]. Available: http://www.i-programmer.info/news/91-hardware/8325-microsoft-band-gets-an-sdk.html. [Accessed 5 10 2015].

[122] Microsoft, "Create amazing apps for Microsoft Band and Microsoft Health," Microsoft, 2015. [Online]. Available: http://developer.microsoftband.com/. [Accessed 6 10 2015].

[123] D. Rubino, "This is how often the Microsoft Band checks your heart rate," Mobile Nations, 3 11 2014. [Online]. Available: http://www.windowscentral.com/how-often-microsoft-band-checks-your-heart-rate. [Accessed 6 10 2015].

[124] Empatica Inc., "OFFER," Empatica Inc., 2016. [Online]. Available: https://www.empatica.com/offer.html.

[125] Empatica Inc., "Utilizing the PPG/BVP signal," Empatica Inc., 31 3 2016. [Online]. Available: https://support.empatica.com/hc/en-us/articles/204954639-Utilizing-the-PPG-BVP-signal. [Accessed March 2016].

[126] Empatica Inc., "What should I know to use the PPG/IBI data in my experiment?," Empatica Inc., 2016. [Online]. Available: https://support.empatica.com/hc/en-

us/articles/203621335-What-should-I-know-to-use-the-PPG-IBI-data-in-my-experiment-. [Accessed March 2016].

[127] Empatica Inc., "Store - E4 WRISTBAND," Empatica Inc., 2016. [Online]. Available: https://store.empatica.com/products/e4-wristband?variant=945527715. [Accessed March 2016].

[128] plux | wireless biosignals, "Sensor – Products," plux | wireless biosignals, 2015. [Online]. Available: http://biosignalsplux.com/index.php/en/products/sensors. [Accessed 2 10 2015].

[129] plux | wireless biosignals, "Blood Volume Pulse (BVP) Sensors," plux | wireless biosignals, 2015. [Online]. Available: http://biosignalsplux.com/index.php/en/bvp-blood-volume-pulse. [Accessed 2 10 2015].

[130] plux | wireless biosignals, "API’s – Software," plux | wireless biosignals, 2015. [Online]. Available: http://biosignalsplux.com/index.php/en/software/apis. [Accessed 2 10 2015].

[131] D. Isacson, Degree Project in Computer Science: Application development for smartwatches: An investigation in suitable smartwatch applications, 2015.

[132] Smartwatch Group, "The History of Smartwatches," Smartwatch Group, 2015. [Online]. Available: http://www.smartwatchgroup.com/history-smartwatches/. [Accessed 9 10 2015].

[133] Peeble Inc., "EVENTS AND SERVICES," Peeble Inc., 2016. [Online]. Available: https://developer.pebble.com/guides/events-and-services/. [Accessed 27 12 2016].

[134] Peeble Inc., "HEART RATE MONITOR," Peeble Inc., 2016. [Online]. Available: https://developer.pebble.com/guides/events-and-services/hrm/. [Accessed 27 12 2016].

[135] Apple Inc., "The HealthKit Framework," Apple Inc., 2015. [Online]. Available: https://developer.apple.com/reference/healthkit. [Accessed 8 10 2015].

[136] Apple Inc., "Now everybody can do their part to advance medical research," Apple Inc., 2015. [Online]. Available: http://www.apple.com/researchkit/. [Accessed 8 10

2015].

[137] D. D'Orazio, "Google reveals Android Wear, an operating system for smartwatches," *The Verge,* 18 3 2014.

[138] D. Bohn, "Motorola, LG announce upcoming Android Wear smartwatches," *The Verge,* 18 3 2014.

[139] Android Developers, "Sensors Overview," Android Developers, 2015. [Online]. Available: https://developer.android.com/guide/topics/sensors/sensors_overview.html. [Accessed 9 10 2015].

[140] S. Rhee, B. H. Yang, K. Chang, and H. H. Assada, "The ring sensor: a new ambulatory wearable sensor for twenty-four hour patient monitoring," *Engineering in Medicine and Biology Society, 1998. Proceedings of the 20th Annual International Conference of the IEEE,* vol. 4, no. 12, pp. 1906-1909, 1998.

[141] E. Gil, M. Orini, R. Bailón, J. M. Vergara, L. Mainardi, and P. Laguna, "Photoplethysmography pulse rate variability as a surrogate measurement of heart rate variability during non-stationary conditions," *Physiological Measurement,* vol. 31, no. 9, p. 1271, 2010.

[142] E. Gil, R. Bailón, J. M. Vergara, and P. Laguna, "PTT variability for discrimination of sleep apnea related decreases in the amplitude fluctuations of PPG signal in children," *IEEE Transactions on Biomedical Engineering,* vol. 57, no. 5, pp. 1079-1088, 2010.

[143] H. Han, M. J. Kim, and J. Kim, "Development of real-time motion artifact reduction algorithm for a wearable photoplethysmography," *Engineering in Medicine and Biology Society, 2007. EMBS 2007. 29th Annual International Conference of the IEEE,* p. 1538–1541, 2007.

[144] A. H. Khandoker, C. K. Karmakar, and M. Palaniswami, "Comparison of pulse rate variability with heart rate variability during obstructive sleep apnea," *Medical engineering and physics,* vol. 33, no. 2, pp. 204-209, 2014.

[145] Y. Han, W. C. Lin, S. C. Huang, C. L. Tsai, and K. P. Lin, "Comparison of Heart Rate Variability and Pulse Rate Variability of Respiratory Control," *submitted for publication.*

[146] N. D. Giardino, P. M. Lehrer, and R. Edelberg, "Comparison of finger plethysmograph to ECG in the measurement of heart rate variability," *Psychophysiology,* vol. 39, no. 2, pp. 246-253, 2002.

[147] B. Wagner, and M. Barr, "Introduction to Digital Filters," *Embedded Systems Programming*, pp. 47-48, 2002.

[148] DSPRelated.com, "HAMMING WINDOW," DSPRelated.com, 2016. [Online]. Available: https://www.dsprelated.com/freebooks/sasp/Hamming_Window.html. [Accessed 02 01 2017].

[149] DSPRelated.com, "USE OF A BLACKMAN WINDOW," DSPRelated.com, 2016. [Online]. Available: https://www.dsprelated.com/freebooks/mdft/Use_Blackman_Window.html. [Accessed 02 01 2017].

[150] T. J. Ulrych, and T. N. Bishop, "Maximum entropy spectral analysis and autoregressive decomposition," *Reviews of Geophysics,* vol. 13, pp. 183-200, 1975.

[151] H. W. Lilliefors, "On the Kolmogorov-Smirnov test for normality with mean and variance unknown," *Journal of the American Statistical Association,* vol. 62, no. 318, p. 399–402, 1967.

[152] J. B. du Prel, B. Röhrig, G. Hommel, and M. Blettner, "Choosing Statistical Tests: Part 12 of a Series on Evaluation of Scientific Publications," *Dtsch Arztebl Int,* vol. 107, no. 19, pp. 343-348, 2010.

[153] J. H. Zar, "Spearman rank correlation," in *Encyclopedia of Biostatistics,* 1998.

[154] J. D. Gibbons, and S. Chakraborti, "The Wilcoxon Rank-Sum Test," in *Nonparametric statistical inference,* Springer Berlin Heidelberg, 2011.

[155] B. Bryant, K. Knights, "Chapter 23: Drugs affecting vascular smooth muscle," in *Pharmacology for health professionals*, Chatswood NSW, Australia, Elsevier

Health Sciences, 2011, p. 472.

[156] CNSystems Medizintechnik AG, "Product Portfolio - Overview / Comparison - The next generation of noninvasive monitoring and diagnosis," CNSystems Medizintechnik AG, 2015. [Online]. Available: http://www.cnsystems.com/index.php?option=com_content&view=article&id=92&Itemid=515&lang=en. [Accessed 09 01 2017].

[157] C.-C. Chang, and C.-J. Lin, "LIBSVM: A library for support vector machines," *ACM Trans. Intell. Syst. Technol.*, vol. 2, p. 27:1–27:27, 2011.

[158] J. B. Allen, "Short term spectral analysis, synthesis, and modification by discrete Fourier transform," *IEEE Trans. on Acoust., Speech, and Sig. Proc.*, vol. 4, pp. 21-24, 1997.

[159] B. P. Grubb, "Pathophysiology and differential diagnosis of neurocardiogenic syncope," *Amer. J. Cardiol.*, vol. 84, pp. 3-9, 1999.

[160] R. Couceiro, P. Carvalho, R. P. Paiva, J. Henriques, M. Antunes, I. Quintal, and J. Muehlsteff, "Multi-Gaussian fitting for the assessment of left ventricular ejection time from the photoplethysmogram," *2012 Annual International Conference of the IEEE Engineering in Medicine and Biology Society*, pp. 3951-3954, 2012.

[161] BAL - Business Analyst Learnings, "MoSCoW : Requirements Prioritization Technique," BAL - Business Analyst Learnings, 05 03 2013. [Online]. Available: https://businessanalystlearnings.com/ba-techniques/2013/3/5/moscow-technique-requirements-prioritization. [Accessed 13 01 2017].

[162] PLUX – Wireless Biosignals, S.A., "Blood Volume Pulse (BVP) – Sensor Data Sheet," Lisbon, 2015.

[163] PLUX - Wireless Biosignals, "bioPlux java API v. 2," Lisbon, 2010.

[164] The MathWorks, Inc., "Class MWArray," The MathWorks, Inc., 2014. [Online]. Available: https://www.mathworks.com/help/javabuilder/MWArrayAPI/com/mathworks/toolbox/javabuilder/MWArray.html. [Accessed November 2016].

[165] Oracle and/or its affiliates, "Class Object," Oracle and/or its affiliates, 2016. [Online]. Available: https://docs.oracle.com/javase/7/docs/api/java/lang/Object.html. [Accessed November 2016].

[166] L. J. Laslett, P. Alagona, B. A. Clark, J. P. Drozda, F. Saldivar, S. R. Wilson, et al., "The worldwide environment of cardiovascular disease: prevalence, diagnosis, therapy, and policy issues: a report from the American College of Cardiology," *Journal of the American College of Cardiology,* vol. 60, no. 25_S, pp. S1-S49, 2012.

[167] M. Nichols, N. Townsend, R. Luengo-Fernandez, J. Leal, A. Gray, P. Scarborough, et al., "European cardiovascular disease statistics 2012," *European Heart Network, Brussels, European Heart Society of Cardiology, Sophia Antipolis,* 2012.

[168] A. S. Go, D. Mozaffarian, V. L. Roger, E. J. Benjamin, J. D. Berry, M. J. Blaha, et al., "Heart disease and stroke statistics-2014 update: A report from the American Heart Society," *Circulation,* vol. 129, no. 3, pp. e28-e292, 2014.

[169] B. Verheyden, J. Gisolf, F. Beckers, J. M. Karemaker, K. H. Wesseling, A. Aubert, et al., "Impact of age on the vasovagal response provoked by sublingual nitroglycerine in routine tilt testing," *Clin Sci (Lond),* vol. 113, p. 329–337, 2007.